

Limitations of Proximity Lithography Printing: Simulations, Experiments, and Applications

THÈSE N° 7723 (2017)

PRÉSENTÉE LE 23 MAI 2017

À LA FACULTÉ DES SCIENCES ET TECHNIQUES DE L'INGÉNIEUR
LABORATOIRE D'OPTIQUE APPLIQUÉE
PROGRAMME DOCTORAL EN PHOTONIQUE

ÉCOLE POLYTECHNIQUE FÉDÉRALE DE LAUSANNE

POUR L'OBTENTION DU GRADE DE DOCTEUR ÈS SCIENCES

PAR

Krishnaparvathy PUTHANKOVILAKAM

acceptée sur proposition du jury:

Prof. L. Thévenaz, président du jury
Prof. H. P. Herzig, Dr T. Scharf, directeurs de thèse
Dr A. Erdmann, rapporteur
Dr U. Zeitner, rapporteur
Dr H. Shea, rapporteur



ÉCOLE POLYTECHNIQUE
FÉDÉRALE DE LAUSANNE

Suisse
2017

ABSTRACT

Photolithography is one of the earliest technologies used to transfer patterns to a substrate. It is also known as optical lithography since it uses light to transfer the pattern. This technology is the backbone of the semiconductor industry. Several types of exposure techniques exist for printing the feature patterns. The main techniques are projection printing, contact printing, and proximity printing. Projection printing technology uses optical elements between mask and wafer to project the feature on the mask to the wafer. This is very expensive and delivers the highest resolution. In contact printing, the mask and wafer are in contact with each other and in proximity printing, the mask is kept at some proximity distance away from the wafer. Proximity printing is an easy and cost effective printing technique because the damage to the mask will be less and also no optical elements between mask and wafer are used. The main drawback of the proximity printing is the diffraction effect caused by the proximity gap between mask and wafer, which limits the resolution. The main objective of this thesis is to study the limitations of proximity printing and to increase its resolution.

To study the limitations, different types of design strategies and verification methods are used in the thesis. First is the simulation technique which is performed with GenISys Layout LAB. This is specially designed for proximity printing. The software gives the aerial image and final resist pattern as output. The most interesting and important aspect is the second verification technique which is the experimental setup. A measurement setup has been built to study the light propagation from different masks and to study the aerial image at different proximity gaps. The setup is known as High Resolution Interference Microscopy (HRIM). The setup is basically a Mach-Zehnder interferometer having different light sources, sample plane and reference arm which are used according to the samples. The final verification is achieved using the mask aligner. Both the simulation and experiments are carried out using a special illumination optics called MO exposure optics from Süss MicroOptics.

There exist several types of Resolution Enhancement Techniques (RET) for increasing the resolution in printing. The thesis mainly focuses on the rule based optical proximity correction technique which is a simple method for mass production. Correction structures are designed for one dimensional and two dimensional features in amplitude masks. Adding lines near the edge to improve the edge slope will be discussed as the one dimensional correction. The different intensity cutting planes and the comparison between simulation and experimental results will be

discussed along with that. A unified correction structure is designed to solve corner rounding problem and will be studied as the two dimensional study. The structure is defined to print different line widths at single proximity gap on single exposure.

Usually, all the structures in the amplitude mask are studied with their aerial image intensities at different proximity gaps. But, here the study extends to phase evaluation also. The measurement technique can measure both intensity and phase evolution from the mask structures. Phase evolution from amplitude correction features will be discussed and how the phase modulates the intensity patterns is also studied. The role of fundamental principles like phase singularities, phase shifts are also discussed to find its effects on proximity printing structures. The study also leads to the intensity and phase propagation from phase shifting mask. The structure evaluated is a group of corners in a phase shifting mask. The propagation evaluation can be evaluated considering Lohmann images and the fractional Talbot effect.

The powerful simulation tool with capable measurement system HRIM helps to design, characterize, and verify the functions of various types of masks. The tools will also help to study fundamental principles of optics and approximations in the near field zone of microstructures and has potential for further studies.

Keywords: Photolithography, proximity printing, resolution enhancement techniques, optical proximity correction, GenISys Layout LAB, high resolution interference microscopy, MO exposure optics, edge slope improvement, corner rounding, phase shifts and phase singularities, phase shifting mask, Lohmann images.

RÉSUMÉ

La photolithographie est l'une des premières technologies utilisées pour transférer des motifs à un substrat. Elle est également connue sous le nom de lithographie optique, car elle utilise la lumière pour transférer le modèle ; cette technologie est à la base de l'industrie des semi-conducteurs. Plusieurs types de techniques d'exposition existent pour imprimer les motifs. Les techniques principales sont l'impression par contact, l'impression de proximité et l'impression par projection. Lors de l'impression par contact, le masque et le wafer sont en contact l'un avec l'autre et dans l'impression de proximité, le masque est maintenu à une certaine distance de proximité du wafer. La technologie d'impression par projection utilise des éléments optiques entre le masque et le wafer pour projeter le motif du masque sur le wafer. L'impression de proximité est une impression facile et rentable car les dommages au masque seront moins importants que pour l'impression par contact et aucun élément optique entre le masque et le wafer n'est utilisé. Mais l'inconvénient principal de l'impression de proximité est l'effet de diffraction causé par l'écart de proximité entre le masque et le wafer et ceci limite également la résolution. Le but principal de la thèse est d'étudier les limites de l'impression de proximité et d'augmenter la résolution.

Pour étudier les limites, différents types de stratégies de conception et de méthodes de vérification sont utilisés dans la thèse. La première est la technique de simulation qui est réalisée avec GenlSys Layout LAB et spécialement conçue pour l'impression de proximité. Le logiciel donne l'image aérienne et le motif final de la résine photosensible comme résultat. L'aspect le plus intéressant est la deuxième technique de vérification qui est la vérification expérimentale. Un système optique de mesure a été construit pour étudier la propagation de la lumière à partir de différents masques et étudier l'image aérienne à différents intervalles de proximité. Le système est connu sous le nom de Microscopie à Interférence Haute Résolution (HRIM). C'est fondamentalement un interféromètre de Mach-Zehnder ayant plusieurs parties : différentes sources de lumière, un bras avec le plan pour l'échantillon et le bras de référence. La source peut être choisie selon l'échantillon. La vérification finale est réalisée en utilisant l'alignement du masque. La simulation et les expériences sont réalisées à l'aide d'une optique d'illumination spéciale appelée « MO Exposure Optics » de Süss MicroOptics.

Il existe plusieurs types de techniques d'amélioration de la résolution (RET) pour augmenter la résolution lors de l'impression. La thèse se concentre principalement sur la technique de

correction optique de proximité basée sur des règles empiriques, qui est une méthode simple pour la production de masse. Les structures de correction sont conçues pour des motifs unidimensionnels et bidimensionnels dans le masque d'amplitude. L'ajout de lignes près du bord pour améliorer la verticalité du bord sera discuté comme correction unidimensionnelle. Les différents plans de coupe d'intensité et la comparaison entre la simulation et les résultats expérimentaux seront discutés avec cela. Une structure de correction unifiée est conçue pour résoudre le problème d'arrondi d'angle et sera étudiée comme le cas bidimensionnel. La structure est définie pour imprimer différentes largeurs de ligne à un seul écart de proximité en exposition unique.

Habituellement, toutes les structures du masque d'amplitude sont étudiées avec leurs intensités d'images aériennes à différents écarts de proximité. Mais, ici, l'étude s'étend à l'évaluation de phase aussi. La technique de mesure peut mesurer à la fois l'intensité et l'évolution de phase à partir des structures du masque. L'évolution de phase à partir des motifs de correction d'amplitude sera discutée et la façon dont la phase module les distributions d'intensité est également étudiée. Le rôle des principes fondamentaux comme les singularités de phase, les déphasages sont également discutés pour en trouver les effets sur les structures d'impression de proximité. L'étude est étendue également à l'intensité et la propagation de phase à partir du masque de déphasage. La structure évaluée est un groupe de coins sur un masque de déphasage. L'évaluation de la propagation porte également sur la création d'images Lohmann et l'effet fractionnaire de Talbot.

Le puissant outil de simulation avec système de mesure HRIM permet de concevoir et de caractériser différents types de masques. Les outils permettront également d'étudier et de vérifier les principes fondamentaux qui existent jusqu'à présent.

Mots clés : Photolithographie, impression de proximité, technique d'amélioration de résolution, correction optique de proximité, GenlSys Layout LAB, microscope à interférence à haute résolution, MO Exposure Optics, amélioration de verticalité de bord, coins arrondis, déphasages et singularités de phase, masque de déphasage, images de Lohmann.

CONTENTS

Abstract	iii
Resume	v
List of figures	x
List of tables	xv
Chapter 1 Introduction	1
1.1 History of photolithography.....	1
1.2 Photolithographic process	2
1.3 Thesis outline	5
References	6
Chapter 2 Proximity printing and Resolution Enhancement Techniques (RETs)	8
2.1 Exposure system technology.....	8
2.2 Comparison between proximity printing and projection printing.....	10
2.3 Resolution Enhancement Techniques(RETs).....	12
2.3.1 Off – Axis Illumination (OAI)	12
2.3.2 Phase Shifting Mask (PSM)	13
2.3.3 Optical Proximity Correction (OPC).....	15
Conclusion	16
References	17
Chapter 3 Design and Verification techniques	20
3.1 Simulation : GenISys Layout LAB.....	20
3.2 MO exposure optics	23
3.3 Measurement : High Resolution Interference microscopy(HRIM).....	26
3.3.1 Mach-Zehnder Interferometer.....	27

3.3.2 Sample stage and microscope	28
3.3.3 Five phase shift mirror	28
3.3.4 MO exposure optics	29
3.3.5 Illumination sources and operation	29
3.4 Comparison of simulation and measurement	30
3.5 Printing : Mask aligner	32
Conclusion	32
References	33
Chapter 4 1D correction structures in amplitude mask - Edge	36
4.1 Structure definition	37
4.2 Simulation and experimental geometries	37
4.3 Measurements and recordings	38
4.4 Parameter definition	42
Conclusion	44
References	45
Chapter 5 Lines characterization	46
5.1 Theoretical definition	46
5.2 Measurements and recordings	47
5.3 Results and findings	55
Conclusion	56
References	56
Chapter 6 2D correction structure in amplitude mask - Corner	57
6.1 Designing of the corner correction structure	57
6.2 Characterization of the corner correction structure	61
6.3 Results and findings of the corner correction structure	64
Conclusion	67
References	67
Chapter 7 Phase analysis of amplitude mask structures - 1D and 2D	69

7.1 Importance of phase in light propagation.....	69
7.2 Phase evolution from edge structure (1D).....	69
7.3 Phase evolution from corner structure (2D).....	71
Conclusion	75
References	76
Chapter 8 Phase and intensity analysis of phase mask structure	78
8.1 Phase mask and structure definition	78
8.2 Measurements and recordings from structures.....	79
8.2.1 Propagation measurement : x-z.....	80
8.2.2 Image plots : x-y	84
8.3 Results and discussion.....	86
Conclusion	89
References	89
Chapter 9 Conclusions.....	91
Acknowledgement.....	94
List of publications	96
List of abbreviations	98
Curriculum Vitae	99

LIST OF FIGURES

Chapter 1

- Figure 1. 1: Different types of exposure techniques. 4
Figure 1. 2: Resist development and pattern transfer on the wafer. 4

Chapter 2

- Figure 2. 1: Different types of projection printing technology. 10
Figure 2. 2: Light intensity profile on the wafer for different printing technologies. Here the light propagates through a slit width, so the design in the resist profile should look like a slit but in reality due to diffraction the shape changes into resist profile as shown for technologies. 11
Figure 2. 3: On-axis and off-axis illumination techniques. Comparing the on-axis and off-axis diffraction orders. The off-axis illumination has shifted the zeroth order. Due to the shift in the illumination angle we can capture a larger angle between zero and first order. Consequently, the resolution increases. 13
Figure 2. 4: Light intensity distribution through conventional mask and phase shifting mask. The mask in the right is the Phase shifting mask. The yellow colored region is where the depth is changed to half a wavelength. So when the light passes through the mask, field amplitude from both will have a phase difference of 180° and final intensity will be as shown above. 14
Figure 2. 5: Different types of PSM. 14
Figure 2. 6: The features on the mask after model based optical proximity correction [2.5]. (a): The mask structure that we need to print; (b): Feature printed on wafer with mask structure in (a); (c): The corrected Structure of (a) with model based Optical Proximity Correction technique; (d): The feature on wafer with corrected structure. 15

Chapter 3

- Figure 3. 1: Simulation module of Layout LAB. 21
Figure 3. 2: Constructing greens function by mirror method. P is the actual observation point to get the diffraction field. P' is mirror point and R and R' are the distance vectors. 22
Figure 3. 3: Köhler illumination technique. 24
Figure 3. 4: MO exposure optics [3.3]. 25
Figure 3. 5: Beam evolution from Köhler integrators. 26

Figure 3. 6: High Resolution Interference Microscopy (HRIM).....	27
Figure 3. 7: Mach – Zehnder interferometer.....	27
Figure 3. 8: MO exposure optics in HRIM.....	29
Figure 3. 9: Propagation measurement (x-z) of a 6 μm line width structure till 50 μm proximity gap. (a) Represents the experimental result and (b) the simulation result. Intensities are normalized from 0 to 1.....	31
Figure 3. 10: The (x-y) intensity images of a 10 μm line with both simulation and experimental results at different proximity gaps respectively. Intensities are normalized from 0 to 1.....	31
Figure 3. 11: Mask aligner set up in clean room [3.23].....	32

Chapter 4

Figure 4. 1: The structure definition to study (a) normal edge, (b) edge with one line correction and (c) edge with two line correction structures respectively.....	37
Figure 4. 2: x-y intensity images from HRIM optimized for 50 μm proximity gap at 0.1 μm (a) one line edge correction and (b) two line edge correction.	38
Figure 4. 3: x-z propagation images from HRIM optimized for 50 μm proximity gap (a) one line edge correction and (b) two line edge correction.....	39
Figure 4. 4: x-z propagation images from HRIM optimized for 30 μm proximity gap (a) one line edge correction and (b) two line edge correction.....	39
Figure 4. 5: x-y line images at 30 μm proximity gap of an optimized structure defined for 30 μm . (a) and (b) are one line edge corrected simulation and HRIM images respectively. (c) and (d) are two line edge corrected simulation and HRIM images respectively.....	40
Figure 4. 6: x-y line images at 50 μm proximity gap of an optimized structure defined for 30 μm . (a) and (b) are one line edge corrected simulation and HRIM images respectively. (c) and (d) are two line edge corrected simulation and HRIM images respectively.....	41
Figure 4. 7: Edge falling position with an example.	42
Figure 4. 8: Example parameters are defined (50 μm two line corrected experimental results). 43	

Chapter 5

Figure 5. 1: Simulation result of light evolution (x-z) from a 6 μm line width structure until 50 μm proximity gap using parallel illumination and MO exposure optics.	47
Figure 5. 2: HRIM and simulation result of light evolution (x-z) from a 2 μm line width structure until 50 μm proximity gap.	48
Figure 5. 3: HRIM and simulation intensity images(x-y) at different proximity gaps. Proximity gaps are written on the top of the images.....	49
Figure 5. 4: HRIM line plots from(x-y) images of 2 μm line width structure at different proximity gaps.....	50

Figure 5. 5: HRIM and simulation result of light evolution (x-z) from a 6 μm line width structure until 50 μm proximity gap.	51
Figure 5. 6: HRIM and simulation intensity images(x-y) at different proximity gaps for 6 μm line. Proximity gaps are written on the top of the images.	52
Figure 5. 7: HRIM line plots from(x-y) images of 6 μm line width structure at different proximity gaps.....	52
Figure 5. 8: HRIM and simulation result of light evolution (x-z) from a 10 μm line width structure until 50 μm proximity gap.	53
Figure 5. 9: HRIM and simulation intensity images(x-y) at different proximity gaps for 10 μm line. Proximity gaps are written on the top of the images.	54
Figure 5. 10: HRIM line plots from(x-y) images of 10 μm line width structure at different proximity gaps.....	54
Figure 5. 11: Intensity line images of characteristic features observed for a line (6 μm) at different proximity gaps.....	55

Chapter 6

Figure 6. 1: Simulated aerial images of different line widths at 30 μm proximity gap. Blue shows the low intensity regions and red shows the high intensity regions.	58
Figure 6. 2:(a) Feature (slit) with no correction, (b) Result obtained with the serif correction methods with conventional feature size and (c) result with the new rule based correction method using sub-resolution features. Here, the images are represented as three sets, first set is the drawing of the pattern, second set is the aerial image and third set is the aerial image in detail with intensity levels.	59
Figure 6. 3: Simulation aerial images of different correction structures at 30 μm proximity gap. The fine black line is printed to guide the eye.	60
Figure 6. 4: Parameter variation in the OPC structure.....	61
Figure 6. 5: The designed rule based structure for corners.	61
Figure 6. 6: The simulation, experimental intensity and SEM images on wafer of 10 μm line width: normal (a, b, c) and corrected structure (d, e, f).	62
Figure 6. 7: SEM images of the 10 μm line width correction structure at different printing doses.	63
Figure 6. 8: Line width variation at different exposure doses.	64
Figure 6. 9: Inner radius of curvature definition for 10 μm line width structure.....	65
Figure 6. 10: Minimum inner radius of curvature of optimized structure having 10 μm line width.	65
Figure 6. 11: The simulation, experimental intensity and SEM images of 40 μm line width: normal (a, b, c) and corrected structure (d, e, f).....	66

Chapter 7

Figure 7. 1: 1D OPC structure for phase analysis.....	70
Figure 7. 2: Intensity and phase behind an OPC structure similar to that one given in Fig.7. 1. (a) and (b) HRIM measurement intensity and phase. (c) and (d) are FDTD simulation results.....	70
Figure 7. 3: 2D OPC structure for phase analysis.....	71
Figure 7. 4: Intensity and phase behind an OPC structure similar to that one given in Fig.7. 3(a).	72
Figure 7. 5: The measured intensity and phase image of the corner structure at different proximity gaps between the mask and observation plane. (a) Image at 0.1 μm proximity gap, (b) image at 20 μm proximity gap and (c) image at 30 μm proximity gap.....	73
Figure 7. 6: Intensity and phase behind an OPC structure similar to that one given in Fig.7. 3(b).	74
Figure 7. 7: The measured intensity and phase image of the corner structure at different proximity gaps between the mask and observation plane. (a) Image at 0.1 μm proximity gap, (b) image at 20 μm proximity gap and (c) image at 30 μm proximity gap.....	75

Chapter 8

Figure 8. 1: Structure considered for our experiments, (a) is the geometry of the structure, (b) amplitude structure [yellow lines are the open areas] and (c) shows the structure with phase shifts [yellow lines are the open areas and violet areas are the etched quartz] of π or half wavelength.....	78
Figure 8. 2: The measured intensity and phase image at 0.1 μm proximity gap between the mask and observation plane. (a) Amplitude mask and (b) Phase shift mask. The intensities are normalized from 0 to 1, and phase values are from $-\pi$ (-3.14) radian to π (3.14) radian.	79
Figure 8. 3: The simulation structure. (a) Amplitude structure with 2 μm openings and 4 μm period (b) represents the PSM Structure of 2 μm openings and 8 μm period with phase changes similar to the measurement structure.	80
Figure 8. 4: The simulated light field propagation through (a) Amplitude structure and (b) PSM structure for a proximity gap of 50 μm . Intensities are normalized to the maximum intensity.	81
Figure 8. 5: The measured intensity and phase image of the light evolution for a proximity gap of 50 μm in amplitude structure.....	82
Figure 8. 6: The measured intensity and phase image of the light evolution for a proximity gap of 50 μm in a phase structure.	83

Figure 8. 7: The measured intensity, phase and line image of the phase shifting mask structure at 5 μm proximity gap.	84
Figure 8. 8: The measured intensity, phase and line image of the phase shifting mask structure at 22 μm proximity gap.	85
Figure 8. 9: The measured intensity, phase and line image of the phase shifting mask structure at 40 μm proximity gap.	86
Figure 8. 10: OPC structure designed in PSM for printing at 30 μm proximity gap. Left side image is the full image figure and right side image represents the zoom in version of the edge position to see the details.	88
Figure 8. 11: The measured intensity and phase images of the OPC phase shifting mask structure at different proximity gaps. (a) and (b) represents the images at 0.1 μm proximity gap. (c) and (d) represents images at 30 μm proximity gap.	88

LIST OF TABLES

Chapter 2

Table 2. 1: Comparison between different printing machines.....	12
---	----

Chapter 4

Table 4. 1: Parameters defined for 30 μ m proximity gap - experimental results.	43
--	----

Table 4. 2: Parameters defined for 30 μ m proximity gap - simulation results.	43
--	----

Table 4. 3: Parameters defined for 50 μ m proximity gap - experimental results.....	44
---	----

Table 4. 4: Parameters defined for 50 μ m proximity gap - simulation results.	44
--	----

Chapter 5

Table 5. 1: Fresnel number for 6 μ m structure	54
--	----

Table 5. 2: Fresnel number for 10 μ m structure.	56
---	----

Chapter 6

Table 6. 1: The radius of curvature of different line width structures at different exposure times.	68
--	----

CHAPTER I

Introduction

Photolithography is a vast and highly progressing field in the micro-fabrication industry. Fabrication can be done with the help of visible optical radiation, which ranges from 400 nm to 780 nm and can also be done with high energy radiations which are of shorter wavelength and in the ultraviolet (UV, $\lambda < 400$ nm), deep ultraviolet (DUV, $\lambda = 248$ nm, 193 nm) or extreme ultraviolet (EUV, $124 \text{ nm} < \lambda < 10$ nm). Because of this property, photolithography is often known as optical lithography, UV lithography, and EUV lithography.

1.1 History of photolithography

The lithographic technology started in 1798. Alois Senefelder was a German theater drama writer who was seeking less costly ways to reproduce his plays [1.1]. He started producing his own copper plate engravings, but reverse engravings were very difficult at that time. So he decided to use limestone instead of copper and he also developed a 'correction fluid' with a mixture of wax, soap, lamp black and rainwater to correct his frequent mistakes. He found out that the image with the correction fluid on limestone would repel water and the surface can hold the water. This made him to use this as the printing plate where the image areas will hold water and the rest will not. The writing ink on the wet stone was then pressed on to the printing plate so that the ink will stay on the image areas only and can be easily transferred to paper. The word "Lithography" was derived from Greek after this process: 'lithos' meaning stone and 'Graphene' meaning to write. The first lithography involving a chemical process started and Senefelder designed his own press with automatic engraving in 1817. Even today, lithography uses the same principle, where ink coated on desired plates are active only on the designed images or structures.

At the same time, Jean Senebier, a Swiss pastor found that some resins become insoluble in turpentine when they are exposed to sunlight. With his inspiration, Nicephore Niepe managed to copy an etched print on oiled paper in 1822[1.2]. He put the oiled paper on top of a glass plate which was coated with asphalt (bitumen) on certain areas and was dissolved in lavender oil. He exposed this to sunlight for some hours and noticed that the unshaded areas of bitumen became hard compared to the shaded areas. The shaded areas became more soluble and could be washed away easily with turpentine and lavender oil. The world's first photograph got introduced by this process.

The photo masking with chemical processing and using light led to “Photolithography”. Photolithography is the process of making lithographic plates by photographic techniques and it was introduced by Louis Poitevin, in August 1855 [1.3]. Poitevin patented photolithographic process and a Parisian writer printed 700 impressions with this technology. The idea of photolithography opened a new era in fabrication and semiconductor industry.

The first application of printed circuit board (PCB) was introduced by Paul Eisler in 1943, after 100 years of photolithography invention [1.4, 1.5]. Just before PCB invention, negative and positive resists were invented. In 1935 Louis Minsk of Eastman Kodak developed the basis of the first negative photo resist and in 1940 Otto Suess at Kalle Division of Hoechst AG developed the first positive photoresist [1.6]. With the above developments, lithography industry was making its entry to the micro fabrication world.

In late 1950's, Jack Kilby of Texas instruments and Robert Noyce of Fairchild semiconductor developed the first integrated circuit (IC) in their research labs [1.7]. Early 1960s was the time when a new chapter in semiconductor industry started: the first Integrated Circuits (IC) were patterned and commercially introduced with the help of photolithography [1.8]. Since then, the semiconductor industry is reaching its limits by creating new goals in patterning and printing [1.9]. In 1960's 5 μm geometries were not properly generated and shadow printing was the technology used at that time. In 1970, Bell Laboratories implemented an integrated mask making system for second generation mask aligners which reduces the feature size to 2 μm . But the damage to the wafer and mask by contact printing got increased and as a result, projection printing was introduced at this stage.

Demand for high throughput and high resolution paved the way for introducing steppers and scanners in the mid-1990s. Every year, the demand increased and critical dimension size decreased from 350 nm in 1990 to 100 nm in 2003. Surprisingly up to now and despite of all challenges the industry faced, semiconductor industry still follows ‘Moore’s law’ [1.10]. The feature size has decreased from 70 nm to 7 nm in the last 10 years. Nowadays, sub nanometer accuracy can be attained by using photolithography, e-beam lithography or x-ray lithography [1.11]. The new resolution limits and size reduction have forced the industry to reconsider Moore’s law to more Moore’s law [1.12].

1.2 Photolithographic process

The main steps involved in photolithographic printing are [1.13]

- Wafer cleaning: Contaminants on the wafer are removed by chemical cleaning. This technique is used to remove traces of organic, ionic and metallic impurities.

- Wafer priming: In order to assist and make the photoresist coat easily, some adhesion promoters are used. For silicon wafers, siloxane linkage (Si – O – Si) based products are used, for eg. HMDS, TCPS, BSA etc. For gallium arsenide, monazoline and xylene are used.
- Photoresist coating: Wafer is placed on the chuck of a spin coater at vacuum. Resist can be either positive or negative depending on the purpose. Resist is uniformly coated on the wafer by spin coating. For positive photoresist, the photoresist region exposed to light exposure is soluble in developer and for negative photoresist, the region exposed to light is insoluble in developer. Resist thickness can be set by resist viscosity and rotational speed of the spin coater.
- Soft baking: It is used to evaporate the coating solvent and also to densify the resist. The thickness of both positive and negative resist is usually decreased by 25% in prebaking.
- Mask alignment and Exposure: The photomask has the master patterns which are transferred to wafers. The photomask is aligned with the wafer surface so that the pattern can be transferred easily. Next step is the exposure, and it is most important step in the lithographic process. Different types of exposure systems exist. They are contact printing, proximity printing and projection printing.
 - Contact printing – The wafer is placed on the vacuum chuck and it is brought into physical contact with the photomask. Since both the wafer and photomask is in contact, high resolution is possible with this printing. The main disadvantage is that mask can be damaged easily, and debris between resist and mask can cause defects in the pattern.
 - Proximity printing – The wafer is kept at some distance with the mask (10 to 25 micron) and the distance is known as proximity gap. The proximity gap reduces the mask damage.
 - Projection printing – Mask designs are projected to wafer using imaging optics. Steppers and scanners are example of projection systems.

Exposure systems strategies are represented in Fig.1.1.

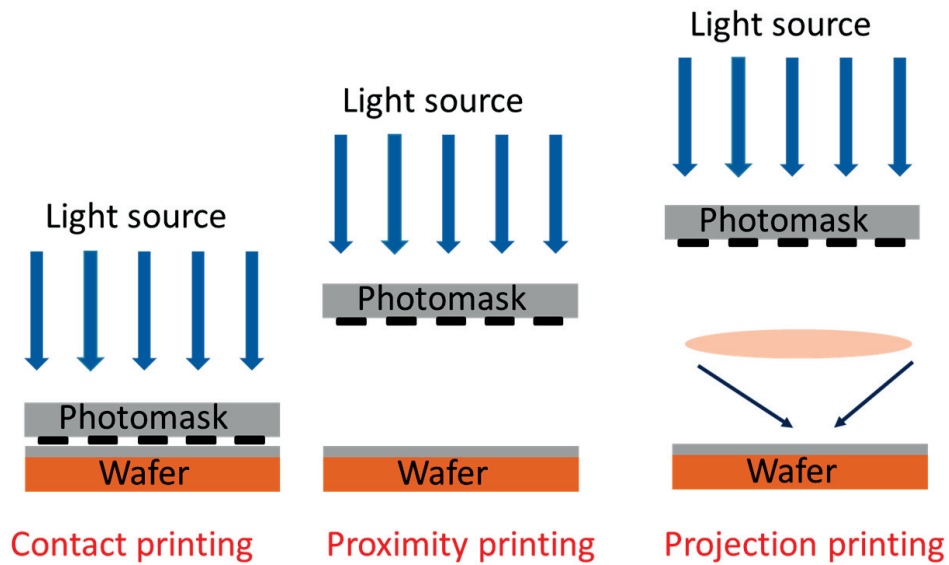


Figure 1. 1: Different types of exposure techniques.

- Post-baking: In order to reduce the standing wave formation in the resist and solvent bust effects, post- baking is performed. It also removes remaining traces of the resist or developer.
- Development: After exposure, photoresists are developed using developer solutions. The resist – developer reactions influence the final pattern to a large extent.

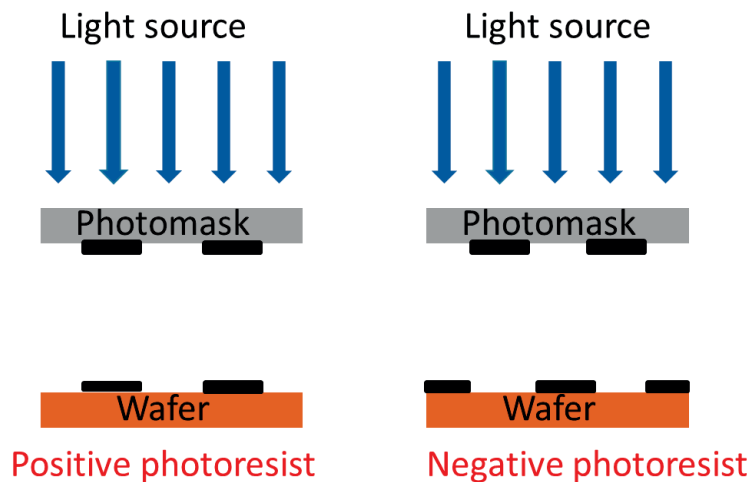


Figure 1. 2: Resist development and pattern transfer on the wafer.

- Hard baking: This step is to stabilize and harden the photoresist. This increases the adhesion of resist to the wafer.
- Photoresist removal and post process cleaning: The hardened resist after hard baking acts as an easy way to etch the oxide layer above the semiconductor in order to expose the

semiconductor. After the oxide etching, the remaining resist is removed with the help of strong acid mixtures. Post process cleaning and drying gives the final window to process.

The history of photolithography and its process steps, paved the way to develop my interest in this technology. This thesis will help to contribute more to the field of proximity lithography.

1.3 Thesis outline

This thesis is a study of proximity lithographic printing and its limits with different characterization techniques. The main motivation of this thesis is to understand the unknown properties of proximity printing with discussing several problems and solutions. The study characterizes the proximity printing technology and to use it in a better way for the future.

Chapter 2 discusses different exposure techniques in detail and the advantages of proximity printing over other techniques. The chapter also discusses how proximity printing can be improved using resolution enhancement techniques (RETs). RETs are mainly classified in to three, phase shifting mask (PSM), off-axis illumination (OAI) and optical proximity correction (OPC) and the chapter discusses these techniques in detail.

Chapter 3 is about design and verification techniques that are used to study proximity printing. The first technique is the simulation. Simulations are carried out with the help of a software called Layout Lab and it is a specialized software for proximity printing. The software gives the result of the final resist pattern. Main technique is the experimental analysis of the aerial images. The main aim is to experimentally analyze the propagation of light from the mask. The aerial images are observed with high resolution interference microscopy (HRIM). HRIM is a Mach- Zehnder interferometer which efficiently measures the intensity and phase of light through different samples. The last and final verification technique is the printing. The analyzed results are printed using MA8 Gen3 mask aligners from Süss MicroOptics.

Chapter 4 starts with the problems and solutions in proximity printing. It describes the analysis of simple 1dimensional structures in an amplitude mask and an example structure is an 'edge'. The chapter presents an idea to improve the edge slope and the line edge roughness with easy optical proximity corrections. This chapter describes how the simulation and experimental results work and how similar the results are. It also describes methods to define the process window for different proximity gaps at different exposure doses.

Chapters 5 and 6 pave the way to a next level hypothesis and solutions: 2 dimensional structures. Study of lines and its diffraction patterns at different proximity gaps are mentioned in chapter 5. The aim of chapter 6 is to find an easy solution for the most severe problem of lithography industry: 'corner rounding'. A new rule based optical proximity correction is designed for the corners and characterized with simulation, experimental and printing results. The newly designed

structure helps to print features of different sizes at single proximity gap with single exposure on a single wafer.

Chapter 7 discusses phase measurements and phase singularities. Printing industry is usually concerned with aerial images or the intensity results. This chapter explains about phase from amplitude mask. The intensity evolution from optical proximity correction structures has been widely studied but the role of phase to get the desired pattern has not yet been revealed. Phase from one dimensional and two dimensional correction features is studied in this chapter.

Chapter 8 is the most interesting chapter and it is about the study of phase shifting mask. The chapter explains the intensity and phase propagation from corner structures in a phase shifting mask. It also gives a chance to rethink about the concept that shorter proximity gaps give better results. The chapter summarizes the Talbot effect and fractional Talbot effect and gives a new definition to design the masks.

Chapter 9 summarizes all of the outputs and results.

The research has received funding from CTI project 12782.1 PFNM-NM.

References

- [1.1] "The history of lithography"; digital media from University of Houston;
http://sites.tech.uh.edu/digitalmedia/materials/3350/History_of_Litho.pdf.
- [1.2] M. Madou; "Fundamentals of Microfabrication"; *CRC Press, USA*; pp. 1-2(1997).
- [1.3] C. G. Willson ; R. R. Dammel and Arnost Reiser; "Photoresist materials: a historical perspective"; *Proc. SPIE Advances in Resist Technology and Processing XIV*, **Vol.3049**; pp. 28-41 (1997);
- [1.4] P. Eisler; "Manufacture of electric circuit components"; *US patent No. 2587568(A)*; (1944).
- [1.5] M. J. Madou; "Fundamentals of MICROFABRICATION and NANOTECHNOLOGY"; *CRC press, USA Vol. II Manufacturing Techniques for Microfabrication and Nanotechnology*; pp. 4-5 (2011).
- [1.6] R. D. Oliveira; "Photolithography and chemical etching";
https://indico.cern.ch/event/34040/contributions/1736942/attachments/667706/917760/TT2008-1_rui.pdf.
- [1.7] "The History of the Integrated Circuit"; Nobelprize.org. Nobel Media AB 2014; Web. 20 Feb2017.
http://www.nobelprize.org/educational/physics/integrated_circuit/history/.
- [1.8] J. Andrus; "Fabrication of semiconductor devices"; *US patent No. 3122817*; (1964).

- [1.9] J. H. Bruning; "Optical Lithography – Thirty years and three orders of magnitude"; *Proc. SPIE Optical Microlithography XX* **Vol. 6520**; pp. 652004 1-13 (2007).
- [1.10] G. E. Moore; "Cramming more components onto integrated circuits"; *Electronics* **Vol. 38, No. 8**; pp. 114-117 (1965).
- [1.11] M. Rothschild, T. M. Bloomstein, T. H. Fedynyshyn, R. R. Kunz, V. Liberman, M. Switkes, N. N. Efremow, S. T. Palmacci, J. H.C. Sedlacek, D. E. Hardy and A. Grenville; "Recent Trends in Optical Lithography"; *LINCOLN LABORATORY JOURNAL* **Vol.14, No.2**; pp. 221-236(2003).
- [1.12] M. M. Waldrop; "More than Moore"; *NATURE* **Vol. 530**; pp. 145-147(2016).
- [1.13] C. A. Mack; "Fundamental Principles of Optical Lithography "; *WILEY press*; pp. 2-6 (2007).

CHAPTER 2

Proximity printing and Resolution Enhancement Techniques (RETs)

Exposure systems and imaging theories are main two factors which define the lithography industry. Other factors are material science properties, micro/nano mechanics etc. Proximity printing is one of the oldest printing technique and this technique will be studied in the chapter. The main aim is to overcome the limits of proximity printing with resolution enhancement techniques. There are various techniques available to increase the resolution and they will be discussed here.

2.1 Exposure system technology

Exposure systems that existed earlier, were contact printing and proximity printing. Kulick and Soffa was one of the early suppliers of contact mask aligners on the market (1965) [2.1]. They were very successful in 1960's and withdrew the company in 1970. At that time Kasper Instruments was founded (1968) and took over the market. Their contact mask aligners were equipped with proximity technology also. In 1970 Canon also announced its first mask aligner and started dominating the market.

In contact and proximity systems, the wafer is held in contact or in close proximity to make the exposure [2.2]. Contact printing provides higher resolution compared to the proximity printing but the risk of mask damage is high. Even if large amount of care was given in cleanliness, some dirt will be there on the surface of the wafer and eventually on the mask. Because of these reasons, contact printing is not used in the mainstream semiconductor industry. In proximity printing, the wafer is held at several micron distance from the mask. The wafer position can be adjusted with respect to the mask with a wafer positioning system. In general, the distance is 20 μm . It is believed that larger proximity gap reduces the resolution. The resolution achieved by proximity lithography is calculated with the formula

$$R = 2b_{\min} = k_1 \sqrt{\lambda \left(g + \frac{z}{2} \right)} \quad (2.1)$$

Where R is the lateral resolution, b_{\min} is the structure width or critical dimension, λ is the wavelength, g is the proximity gap, z is thickness of the resist and k_1 is the factor which depends on illumination and resist parameters. In the proximity printing situation k_1 takes a value of 3/2. [2.3]. If we insert the values in the formula for a thin resist of thickness 1 μm , wavelength of 405 nm and the proximity gap 20 μm , the minimum feature size possible is 2.02 μm .

The proximity technology started losing its market because of failure in reducing the resolution beyond 2 μm . The market was good from 1959 to 1970. The half pitch of the feature in 1959 was 120 μm and in 1980, the feature size reduced to 1.5 μm . Using ultraviolet band (450 nm – 350nm), and deep UV (248 nm, 193 nm) the maximum resolution attained was 2 μm and 1.5 μm respectively.

In 1970s 1X projection printers replaced the proximity printing technology. The first scanning projection printer was invented by Perkin Elmer in 1973. The diffraction limited optics reached the quality to meet the requirements of the semiconductor industry in early 1970s. Projection technology uses an additional imaging lens between mask and wafer. The typical mask to wafer distance in projection printing was 80 cm or larger. This made the mask and wafer movement easy without any damages. The resolution and Depth of Focus (DOF) of a projection printer is described as follows

$$W = k_1 \frac{\lambda}{NA} \quad (2.2)$$

$$\text{DOF} \propto \frac{\lambda}{NA^2} \quad (2.3)$$

Where W is the printable minimum feature width, λ is the wavelength, k_1 is the process related factor and NA is the numerical aperture [2.3]. Increasing NA , decreases the minimum printable feature width W . But DOF will be less with high NA values. Small NA results in large DOF and large NA results in small DOF . So a comparable situation should be selected between NA and DOF . Consider a system using a wavelength of 248 nm, k_1 of 0.5, DOF of 0.6 μm and having a NA of 0.7, then printable minimum feature width W will be 150 nm.

There are two major projection lithography printers: one is the scanning printers and other is the step and repeat printers [2.4]. Scanners replaced proximity printing in 1970 and steppers took the market at 1980 from scanners. Printing 1 μm feature was difficult with 1X scanners (mask and image 1:1 ratio). The early step and repeat system was introduced in 1978 by GCA. Semiconductor market got revolutionized by steppers. Steppers dominated until the feature size reached 250 nm. In early 1990s, hybrid step and scan method was introduced and used for manufacturing below 250 nm. Till now it is continuing with reaching the resolution limit of 20 nm [2.5]. The main producers of projection printing machines are ASML, Nikon, Canon, and Ultratech. Different types of projection printing technologies are explained in Fig. 2.1.

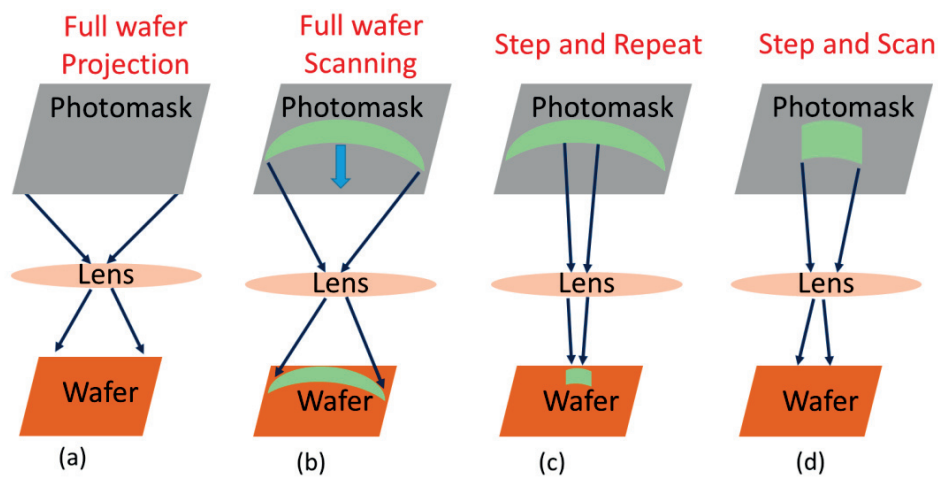


Figure 2. 1: Different types of projection printing technology.

Figure 2.1(a) represents a full wafer projection system without any demagnification. It is one of the earlier 1X projection systems. Next is the scanning projection printing system (Fig.2.1 (b)), the feature is projected on the wafer by scanning a ring shaped image field. Because of increase in wafer size, full wafer printing in 1X magnification was getting difficult. The process of demagnification of the image on the wafer started with step and repeat systems (Fig.2.1(c)). With the increase in chip size reduction, a new system was introduced. It is a hybrid of full wafer scanning systems and step and repeat systems. The hybrid system is represented in Fig.2. 1(d).

2.2 Comparison between proximity printing and projection printing

Most prominent effect with proximity printing is the diffraction effect due to propagation (since the wafer is kept at a distance from the mask). Diffraction effect causes resist exposure outside the projected pattern and the resulting feature will be different from the mask feature in proximity printing. In projection printing, the aerial image will be inside the resist threshold but the feature shape will vary.

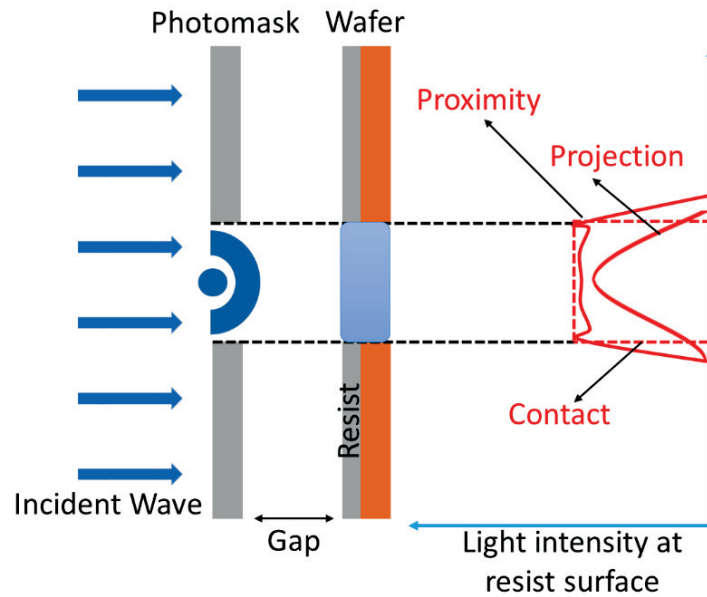


Figure 2. 2: Light intensity profile on the wafer for different printing technologies. Here the light propagates through a slit width, so the design in the resist profile should look like a slit but in reality due to diffraction the shape changes into resist profile as shown for technologies.

- Proximity image is the shadowing effect of the mask feature on the wafer, on the other hand projection image depends on the lens system used for the exposure.
- Proximity printing failed to go below $2\ \mu\text{m}$ with UV illumination source and $20\ \mu\text{m}$ proximity gap. Printing below that gap can damage the mask or the wafer. Projection printing made the 1X printing at lower resolution limit. The distance between mask and wafer were also in centimeters. Projection printing allows the placement of mask protecting pellicles at both sides which defocuses the foreign particle that may fall on the mask.
- For both these types of printing, resolution increases when the wavelength is reduced. But for projection printing, depth of focus (DOF) plays a vital role and it gives negative effect on resolution with reduction of wavelength. So a balance needs to be maintained between DOF and wavelength in projection printing. On the other hand, for proximity printing, wavelength reduction always gives a positive effect.
- Other important factor is the exposure field. In proximity printing, exposing a $100\ \text{mm}$ wafer at one shoot is not difficult. But in projection printing, it is decided by the imaging lens parameters [2.6, 2.7].

Type	Parameters	Proximity printing (Süss MA300 Gen2)	Projection Printing (Canon FPA-5500 (I-line))
Technical Parameters	System size	Small	Large
	Cost/Investment	Low (<1.0M\$)	High (3.1 – 4.0M\$)
	Field size	High (300mm)	Small(52x34mm)
Optical Parameters	Resolution	Low (2-4 μ m)	High(<1/1.5/>2 μ m)
	Propagation	Free space, Diffraction effects	Diffacted limited imaging(NA 0.10/0.18)

Table 2. 1: Comparison between different printing machines.

As seen from the table, the comparison is made with two different type of machines – Süss MA300 Gen2 (proximity printing) and Canon FPA -5500 I- line (projection printing). The technical parameters give a clear idea that proximity printing is better than projection printing comparing the system size, cost and field size. Cost and investment is low for proximity printing and also larger wafer can be printed at the same time. But the optical parameters like propagation and resolution are compared, then projection printing will give better results [2.8]. Free space propagation in proximity printing will create diffraction effect and reduces the resolution. Proximity printing has been used for different applications like microlens making, wave guide fabrication etc. [2.9 - 2.12]. **The main challenge in our project is to increase the resolution of the proximity printing by overcoming these limits. Study the proximity printing technology, its limitations and propose ideas and solutions to increase the process window.**

2.3 Resolution Enhancement Techniques (RETs)

Resolution Enhancement Techniques (RETs) are used to enhance the contrast and resolution of the image on the wafer by adjusting or manipulating the wave front that falls on the photomask. In general, a normal optical wave can be defined using an amplitude, phase and direction. So the parameters that can be modified for a wave are these three [2.13]. Three principle techniques used to increase resolution are Optical Proximity correction (amplitude variation), Phase Shifting mask (Phase variation) and Off- Axis Illumination (direction variation).

2.3.1 Off- Axis Illumination (OAI)

As the name suggest the aim of this technology is to tilt the light beam from its axis such that the light beam is off-axis. The normal incident beam is shifted to reduce the on-axis illumination component [2.14]. By changing the illumination angle, the diffraction pattern of the mask feature is also shifted. The shift is within the illumination lens. If the incident light is at a normal angle, then the zero-th diffracted order continues to be along the optical system axis, while the other orders are diffracted sideways. For small pitch of grating, only the zero-th diffraction order manages to make it through the projection lens, with the other orders being lost and no pattern will be created on the wafer. By making the illumination off-axis, all the diffraction orders are tilted, which makes it more likely that the higher diffraction orders can make it through the projection lens and help form the image of the mask onto the wafer. The angle shift is decided by the distance between zeroth order and first order and it depends on the feature size opening. Different shapes are introduced to modify the angle in the photomask illumination. Some examples of shapes are annular, quadruple, dipole [2.15]. In order to use it efficiently, the shape and size of the illumination shape should be optimized for the specific mask designs.

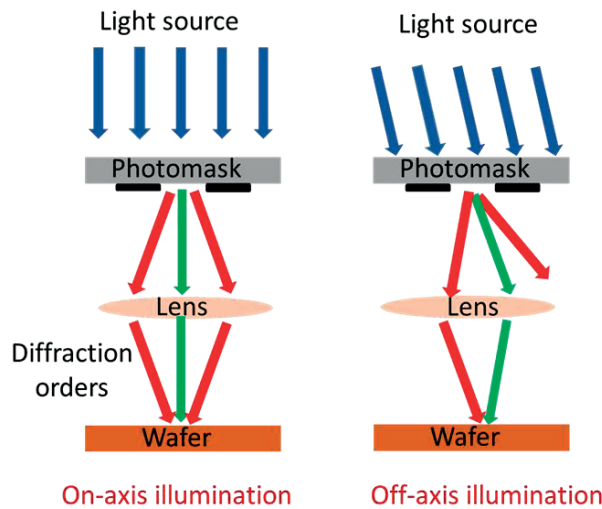


Figure 2. 3: On-axis and off-axis illumination techniques. Comparing the on-axis and off-axis diffraction orders. The off-axis illumination has shifted the zeroth order. Due to the shift in the illumination angle we can capture a larger angle between zero and first order. Consequently, the resolution increases.

2.3.2 Phase Shifting Mask (PSM)

PSM technology is one of the widely used techniques in lithography industry to increase the resolution. As the name suggests, the phase of the wave is varied here. The technology was invented by M. D. Levenson in 1982 [2.16]. Constructive interference of light fields from the mask features maximizes the amplitude and reduces the resolving power. The idea he used is to create a destructive interference, creating a phase difference of 180° between two adjacent features. To

create the phase difference a phase shifter or an extra chemical layer is added in the required feature areas. These masks are named as phase-shifting mask or ϕ -mask. This technique increased the resolutions of fine line lithography. Scientist Lord Rayleigh mentioned about the resolving power of light from the microscope images by creation of a black line in one of his manuscript - "On the Theory of Optical Image, with Spatial Reference to the Microscope" [2.17]. These days, instead of adding an additional phase layer, quartz mask are etched deeply to create the phase difference on the required areas. Phase masks have structures which are etched in such a way that, for particular wavelengths, the phase shift becomes π .

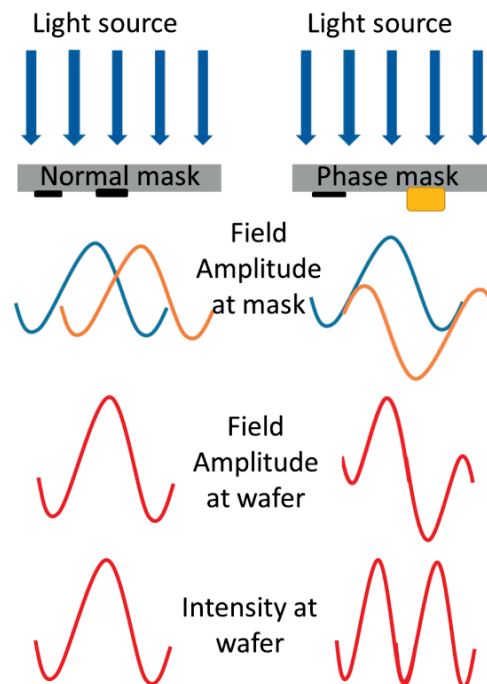


Figure 2. 4: Light intensity distribution through conventional mask and phase shifting mask. The mask in the right is the Phase shifting mask. The yellow colored region is where the depth is changed to half a wavelength. So when the light passes through the mask, field amplitude from both will have a phase difference of 180° and final intensity will be as shown above.

There are several types of phase shifting masks that exist [2.18]. The main two are Attenuated Phase Shift Mask (AttPSM) and Alternating Phase Shift Mask (AltPSM) [2.19]. In AttPSM, an extra layer is coated on the quartz mask (eg: MoSi) on the desired areas which allows small percent of light transmission through the area (normally 6% to 18%). Thickness of the extra layer is selected according to the phase. The light passing through the feature is 180° out of phase with the neighboring quartz area but with transmission of light. In AltPSM, chrome and 180° etched quartz are placed alternatively.

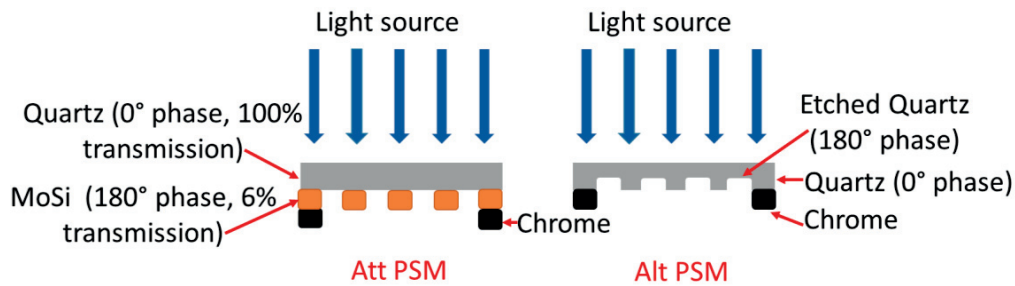


Figure 2. 5: Different types of PSM.

PSM mask is used for different applications in semiconductor industry and each time it sets high resolution targets [2.20, 2.21, and 2.22]. The main disadvantage with this technology is the mask fabrication cost. The phase mask costs more than twice that of the normal amplitude mask which makes this technique less accessible to the small scale industries.

2.3.3 Optical Proximity Correction (OPC)

As discussed earlier, because of the diffraction of the propagating wave and interference, features on the wafer can change its shape and won't be the same as the feature on the mask in appearance. The change in pattern line width or length to the desired pattern and its effects are called Optical Proximity Effects (OPE). These effects can be originated from mask designs, printing gap, or resist used. Optical Proximity Correction (OPC) is a simple and cost efficient technique to reduce OPEs. Here the modification is done in the amplitude of the wave. OPC is the method where adding or subtracting some features like lines or spaces on the mask makes the feature on the wafer as close to the desired design [2.23]. There are two methods to do the correction. One is the Rule based OPC and other is the Model based OPC.

- Rule Based OPC – A set of rules are introduced with lot of analysis to solve the common problems in printing. The first automated rules were introduced by O. W. Otto [2.24]. Mask patterns are modified by pre written rules by adding sub resolution features or moving the edge positions [2.25, 2.26]. It is a more practical approach for full chip correction since the rules are clearly defined.
- Model Based OPC – This is the most common technique used in OPC. This method is done with iteratively simulating the structure until the precision or the perfect match with the desired structure is formed [2.27 - 2.30]. It is a time consuming process since each structure needs to be taken care to get the uniform precision.

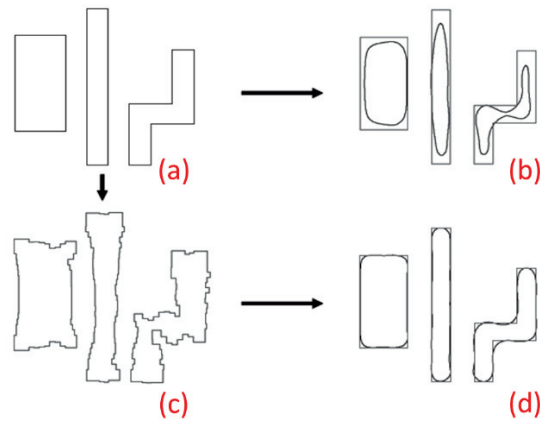


Figure 2. 6: The features on the mask after model based optical proximity correction [2.5]. (a): The mask structure that we need to print; (b): Feature printed on wafer with mask structure in (a); (c): The corrected Structure of (a) with model based Optical Proximity Correction technique; (d): The feature on wafer with corrected structure.

From Fig. 2.6, it is visible that corrected structures give better results than the exact structures. OPC is an easy and cost efficient method compared to the other two RETs. The aim of the thesis is to create easy and cost efficient solutions for mask aligner industry to increase their resolution limit. The method we chose is by creating rules for one dimensional structure and to higher dimensional structure by optical proximity correction method. There exist many rule based OPC methods for projection printing but not for proximity printing. This is the main challenge of project. Study each structure carefully and create and establish the rules on wafers. The next chapter explains the methods used to create and analyze the structures.

Conclusion

Several exposure techniques exist in lithography industry and they all have advantages and disadvantages. The main two techniques like proximity printing and projection printing are studied with example machines and comparisons are figured out. The chapter also discussed the various Resolution Enhancement Techniques that exist in the industry and its detailed explanations. The main aim of the chapter is to understand the limitations of proximity printing (mask aligners) and find a way to solve the limitations with a cost effective method. The discussions ended up with selecting OPC as the cost efficient method and to apply the technique to increase the resolution in mask aligners. The methods used to develop and study the OPC techniques will be discussed in the following chapter.

References

- [2.1] A. Kato; "Chronology of Lithography Milestones"; Version 0.9 (2007).
http://www.lithoguru.com/scientist/litho_history/Kato_Litho_History.pdf
- [2.2] J. R. Sheats, B. W. Smith; "Microlithography: Science and Technology"; *Marcel Dekker Inc., New York*; pp. 2-3 (1998).
- [2.3] A. K. Wong; "Resolution Enhancement Technologies in optical lithography"; *SPIE Press, USA*, pp. 13-18 (2001).
- [2.4] M. V. Brink, H. Jasper, S. Slonaker, P. Wijnhoven and F. Klaassen; "STEP-AND-SCAN AND STEP-AND-REPEAT, A TECHNOLOGY COMPARISON"; *SPIE International Symposium on Microlithography*; (1996).
- [2.5] C. A. Mack; "Fundamental Principles of Optical Lithography "; *WILEY press*; pp. 19-22 (2007).
- [2.6] B. J. Lin; "Optical Lithography Here Is Why"; *SPIE press USA*; pp. 9-10(2009).
- [2.7] B. J. Lin; "A Comparison of Projection and Proximity Printing – From UV to X-ray"; *Elsevier Science Vol. 11*; pp. 137-145(1990).
- [2.8] J. C. Tsai, M. Y. Hsieh and H. Yang; "Diffraction effects in Proximity Printing of Circular Aperture Array"; *Key Engineering Materials Vols. 364-366*; pp. 955-960 (2008).
- [2.9] L. Stuerzebecher, F. Fuchs, T. Harzendorf and U. D. Zeitner; "Pulse compression grating fabrication by diffractive proximity photolithography"; *OPTICS LETTERS Vol. 39, No. 4*; pp. 1042-1045(2014).
- [2.10] T.-H. Lin, H. Yang, R. F. Shyu and C.-K. Chao; "New horizontal frustum optical waveguide fabrication using UV proximity printing"; *Microsyst Technol Vol.14*, pp. 1035-1040(2008).
- [2.11] H. Yang, C.-K. Chao, T.-H. Lin and C.-P. Lin; "Fabrication of microlens array with graduated sags using UV proximity printing method"; *Microsyst Technol Vol.12*, pp. 82-90(2005).
- [2.12] T.-H. Lin, H. Yang, C.-K. Chao, S.-Y. Hung and J.-S. Hsu; "New high fill-factor dual-curvature microlens array fabrication using UV proximity printing"; *Microsyst Technol Vol.17*, pp. 601-607(2011).
- [2.13] F. M. Schellenberg; "A History of Resolution Enhancement Technology"; *OPTICAL REVIEW Vol. 12, No. 2*; pp. 83-89 (2005).
- [2.14] C.A Mack; "Off-Axis Illumination"; (2003)
[http://lithoguru.com/scientist/litho_tutor/TUTOR42%20\(Aug%2003\).pdf](http://lithoguru.com/scientist/litho_tutor/TUTOR42%20(Aug%2003).pdf)
- [2.15] M. L. Rieger; "Communication theory in optical lithography"; *Journal of Micro/Nanolithography, MEMS, and MOEMS, Vol.11, No. 1*, pp. 013003 1-10 (2012).

- [2.16] M. C. Levenson; "Improving Resolution in Photolithography with a Phase – Shifting Mask"; *IEEE Transactions and electron devices* **Vol. ED-29, No. 12**; pp. 1828-1836 (1982).
- [2.17] L. Rayleigh; "On the Theory of Optical Images, with Special Reference to the Microscope"; *PHILOSOPHICAL MAGAZINE AND JOURNAL OF SCIENCE* **Vol.42**; pp. 167 (1896).
- [2.18] M. C. Levenson; "Phase-Shifting Mask Strategies: line-Space Patterns"; *Microlithography world*; pp. 6-10 (1992).
- [2.19] "The Phase Shift Photomask Family"; from TOPPAN photomasks, INC.
<https://www.photomask.com/products/phase-shift-masks>.
- [2.20] G. A. Cirino, R. D. Mansano, P. Verdonck, L. Cescato and L. G. Neto; "Diffractive phase-shift lithography photomask operating in proximity printing mode"; *OPTICS EXPRESS* **Vol.18, n. 16**; pp.16387-16405 (2010).
- [2.21] S. Buhling, F. Wyrowski, E.-B. Kley, A J M Nellissen, L. Wang and M. Dirkzwager; "Resolution enhanced proximity printing by phase and amplitude modulating masks"; *J. Micromech. Microeng.* **Vol. 11**; pp. 603–611 (2001).
- [2.22] M. Fritze, B. M. Tyrrell, D. K. Astolfi, R. D. Lambert, D.-R. W. Yost, A. R. Forte, S. G. Cann and B. D. Wheeler; "Subwavelength Optical Lithography with Phase-Shift Photomasks"; *Lincon Laboratory Journal* **Vol.14**; pp. 237 – 250 (2003).
- [2.23] L. Capodieci; "From Optical Proximity Correction to Lithography-Driven Physical Design (1996-2006): 10 years of Resolution Enhancement Technology and the roadmap enablers for the next decade"; *Proc. SPIE Optical Microlithography XIX* **Vol. 6154**; pp. 615401 1 -12 (2006).
- [2.24] O. W. Otto, J. G. Garofalo, K. K. Low, C.-M. Yuan, R. C. Henderson, C. Pierrat, R. L. Kostelak, S. Vaidya and P. K. Vasudev; "Automated optical proximity correction: a rules-based approach"; *Proc. SPIE Optical/Laser Microlithography VIII* **Vol. 2197**; pp. 278–293 (1994).
- [2.25] Y.-H. Oh, J.-C. Lee and S. Lim; "Resolution Enhancement through a Rule-free Optical Proximity Correction in Optical Lithography"; *Journal of the Korean Physical Society* **Vol. 33**; pp. S63-S66 (1998).
- [2.26] R. Shi, Y. Cai, X. Hong, W. Wu and C. Yang; "The selection and creation of the rules in rules-based optical proximity correction"; *4th International conference ASIC*; (2001).
- [2.27] S. Shioiri and H. Tariabe; "Fast Optical Proximity Correction: Analytical Method"; *Proc. SPIE Optical/Laser Microlithography VIII* **Vol. 2440**; pp. 261–269 (1995).

- [2.28] A. B. Kahng, S. Muddu and C.-H. Park; "Auxiliary pattern-based optical proximity correction for better printability, timing, and leakage control"; *Journal of Micro/Nanolithography, MEMS, and MOEMS* **Vol. 7, No. 1**; pp. 013002 1-13 (2008).
- [2.29] P. Yu and D. Z. Pan; "Novel Intensity Based Optical Proximity Correction Algorithm with Speedup in Lithography Simulation"; *IEEE/ACM International Conference on Computer-Aided Design*; pp. 854-859 (2007).
- [2.30] L.-D. Huang and M. D. F. Wong; "Optical Proximity Correction (OPC)-Friendly Maze Routing"; *IEEE 41st Design Automation Conference*; pp. 186-191 (2004).

CHAPTER 3

Design and Verification techniques

This chapter describes the design and verification techniques that are used to obtain and characterize the results of this research on proximity printing. To start any study, simulation is the best technique. Simulation helps us to picturize the output which leads to a fast optimization of the results. The simulation software that is used for the study is GenISys Layout LAB-software which is designed for lithography simulations [3.1]. The software and its working is explained in the following sections. Once the results are optimized with simulation, experimental analysis is the next step. A specialty here is that, the amplitude and phase propagation are analyzed from the samples at different proximity positions with a High Resolution Interference Microscopy (HRIM) [3.2]. HRIM is an optical interferometer which can record 3D interferograms and both amplitude and phase can be tabulated with a mathematical algorithm. The working principle and recording of interferograms are explained in detail in the second part of this chapter. Both simulation and characterization techniques use a specialized optical system setting for modeling or mimicking the uniform illumination. The uniform illumination system applied here is known as MO exposure optics and available from Süss MicroOptics [3.3]. MO exposure optics is a specialized homogenization optics which uses micro-lens arrays, illumination filter plate (IFP) and a Fourier lens to obtain a uniform intensity illumination keeping a well-defined illumination angle. The final characterization technique is the Süss MicroTech MA/BA8 GEN3 mask aligner, to print at proximity distance. In this chapter, we also compare the results obtained with simulation and experimental analysis to prove the credibility and similarity of the results.

3.1 Simulation: GenISys Layout LAB

GenISys Layout Lab is a specialized simulation software for lithographic simulations. It includes the possibility of simulating proximity printing, projection printing, laser and e-beam lithography. Integrated circuit (IC) development and process optimization is a time consuming process if we do it experimentally; but the simulation techniques make it easier [3.4] especially if many parameters are involved. Layout LAB is a single platform for all the lithographic simulations and helps to visualize the final resist patterns on the wafers. Software accurately calculates aerial images and intensity patterns which help to optimize the mask layout, resist parameters and

verify the process flow. This reduces the wastage of wafers and a fast optimization of process window can be done. Figure 3.1 shows the layout of the simulation with its main features.

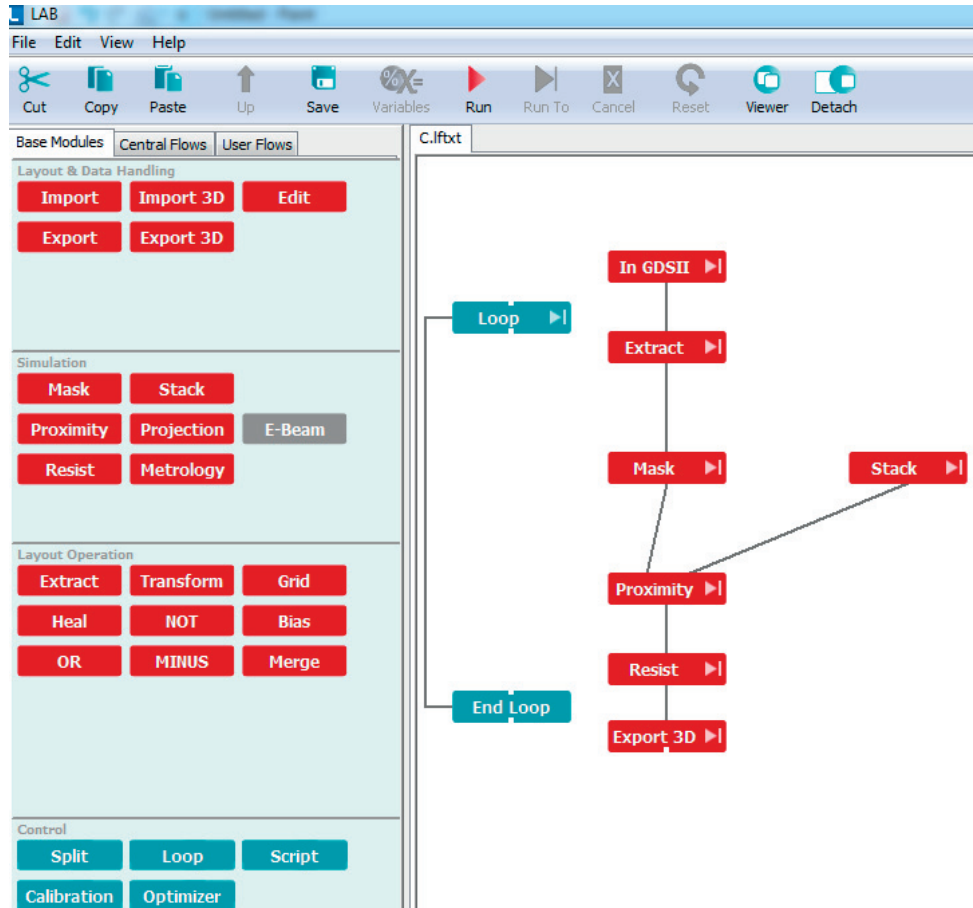


Figure 3. 1: Simulation module of Layout LAB.

Different modules in Fig.3.1 are explained here. In general mask designs are stored in formats like GDSII, OASIS, CIF, and DXF and are loaded to layout LAB by the 'Import' function. 'Mask' definition is used to define the mask properties. Mask can be a normal amplitude mask, grey tone mask or a phase shifting mask. The mask properties (bright field or dark field) and phase levels of each layer and cell are also mentioned. Next is the stack module which is used to define the wafer properties. Material properties, thickness of the substrate and resist coating are defined here. Exposure is one of the most important part of the simulation. We are using proximity exposure for our calculation since we use mask aligners [3.5]. The illumination parameters are defined in the module. Source and wavelength of the spectrum, exposure dose (mJ/cm^2), proximity gap, illumination angle and type of illumination can be defined here. Illumination can be parallel or user defined. It is indeed an advantage that a special illumination technique called

$$G = \frac{e^{ikR}}{R} + \frac{e^{ikR'}}{R'} \quad (3.2)$$

Inserting these two greens functions in Kirchhoff integral will yield first and second Rayleigh – Sommerfeld diffraction integrals (RS1 and RS2).

Diffraction field $U_1(\vec{r})$ and $U_2(\vec{r})$ with respect to above functions may be expressed as,

$$U_1(\vec{r}) = \frac{1}{2\pi} \iint U(\vec{r}') \frac{\partial}{\partial \vec{s}} \frac{e^{ik|\vec{r}-\vec{r}'|}}{|\vec{r}-\vec{r}'|} d\sigma \quad (3.3)$$

$$U_2(\vec{r}) = -\frac{1}{2\pi} \iint \frac{e^{ik|\vec{r}-\vec{r}'|}}{|\vec{r}-\vec{r}'|} \frac{\partial}{\partial \vec{s}} U(\vec{r}') d\sigma \quad (3.4)$$

It is assumed that Rayleigh – Sommerfeld integral is valid throughout the space. In general, there is no maximum size for the aperture size and observation field for the Rayleigh – Sommerfeld theory. This makes the proximity printing calculation easy. One of the other methods used for calculating field is the transfer matrix method [3.8]. This method is used to analyze the propagation of electromagnetic waves through a medium. It is based on Maxwell equations and matrix operations defined for transmission and reflection. It becomes particularly useful if the refractive index change is along the propagation direction and the gradients (or surface normal of multilayers) are also parallel to the propagation direction.

After the aerial image calculation, next important factor is the resist calculation. In general, a method called Mack4 is used for positive resist calculation and inverse Mack is used for negative resist model calculations. Mack4 is the resist development model suggested by Chris Mack which considers four parameters and is based on simple kinetic considerations [3.9]. Calibration of the data is done in user defined resist positions and resist heights. To make the calibration simple and to get the target values, one can use specialized functions like ‘Loop’, ‘Optimizer’ and ‘Split’. 2D and 3D visualization of the resist profile and aerial image are possible with the software. It also gives the advantage of viewing in continuous color mode or in the discrete line mode with user defined cut lines and the results can be exported as ASCII files or .PNG files.

3.2 MO exposure optics

As it is known, most of the printing machines today employ some special optical systems to make uniform illumination on the wafer. Köhler illumination is one of the optical techniques for making uniform illumination [3.10]. August Köhler invented a technique for microscopy which

allowed for adjusting the numerical aperture and size of the illumination area independently of each other. Köhler illumination works with two lenses and two diaphragms (collector lens, condenser lens, field diaphragm and aperture diaphragm). The first lens called collector lens images the light source to a plane where the aperture diaphragm is placed. This aperture diaphragm is at the same position of the front focal plane of the condenser lens. With this arrangement all the rays from aperture diaphragm are imaged to infinity, refer to Fig 3.3 red colored rays. The field diaphragm is placed just after the collector lens. The condenser lens images it to the object plane and a proper adjustment of the distance between condenser lens and object plane is needed.

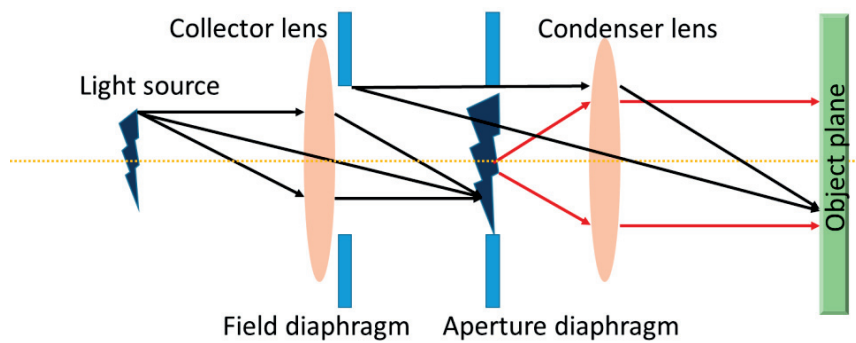


Figure 3. 3: Köhler illumination technique.

Köhler illumination provides a uniform illumination in the object plane independent of source size, shape and angular spectrum. It decouples the information from source spectrum and creates each point as source of homogenous illumination.

Süss MicroTech have developed their own uniform illumination optics with the concept of Köhler illumination using microlens arrays. The special illumination technique is named as MO exposure optics [3.11, 3.12] and is represented in Fig. 3.4.

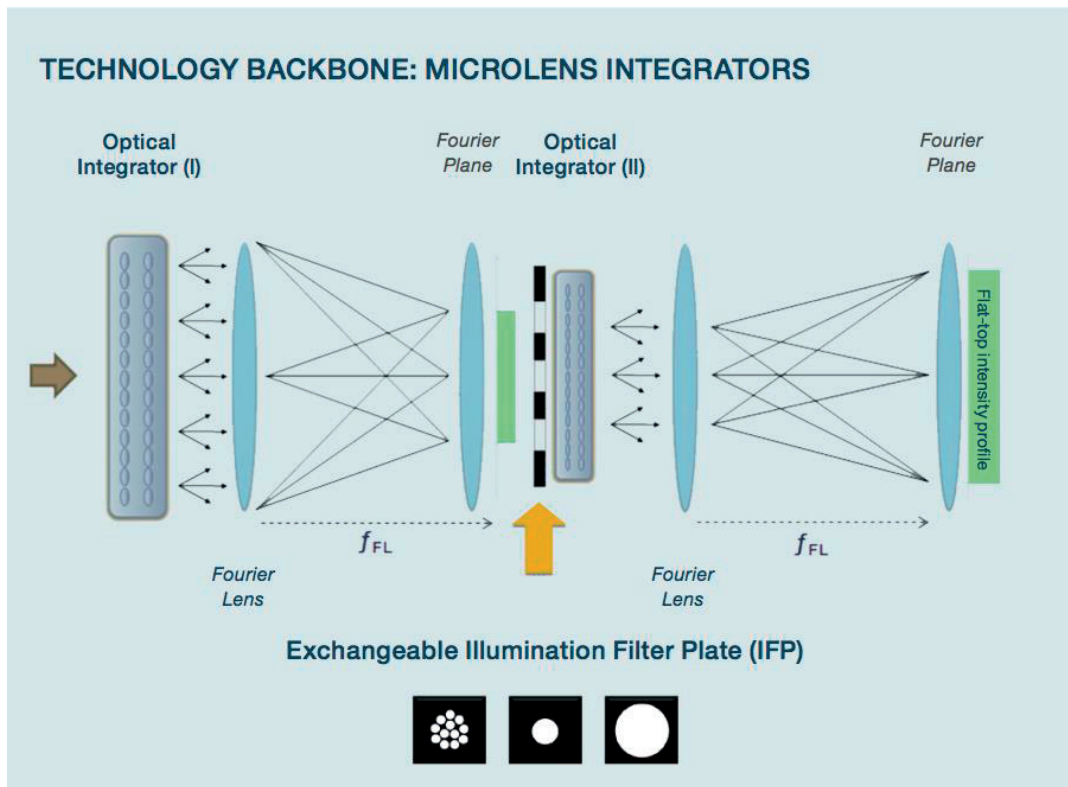


Figure 3. 4: MO exposure optics [3.3].

A microlens array divides the single lens illumination channel to multiple Köhler illumination channels and is then summed up. The technique is known as optical integrators or Köhler integrators [3.13, 3.14]. The first lens array will split the incoming light from a mercury lamp in form of an ellipsoidal reflector to beamlets followed by a condenser lens (Fourier lens), an assembly which is presented in Fig. 3. 5. The collimated beam will be collected by a collector lens which makes the beam telecentric (ray from all points are perpendicular to the direction of arrival and therefore generates a homogenous illumination). There exist a pair of Illumination Filter Plates (IFPs) at the image plane of first set of lenses. IFPs are just metals having different shapes engraved in to it, to get a homogenous illumination. They are used to change the angular setting of the beam. The IFPs that are commonly used are small ring, large ring, maltese shape and quadrupole shape etc. Each IFP helps to provide a different angular light spectrum by changing the light propagation behind the mask pattern and also helps to select the incidence angle on the mask plane. Second set of optical integrators are placed just after the IFPs. More number of integrators means a greater light mixing which gives more uniformity. The principle of beam operations is same as the first set of lenses and the final beam will be redirected to the mask plane. This technique was mainly invented as an advanced mask aligner lithography technique [3.15].

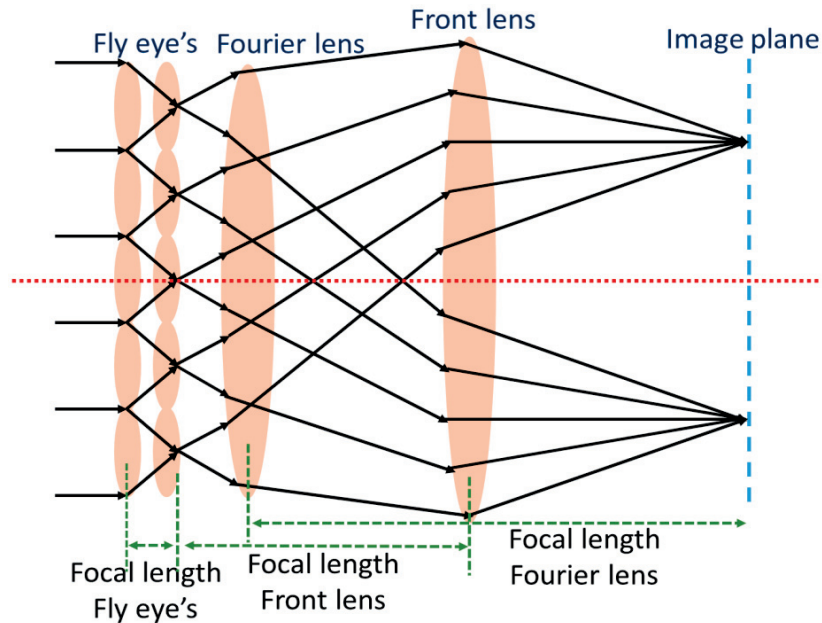


Figure 3. 5: Beam evolution from Köhler integrators.

3.3 Measurement: High Resolution Interference Microscopy (HRIM)

High Resolution Interference Microscopy (HRIM) is an interference microscope technique. As the name suggests, it works with the principle of interferometry and calculates the light propagation factors like amplitude and phase from different samples and records 3D interferograms. Interferometers are widely used for surface profiling, wave analysis in different fields like astronomy, defense and aerospace and vision systems etc. [3.16]. Recently, gravitational waves have been observed with an interferometric technique called LIGO (The Laser Interferometer Gravitational-Wave Observatory) [3.17]. The observatory uses Michelson interferometer concept to observe gravitational waves. In contrast to the LIGO, here a two arm interferometer is used that allows to put optical elements under investigation in one arm. HRIM is a proven interferometric measurement system for observing fundamental optical principles like nano jet and spot of arago with micro or macro optical samples [3.18, 3.19, and 3.20]. The concept of HRIM is explained below using an example from our lithographic studies in the following sections. The instrument setup is represented in Fig. 3.6.

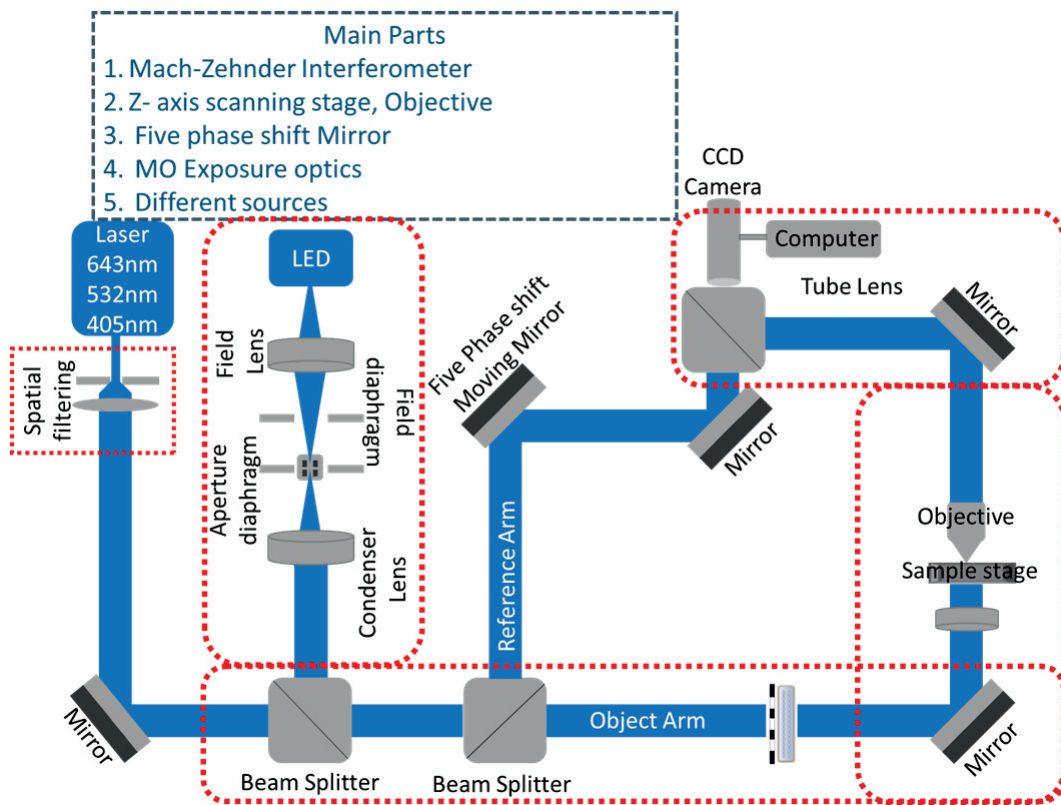


Figure 3. 6: High Resolution Interference Microscopy (HRIM).

3.3.1 Mach- Zehnder Interferometer

The instrument works as a Mach- Zehnder interferometer. In normal mode, Mach - Zehnder interferometer has two beam splitters [3.21].

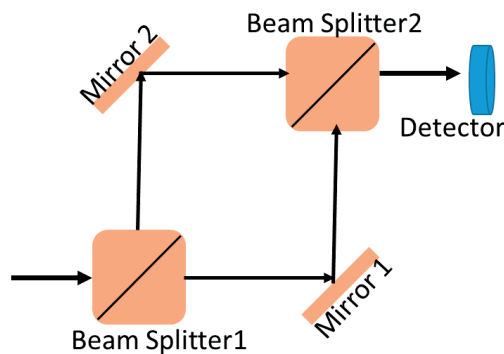


Figure 3. 7: Mach - Zehnder interferometer.

As shown in Fig. 3.7, a light beam will be split into two by a first beam splitter and a second beam splitter recombines both beams. Depending on the path length, both constructive and destructive interference can take place. Usually one path is called measurement arm and the other, reference arm. In a Mach Zehnder interferometer, the light passes through the measurement arm

only once in contrary to the Michelson interferometer. This technique is widely used in optical setups for measuring phase and amplitude information. Our high-resolution interference microscope HRIM works in transmission mode and all the light propagations are in free space. The first beam splitter that splits the beam to object and reference arm is a polarizing beam splitter. The object arm is the path where the sample is placed and reference arm is used to create phase difference. Both the beams are combined at the second beam splitter and interferograms are recorded by a charge coupled device (CCD) camera - Scion Corporation, CFW1312M camera having SONY ICX205AK image sensor of 1360 x 1024 pixels.

3.3.2 Sample stage and microscope

As mentioned earlier, the object arm contains a sample stage. The sample stage is connected to a piezo actuator to achieve a scan range in propagation direction of 500 μm with a nominal accuracy of 1 nm (Mad City Labs Inc., Nano-Z500). The CCD camera usually records 2D interferograms but with the piezo actuated sample stage, 3D measurement of data is possible by scanning the focal plane. In order to get the micro feature sample size and accuracy, a microscope is built in the object arm. Microscope objectives are placed with the corresponding tube lens and magnification of the objective decides the field of view of the camera. High numerical aperture objectives are used to get high resolution measurements. For example, 100X/NA 0.9 dry objective (Leica Microsystems, HC PL FLUOTAR) gives a field view of 64 x 48 μm^2 . With the number of pixels of the camera (1360 x 1024 pixels), the sampling interval becomes roughly 50 nm in object space. This value is smaller than the optical resolution of the microscope objective. All the recorded interferograms are tabulated with numerical algorithms in Matlab to get the amplitude and phase information.

3.3.3 Five phase shift mirror

In the reference arm of the HRIM, a piezo actuated (Mad City Labs Inc., Nano-P15) optical mirror is placed to change the optical path length. This is necessary to reconstruct the phase information of the recorded data for each plane. A common algorithm known as Schwider-Hariharan algorithm (five - phase shift algorithm) is used to retrieve phase information [3.22]. The mirror introduces a phase shift of 90° ($\lambda/4$) for five times in order to get an unambiguous measurement of the phase. For each phase and intensity, I_m ($m=1.5$) is recorded and a phase value can be calculated using the algorithm. One finds

$$\varnothing = \tan^{-1} \left(\frac{2(I_2 - I_4)}{2I_3 - I_5 - I_1} \right) \quad (3.5)$$

Where, \varnothing is the phase and I_1, I_2, I_3, I_4, I_5 are the five interferograms at different phase shifts.

3.3.4 MO exposure optics

HRIM usually works with a monomode laser in plane wave illumination. But for some measurements, it is necessary to change the coherence of the light or control the illumination angle. A specialized micro optics illumination setting, the MO optics from SüSS MicroOptics has been installed in the object arm of the interferometer (Fig. 3.8) for selected experiments to simulate real world conditions. The fly eye condensers, an illumination filter plate (IFP) and the final lens are placed to get the same optical characteristics as that of a mask aligner.

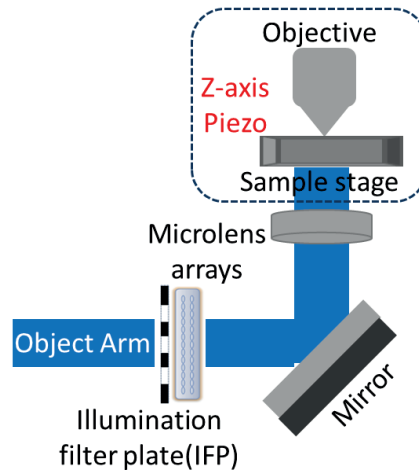


Figure 3. 8: MO exposure optics in HRIM.

3.3.5 Illumination sources and operation

There are two different types of sources for illumination. One is the coherent illumination source, usually lasers, and the other is a non-coherent illumination source, an LED. Single mode lasers of different wavelengths are used in HRIM (CrystaLaser, 642nm: DL640-050-3, 532nm: IR-GCL- 025-S and TOPTICA TopMode CHARM 405 nm, 50 mW). LEDs of 405 nm wavelength, both as single chip and with 4 chips are used as non-coherent illumination source. A source of 405 nm wavelength is used because this is one of the peak wavelengths in a mercury high pressure lamp. The experiment which intends to measure phase is carried out solely with lasers as the light source. Experiments which need only aerial images can be done with LED or laser. For amplitude/intensity results only the object arm of the HRIM is used.

To create a uniform illumination, laser beams are focused through pinholes to do spatial filtering which are placed at the front focal length of a second lens that expands and collimates the beam. It will then pass through a polarizing beam splitter which makes the beam to travel in two paths: object arm and reference arm. Object arm is having the sample stage and sample is enlarged by the microscope objectives. The light from the sample will pass through the tube lens and then to the recombining beam splitter. The beam splitter will combine both the beams and

interferograms are recorded. The intensity and phase from the interferograms are tabulated using Matlab scripts.

The light from the LED source will first pass through a Köhler illumination set up. The setup has two lenses and two diaphragms to get a uniform illumination. The uniform beam then passes through a non-polarizing beam splitter to the object arm. To get the full optical power of the beam, the beam splitter is sometimes replaced by a mirror. In general, plane wave illumination is used for the experiments but sometimes special illumination regimes are required to create the same conditions of a mask aligner. We add micro lens arrays, front lenses and IFPs to create MO exposure illumination. The light will propagate through the sample and get recorded by the CCD camera.

3.4 Comparison of simulation and measurement

The simulation and measurement are the two main techniques used to find the limitations of proximity printing. In order to do a performance evaluation and comparison of the techniques, an example of light evolution in both techniques is presented. The main research subjects are presented in chapters 4 to 8. Here the light propagation through a sample having line is shown for illustration.

The simulations are done with parallel illumination (no MO exposure optics) using 405 nm as the wavelength. The measurements are done with LED (RSW-P05-400-0) with a wavelength of 405 nm to simulate the same illumination regime. The beam will pass through a Köhler illumination setup. The objective used for the measurement is high resolution 20X/ NA 0.75 dry objective (NIKON CFI Apochromat VC) corrected for 405nm. The measurement starts with the smallest feature 2 μm . The light evolution from structure till 50 μm behind the structure is theoretically studied and experimentally measured with the help of LAB software and z- axis scanning stage in HRIM respectively.

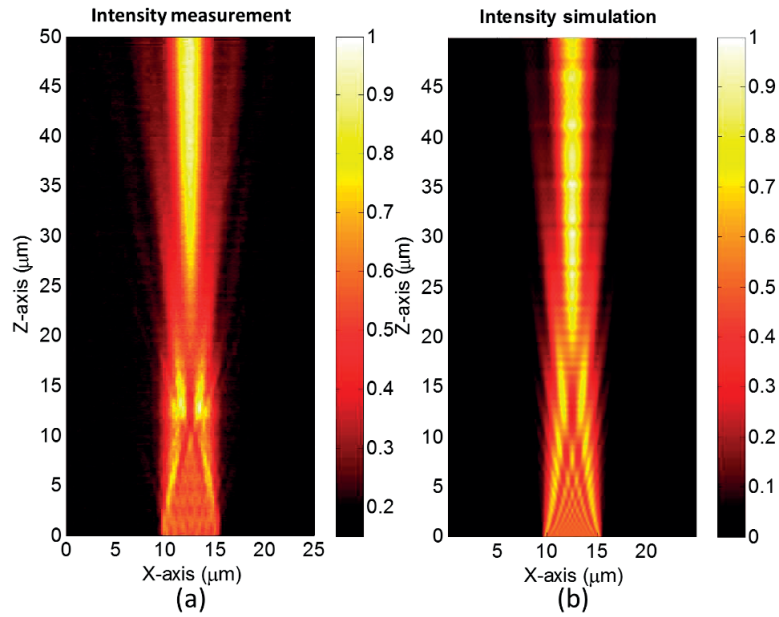


Figure 3. 9: Propagation measurement (x - z) of a $6\ \mu\text{m}$ line width structure till $50\ \mu\text{m}$ proximity gap. (a) Represents the experimental result and (b) the simulation result. Intensities are normalized from 0 to 1.

The experimental system performance is reliable to the theoretical studies with simulation and the results look very similar in Fig. 3.9. To prove it will also work for x - y measurements, another example which is observed with lines of $10\ \mu\text{m}$ at different proximity gaps is provided in Fig. 3.10. This is just to quantify that the HRIM can perfectly set the proximity gaps with $1\ \text{nm}$ step size.

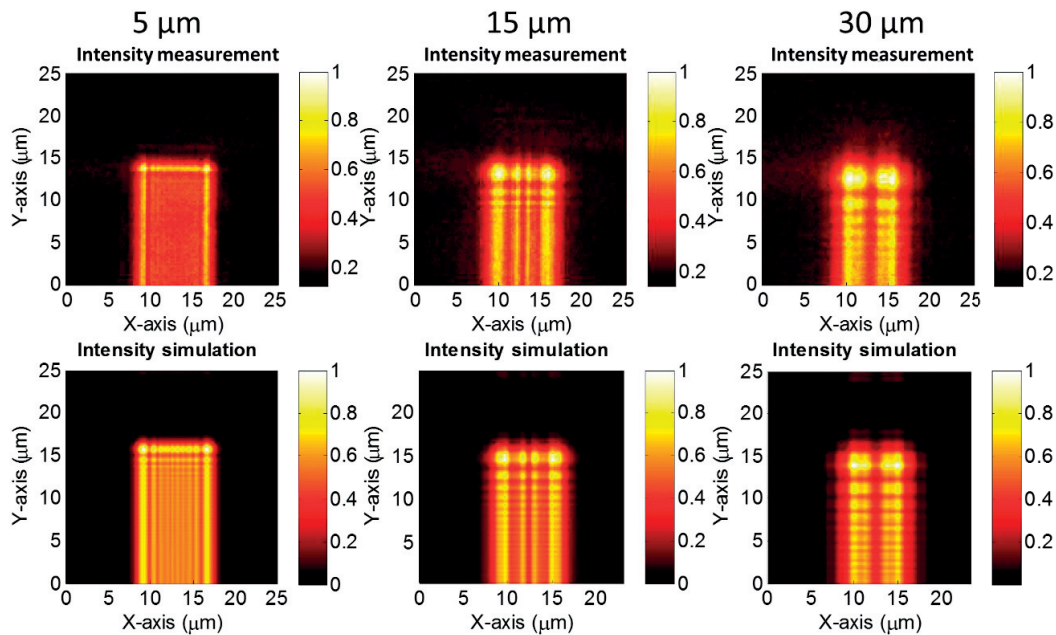


Figure 3. 10: The (x - y) intensity images of a $10\ \mu\text{m}$ line with both simulation and experimental result at different proximity gaps respectively. Intensities are normalized from 0 to 1.

Intensity images at different proximity gaps of 10 μm width are observed in Fig. 3.10. The simulation and experimental images can be accurately calculated at different proximity gaps. It can also be noticed that diffraction effects of a line at different proximity gaps and the simulation and measurement results looks similar.

3.5 Printing: Mask aligner

The mask aligner, shown in Fig. 3.11, that is used for printing the structures is a last generation Süss MicroTech MA/BA8 GEN3 system with a 350 W lamp house [3.21]. It is used to produce optical components, in MEMS production and also for compound semiconductor products. The Mask aligner comes with a special tooling called SMILE (SUSS MicroTech Imprint Lithography Equipment). The main features of the mask aligner are wafer handling of up to 200mm diameter, precise alignment down to 250 nm and it is equipped with MO exposure optics which guarantees an excellent light uniformity over the whole field (typically +/-2%). In our experiments, the wafers are made of silicon and coated with thin resist AZ1518 for our exposures. The proximity gap and printing doses varies according the resist thickness and the structure definitions.



Figure 3. 11: Mask aligner set up in clean room [3.23].

Conclusion

Different characterization techniques that are used in the study to get the limitations of proximity printing are reviewed. A brief overview of the simulation software Layout LAB, which is a powerful tool for lithographic printing technologies, has been discussed. The software works with easy graphical user interfaces and calculates the results efficiently with less time. With this framework, the special illumination techniques, called MO exposure optics from Süss MicroOptics, that have been used within the scope of this research work have also been discussed. MO exposure provides uniform illumination using microlens arrays. They use basic Köhler illumination setting

with micro lens arrays and Illumination Filter Plates to generate a homogenous illumination on the mask plane. The main advantage is that one can import MO exposure optics parameters into simulation software to create one's own illumination. As a third description, the measurement method (HRIM) that is used to study the evolution of light from samples and to study the intensity and phase propagation have been explained. The important parts of the measurement system like illumination sources, sample stage, interferometric technique etc. have also been discussed. The measurement system is also adapted to MO exposure optics. An example study with lines with simulation and measurement results to show the capability and similarity of both characterization techniques has been shown. Lastly, some details about the mask aligner which is used to print the samples have been provided. It is an MA/BA8 mask aligner from Süss MicroTech.

References

- [3.1] "LAB - All in One Lithography Simulation"; from GenISys.
<https://www.genisys-gmbh.com/web/products/lab.html>
- [3.2] C. Rockstuhl, I. Märki, T. Scharf, M. Salt, H. P. Herzig and R. Dändliker; "High Resolution Interference Microscopy: A Tool for Probing Optical Waves in the Far-Field on a Nanometric Length Scale"; *Current Nanoscience* **Vol.2, No.4**; pp. 337-350(2006).
- [3.3] M. Hornung, U. Vogler and R. Voelkel; "Customized illumination for process window optimization and yield improvement in mask aligner lithography systems"; *Journal of Vacuum Science & Technology B* **Vol. 28, No. 6**; pp. C6Q6-C6Q11(2010).
- [3.4] C. A. Mack; "Thirty years of lithography simulation"; *Proc. SPIE: Optical Microlithography XVIII* **Vol. 5754**; pp. 1-12(2005).
- [3.5] K. Motzek, S. Partel, A. Bramati, U. Hofmann, N. Ünal, M. Hennemeyer, M. Hornung, A. Heindl, M. Ruhland, A. Erdmann and P. Hudek; "Mask aligner lithography simulation – From lithography simulation to process validation"; *Journal of Microelectronic Engineering* **Vol. 98**; pp. 121-124(2012).
- [3.6] A. Bramati, U. Vogler, B. Meliorisz, K. Motzek, M. Hornung and R. Voelkel; "Simulation tools for advanced mask aligner lithography"; *Proc. SPIE: Optical Design and Engineering IV* **Vol. 8167**; pp. 81670U 1-9(2011).
- [3.7] W. Singer, M. Totzeck and H. Gross; "Handbook of Optical Systems"; *WILEY-VGH Verlag GmbH & Co. KGaA, Weinheim*, **Vol. 2**; pp. 47-51(2005).
- [3.8] J.B. Pendry; "Photonic Band Structures"; *JOURNAL OF MODERN OPTICS* **Vol. 41, No. 2**; pp. 209-229(1994).
- [3.9] C. A. Mack; "Development of Positive Photoresists"; *Journal of the Electrochemical Society* **Vol. 134, no. 1**; pp. 148-152(1987).

- [3.10] A. Köhler; "Ein neues Beleuchtungsverfahren für mikrographische Zwecke"; *Zeitschrift für wissenschaftliche Mikroskopie und für Mikroskopische Technik* **Vol. 10, No. 4**; pp. 433–440 (1983).
- [3.11] R. Voelkel, U. Vogler and A. Bich; "Illumination system for a microlithographic contact and proximity exposure apparatus"; *European patent* **No. EP 2 253 997 A2**; (2010).
- [3.12] T. Harzendorf, L. Stuerzebecher, U. Vogler, U. D. Zeitner and R. Voelkel; "Half-tone proximity lithography"; *Proc. SPIE Micro- Optics* **Vol. 7716**; pp. 77160Y 1-10(2010).
- [3.13] O. Dross, R. Mohedano, M. Hernández , A. Cvetkovic, J. C. Miñano and P. Benítez; "Köhler integrators embedded into illumination optics add functionality"; *Proc. SPIE Illumination Optics* **Vol. 7103**; pp. 71030G 1-12(2008).
- [3.14] R. Voelkel and K. J. Weible; "Laser Beam Homogenizing: Limitations and Constraints"; *Proc. SPIE Optical Fabrication, Testing, and Metrology III* **Vol. 7102**; pp. 71020J 1-12(2008).
- [3.15] R. Voelkel, U. Vogler, A. Bich, P. Pernet, K. J. Weible, M. Hornung, R. Zoberbier, E. Cullmann, L. Stuerzebecher, T. Harzendorf and U. D. Zeitner; "Advanced mask aligner lithography: new illumination system"; *OPTICS EXPRESS* **Vol. 18, No. 20**; pp. 20968-20978(2010).
- [3.16] H. Komatsu; "Interferometry: Principles and Applications Of Two-Beam And Multiplebeam Interferometry"; Nikon Brochures (1991).
<http://www.tecnicaenlaboratorios.com/Nikon/Brochures/Technical%20Bulletin%20Interferometry%201991.pdf>.
- [3.17] A. Cho; "Gravitational waves, Einstein's ripples in space time, spotted for first time"; *Science News*; (2016).
<http://www.sciencemag.org/news/2016/02/gravitational-waves-einsteins-ripples-spacetime-spotted-first-time>.
- [3.18] M-S. Kim, T. Scharf, S. Mühlig, C. Rockstuhl and H. P. Herzig; "Gouy phase anomaly in photonic nanojets"; *Applied Physics Letters* **Vol. 98, No. 19**; pp. 191114 1-3(2011).
- [3.19] M-S. Kim, T. Scharf and H. P. Herzig; "Small-size microlens characterization by multiwavelength high-resolution interference microscopy"; *OPTICS EXPRESS* **Vol. 18, No. 14**; pp. 14319-14329(2010).
- [3.20] T. Scharf, M-S. Kim and H. P. Herzig; "Measuring amplitude and phase of light emerging from microstructures with HRIM"; *Proc. SPIE Optical Measurement Systems for Industrial Inspection VII* **Vol. 8082**; pp. 808210 1-8(2011).
- [3.21] K P Zetie, S F Adams and R M Tocknell; "How does a Mach-Zehnder interferometer work?"; *Phys. Educ.* **Vol. 35, No.1**; pp. 46-48(2000).

- [3.22] P. Hariharan, B. F. Oreb and T. Eiju; “Digital phase-shifting interferometry: a simple error-compensating phase calculation algorithm”; *APPLIED OPTICS* **Vol. 26, No. 13**; pp. 2504-2505(1987).
- [3.23] Photolithography, EPFL AT MICROCITY clean room,
<http://microcity.epfl.ch/cms/lang/fr/pid/119309>.

CHAPTER 4

1D correction structures in amplitude mask - Edge

In the following chapters, theoretical aspects of proximity printing and the characterization techniques used to study those aspects will be explained. From this chapter onwards, studies are applied to real problems and an attempt is made to find solutions for them. All the studies begin from 1D structures and then continue to higher dimensional structures. Here also, the study starts with a 1D structure – a simple edge. Edge and its characteristic study is one of the early stage study in the field of lithographic printing. This chapter gives details about the optical proximity correction designed for edge slope improvement. Studies are done both theoretically and experimentally by simulation and experimental set up using HRIM. The results have been published partially in SPIE conference proceedings [4.1].

As the resolution of the features is increasing, at one time it can reach its limits. There are several factors which pull back the resolution limits. One such factor is Line Edge Roughness (LER) and Line width Roughness (LWR). These are the deviations of a feature that occur on a dimensional scale (~100 nm) much smaller the resolution limit of the imaging tool. They are basically spatial frequency effects. It is caused by several factors like shot noise, chemical property fluctuation on the resist etc [4.2, 4.3]. Mask Error Enhancement Factor (MEEF) is a way to calculate these reticle errors in printing [4.4]. MEEF is calculated by finding the incremental change in the resist feature to the ideal mask feature size. MEEF depends on how the structure is disturbed not only by the structure itself but also by neighboring parameters. These days, MEEF is calculated in a matrix form to get a bigger picture [4.5]. Earlier days MEEF considers mainly process related factors like illumination parameters and exposure dose. But mask error enhancement matrix (MEEM) takes care of feature size change, proximity effects from neighboring feature etc. For edges, the MEEF is mainly calculated for edge slope improvement or Edge Placement Error (EPE). EPE is the difference in margin between the final edge placements on the wafer to the ideal. EPE and edge slope can be improved using OPC method [4.6, 4.7, and 4.8].

Here, the aim is to find a simple OPC solution to focus light at the desired proximity gap to print the edges with an improved slope. In general, the proximity gaps used in mask aligners for printing starts at 20 μm and it goes larger. The current study concentrates more on the

comparison of intensity field measurements both from simulation and experiments and considers also large proximity gaps up to 100 μm .

4.1 Structure definition

The idea is to add fine structures near the edges to shape the intensity on the edges. As we know from the design of Fresnel zone plates [4.9], adding rings of a certain size will focus light at certain distance [4.10]. Here, the aim is to check whether adding lines to edges will focus the light at certain proximity gaps or not to increase the slope. The following geometries in Fig. 4. 1 are the optimized features for printing edges at different proximity gaps with different degree of complexity.

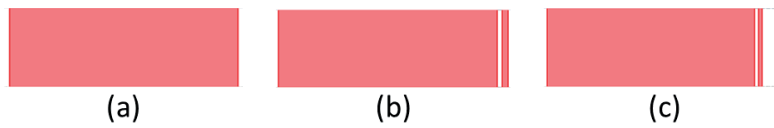



Figure 4. 1: The structure definition to study (a) normal edge, (b) edge with one line correction and (c) edge with two line correction structures respectively.

4.2 Simulation and experimental geometries

The optimized examples of one line and two line corrections near the edges for proximity gaps of 30 μm and 50 μm are presented below. The optimization was performed with the help of our former colleague Qing Tan. The values are optimized by linearly varying each gap from side wall (edge) to the sub resolution line and the finding the best fit to the ideal structure in the mask. Several number of iterations are performed to get the optimized structure.

- For 30 μm


a) Simple edge = 40 μm . 

b) Edge with one line: - one line and one space; Total = $40+0.9+1 = 41.9 \mu\text{m}$. 

c) Edge with two line–two lines and two spaces; Total = $40+0.7+0.7+3.1+0.7= 45.2 \mu\text{m}$.



- For 50 μm

a) Simple edge = 40 μm . 

b) Edge with one line: - one line and one space; Total = $40+1.1+1.5 = 42.6 \mu\text{m}$. 

c) Edge with two line–two lines and two spaces; Total = $40+1.1+0.7+3.5+0.7 = 46 \mu\text{m}$.



Simulations are performed with the normal parallel illumination (405 nm) setting from Layout Lab. The structure is imported to the module and aerial images are observed at desired proximity gaps. The result files are exported as an ASCII file and tabulated using Matlab codes.

4.3 Measurements and recordings

The target is to get the result of propagation and aerial image at different proximity gaps. Experimental measurements are done by 405 nm laser and using 20X/ NA 0.75 dry objectives (NIKON CFI Apochromat VC). 20X objective gives a field size of $316 \times 239 \mu\text{m}^2$ and 1 pixel in the image plane equals to 233 nm in the object plane.

To start with, the intensity image at the starting point of light propagation is important. In measurements, the mask plane is represented by the x-y plane. Fig 4. 2 represents the one line and two line correction structures of edges which are optimized for 50 μm proximity gap and intensity profile at 0.1 μm proximity gap is shown as a top view.

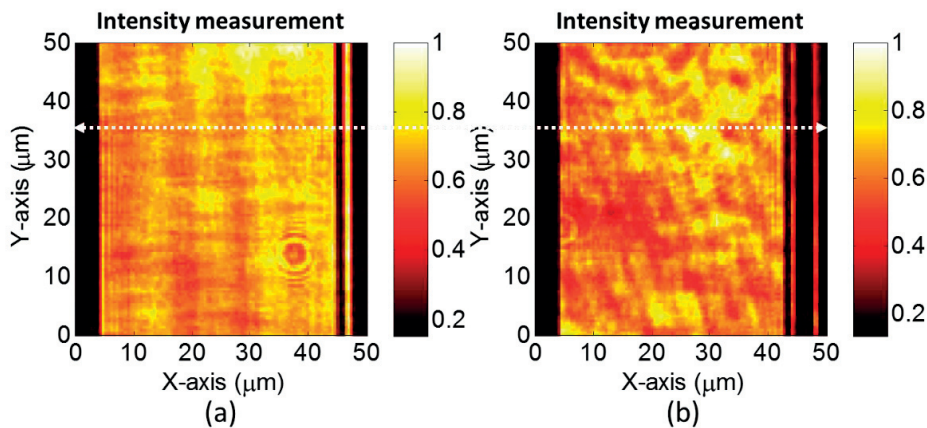


Figure 4. 2: x-y intensity images from HRIM optimized for 50 μm proximity gap at 0.1 μm (a) one line edge correction and (b) two line edge correction.

As we know HRIM can measure and record 3D interferograms. The propagation axis of HRIM is mentioned as z axis. To study the light evolution from the mask level to different proximity gaps, we will have a closer look at the propagation of light from the line cut region which is represented by a white dotted line in Fig. 4. 2.

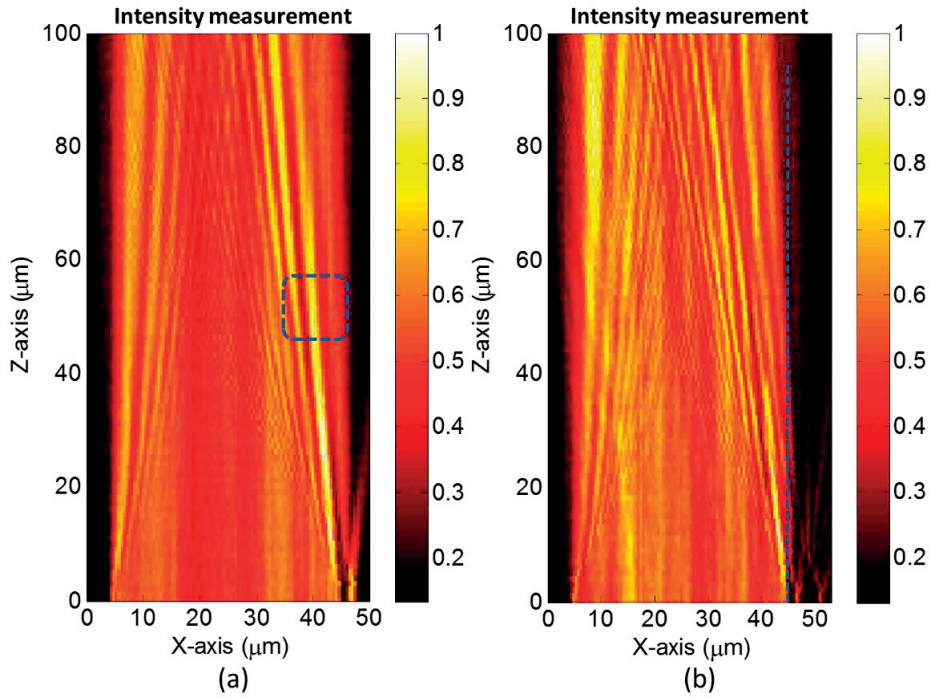


Figure 4. 3: *x-z* propagation images from HRIM optimized for 50 μm proximity gap (a) one line edge correction and (b) two line edge correction.

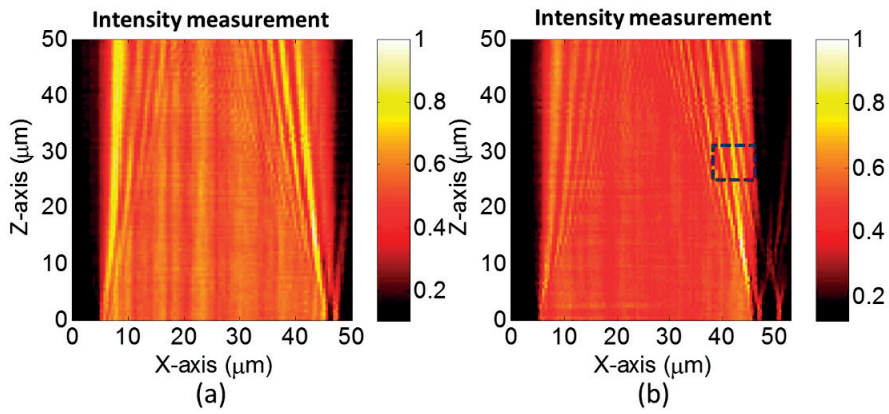


Figure 4. 4: *x-z* propagation images from HRIM optimized for 30 μm proximity gap (a) one line edge correction and (b) two line edge correction.

The propagation measurements of optimized edge at 50 μm and 30 μm are shown in Fig. 4.3 and Fig. 4.4 respectively. The one-line edge correction and two line edge correction propagations are represented. The propagation images of 50 μm optimized structure were measured until a propagation distance of 100 μm proximity gap and for 30 μm optimized structure, the propagation measurement was done until 50 μm proximity gap. The main criteria is to minimize the edge placement error. The interest in the measurement is to see the changes

(slope improvement) and the concentration of light at the desired proximity gap points. In Figure 4. 3 (a) the intensity concentration can be noticed in the corrected edge side and that is represented with blue dotted rectangle in the figure. Considering the edge placement error, two-line correction shows better edge falling and gives better slope. (Fig. 4. 3 (b)). The concentration or focusing of light can reduce the edge placement error. The light transformation can be noticed with the 30 μm two-line edge optimized structure (Fig. 4. 4(b)). Constructive and destructive interference is happening near the edge and plotted with blue dotted rectangle. To study the importance of slope in more detail, intensity line plots will be used. The line plots have been deducted from the above images and shown in Fig. 4. 5 and Fig. 4. 6. The simulation results are also added to do the comparison and to study the OPC structure effects. The intensity line plots are made from the x-y image plots at desired proximity gaps with one line and two line OPC correction edges.

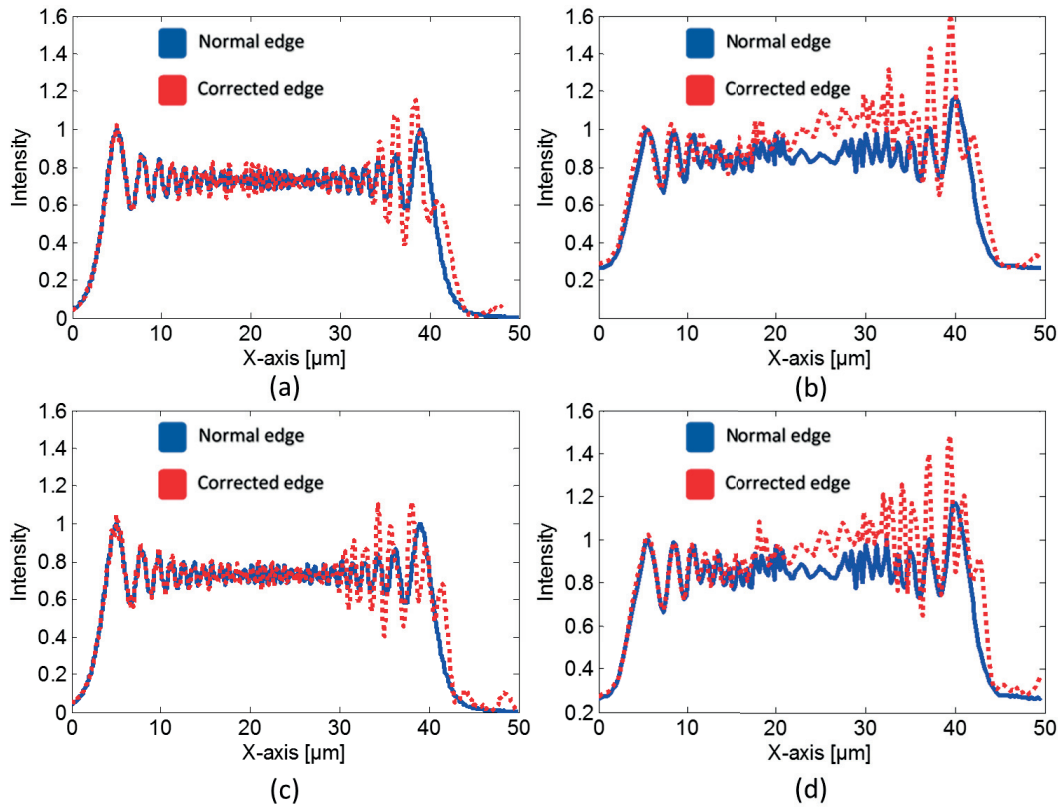


Figure 4. 5: x-y line images at 30 μm proximity gap of an optimized structure defined for 30 μm . (a) and (b) are one line edge corrected simulation and HRIM images respectively. (c) and (d) are two line edge corrected simulation and HRIM images respectively.

Figure 4.5 gives different intensity profiles at 30 μm proximity gap and the peaks are normalized with normal edge peak. One thing that is noticeable is slope getting better with

corrected structures and also the edge falling position changing. There is a slight modulation in measurement results but agreement with simulation result is good.

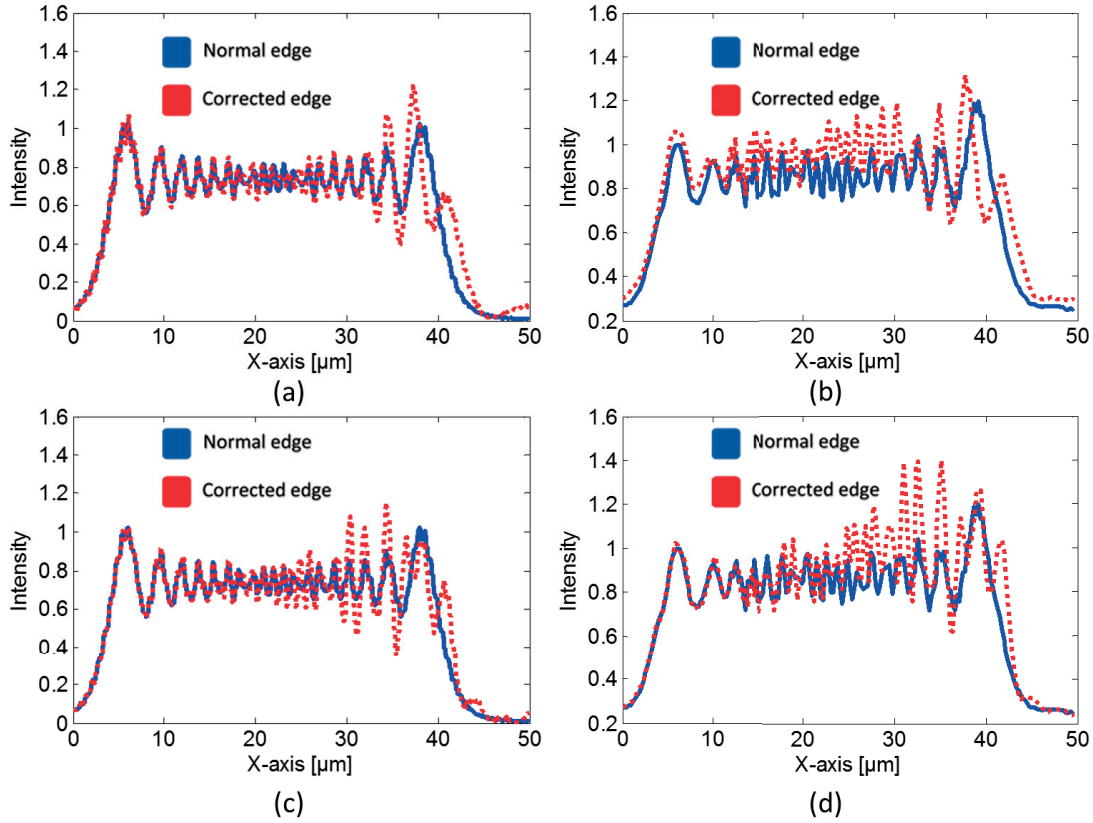


Figure 4. 6: x-y line images at 50 μm proximity gap of an optimized structure defined for 30 μm . (a) and (b) are one line edge corrected simulation and HRIM images respectively. (c) and (d) are two line edge corrected simulation and HRIM images respectively.

The intensity line images of both simulation and HRIM results are shown in Fig. 4. 6. From the figure, two line corrected slopes are better than the one line corrected slopes. It also gives a proof that normal structure edge falling position is not at the desired position but corrected edges try to fall at the desired positions. This is the edge placement error. To validate the statement, we are considering the line width as a parameter (Fig. 4.7).

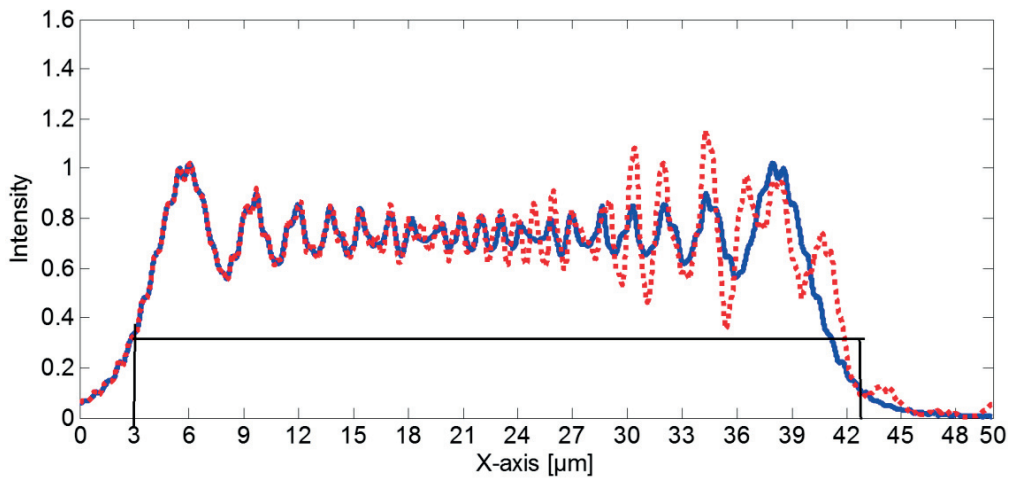


Figure 4. 7: Edge falling position with an example.

The line width of the designed structure is $40\ \mu\text{m}$ ($3\ \mu\text{m}$ to $43\ \mu\text{m}$). In general, edge falling position of a normal edge should be at $43\ \mu\text{m}$ (x-axis position from Fig.4.7), since the ideal line width of the structure is $40\ \mu\text{m}$. From Fig.4.7 it is noted that the edge falling or the side wall is not at $43\ \mu\text{m}$ for normal edge, but for the edge with two line correction the edge tries to fall near to $43\ \mu\text{m}$. An improvement has shown in falling with correction structure (black line in Fig. 4.7 represents the actual line width of the structure). The results in Fig 4.6 show a good agreement between measurement and simulation but needs to be further analyzed. Certain parameters that allow access to process window calculations have been defined. An example calculation indicating the definition of parameters is shown in Fig. 4. 8.

4.4 Parameter definition

Defining parameters allows us to understand and compare the result of simulation and measurements. Main parameters are the slope and working range for every design. Specific intensity values have been set to define contrast and the working range. It is important to define the minimum and maximum intensity level in the process window (the points between light transmission region and non-transmission region). I_{\min} is the maximum point of the intensity variations in the falling position (non-transmission zone - this is the zone which should not be exposed) and I_{\max} is the minimum intensity variation point in the light transmission region. If exposed below I_{\min} , no structure can be printed and if the intensity is chosen higher than I_{\max} everything is overexposed and would not lead to useful results. The range between these two points (I_{\max} and I_{\min}) is called the process window. In the process window, resist profile cut off can be defined at different positions according to the exposure conditions. Usually, two third of the interval between I_{\max} and I_{\min} is defined as I_1 and it is the normal cut off resist profile.

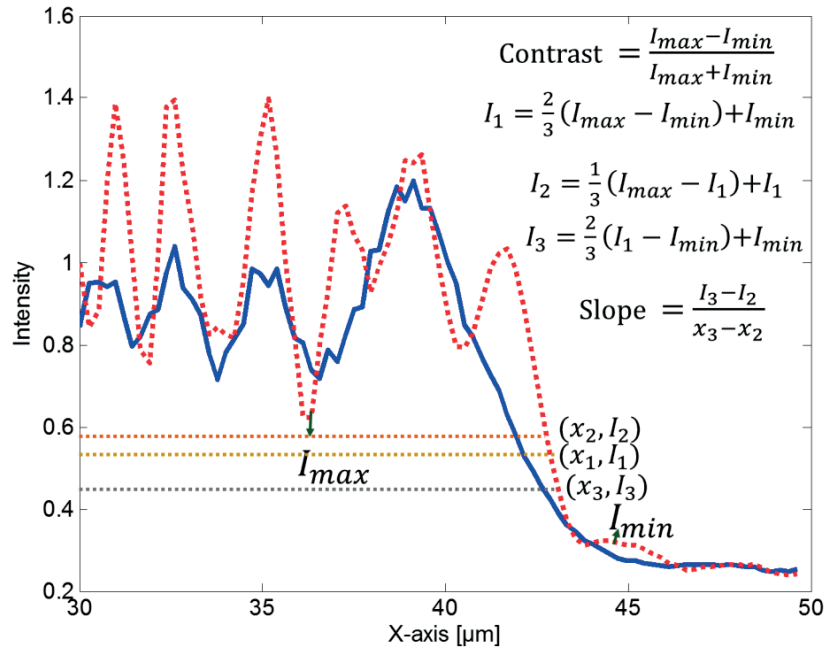


Figure 4. 8: Example parameters are defined (50 μm two line corrected experimental results).

Here, the working region between two intensity points named as I_{max} and I_{min} . (x_1, I_1) is the normal printing region in the masks. But according to the exposure conditions, it is useful to define a higher working region and a lower working region. Higher working region is defined as I_2 , it is at one third between I_{max} and I_1 . Lower working region is defined as I_3 , it is at one third between I_1 and I_{min} . Slope is calculated between the range I_2 and I_3 by linear interpolation. Figure 4. 6 shows that the normal edge is not giving sharp slopes. The OPC structures are defined with an assumption that sharper edge gives better results and the structures are optimized for slope steepness. The tables below summarize the parameters and findings for the proximity gaps and designs studied here.

	I_{max}	I_{min}	I₁	x₁	I₂	x₂	I₃	x₃	Slope
30_edge	0.73	0.29	0.58	42.39	0.63	42.22	0.39	43.44	0.200
30_online	0.66	0.33	0.55	43.57	0.58	43.42	0.40	44.19	0.233
30_twoline	0.65	0.33	0.54	43.57	0.58	43.52	0.40	43.90	0.465

Table 4. 1: Parameters defined for 30 μm proximity gap - experimental results.

	I_{max}	I_{min}	I₁	x₁	I₂	x₂	I₃	x₃	Slope
30_edge	0.40	0.02	0.27	41.08	0.32	40.77	0.10	42.24	0.144
30_online	0.28	0.05	0.20	43.59	0.23	43.38	0.10	44.24	0.146
30_twoline	0.29	0.08	0.22	43.21	0.24	43.16	0.13	43.44	0.417

Table 4. 2: Parameters defined for 30 μm proximity gap - simulation results.

	I_{max}	I_{min}	I₁	x₁	I₂	x₂	I₃	x₃	Slope
50_edge	0.72	0.27	0.57	42.00	0.62	41.76	0.37	43.26	0.164
50_oneline	0.63	0.31	0.52	43.58	0.56	43.38	0.38	44.59	0.151
50_twoline	0.62	0.32	0.52	42.90	0.55	42.84	0.39	43.30	0.361

Table 4. 3: Parameters defined for 50 μ m proximity gap - experimental results.

	I_{max}	I_{min}	I₁	x₁	I₂	x₂	I₃	x₃	Slope
50_edge	0.57	0.05	0.40	40.70	0.45	40.58	0.17	42.00	0.203
50_oneline	0.41	0.06	0.29	43.87	0.33	43.67	0.14	44.72	0.185
50_twoline	0.38	0.13	0.30	42.90	0.32	42.85	0.18	43.22	0.381

Table 4. 4: Parameters defined for 50 μ m proximity gap - simulation results.

The above tables give access to the parameters that are defined from Fig. 4. 5 and Fig. 4. 6. The parameters are given for both simulation and experiment. The behavior of results are exactly the same and compare very well for both measurement and simulation (an example result in the blue dotted rectangle). The little differences appear since measurements are of high resolution, small noises can disturb the system if the chromium in the mask is not perfectly opaque for instance. This will give rise to measurement intensity value higher than the simulated intensity value. But the different intensity x values for corrected structures are similar for both simulation and experiment with less error. If one assumes that steep slopes give sharper corners, there is a pronounced slope improvement with correcting structures from tables. There is an interesting improvement in steepness (slope) with the corrected structures, mainly with the two line correction. The values of one line correction slope improvement is not good when compared to two line correction improvement. The slope values are decreasing for 50 μ m one line correction in comparison to the normal structure. The behavior in slope for measurements and simulation results are the same. Now, there are three regions to work for the resist profile from the intensity results and can be used according to the need.

Conclusion

For the first time, measurements and simulation of OPC structures have been compared. With the definition of key parameters, we try to systematize the results. The optimized structures of 30 μ m and 50 μ m have been studied. It could be shown that tendencies found in simulation predict trends in the measurements. The slope has been improved by adding lines and spaces to the normal edge. Adding two lines makes higher improvement than adding single lines in the steepness of the edge fall. Three regions defined gives more freedom of exposure window for

resist profile printing. 1D correction structure has been studied successfully and next chapters will follow 2D structures and corrections.

References

- [4.1] K. Puthankovilakam, T. Scharf , Q. Tan, H. P. Herzig, U. Vogler, A. Bramati and R. Voelkel; "Shaping intensity behind amplitude masks for proximity correction lithography: design, measurement, and realization"; *Proc. SPIE interferometry XVII: Techniques and Analysis* **Vol. 9203**; pp. 92031B 1-8(2014).
- [4.2] C. A Mack; "Line Edge Roughness"; The Lithography expert (2007).
[http://www.lithoguru.com/scientist/litho_tutor/Tutor56%20\(Feb%2007\).pdf](http://www.lithoguru.com/scientist/litho_tutor/Tutor56%20(Feb%2007).pdf).
- [4.3] C. A. Mack; "Line-Edge Roughness and the Ultimate Limits of Lithography"; *Proc. SPIE Advances in Resist Technology and Processing XXVII* **Vol. 7639**; pp. 76391-16(2010).
- [4.4] F.M. Schellenberg and Chris Mack; "MEEF in Theory and Practice"; *Proc. SPIE 19th Annual Symposium on Photomask Technology* **Vol. 3873**;pp. 189-202(1999).
- [4.5] Y. Granik and N. Cobb; "MEEF as a matrix"; *Proc. SPIE 21st Annual BACUS Symposium on Photomask Technology* **Vol. 4562**; pp. 980-991(2002).
- [4.6] N. Cobb and Y. Granik; "OPC methods to improve image slope and process window"; *Proc. SPIE Design and Process Integration for Microelectronic Manufacturing II* **Vol. 5042**; pp. 116-125(2003).
- [4.7] J. Mulkens, M. Hanna, H. Wei, V. Vaenkatesan, H. Megens and D. Slotboom; "Overlay and Edge Placement Control Strategies for the 7-nmnode using EUV and ArF lithography"; *Proc. SPIE Extreme Ultraviolet (EUV) Lithography VI* **Vol. 9422**; pp. 94221Q 1-13(2015).
- [4.8] C. Maloney; "Compensation of Extreme Ultraviolet Lithography Image Field Edge Effects Through Optical Proximity Correction"; *Thesis. Rochester Institute of Technology*; (2014).
- [4.9] M. Luque; Melusine directory.
<https://melusine.eu.org/syracuse/mluque/fresnel/fresnel.pdf>.
- [4.10] A. W. Lohmann and D. P. Paris; "Variable Fresnel Zone Pattern"; *APPLIED OPTICS* **Vol. 6, No. 9**; pp. 1568-1570(1967).

CHAPTER 5

Lines characterization

After edges, lines and spaces are the next structures which are known as the building blocks of the printing industry. Printing industry is always in need of new correction methods to print the desired pattern in the best way. For new correction methods, analyses of the real problems are necessary. Here, the parameters for analysis are used in real situations. Proximity gaps up to 50 μm and structure sizes down to 2 μm are studied. The main aim is to analyze the propagation of light in independent lines in a dark field mask. The chapter describes the diffraction effects during propagation with the help of Fresnel number.

5.1 Theoretical definition

Effects of Fresnel number in focusing and imaging have been studied by C. J. R Sheppard and P. Török in early days [5.1]. The fact that diffraction effects at different proximity gaps are related to the Fresnel number at a specific distance is known [5.2]. Fresnel number and Fresnel zone region gives the possibility to interpret aerial image intensity of the structure at that plane of observation. Analysis of diffraction pattern using Fresnel number is already in use for the x-ray lithography process optimization [5.3]. The Fresnel number, N_F , of a structure with width $2a$, at a distance z and for a wavelength of λ is defined as [5.4]

$$N_F(z) = \frac{a^2}{\lambda z} \tag{5.1}$$

As we know, proximity printing regions usually falls in the near field diffraction regions. The resolution a and the distance z are defined by Fresnel Number $N_F > 0.5$ [5.1]. The main two factors which decide on the minimum feature width of proximity printing is the proximity distance and the photoresist parameters. The understanding of minimum feature width will be easy by studying the Fresnel number and the effects can be clearer when propagation analysis of different line widths are studied. The diffraction pattern through different slit widths with different diffraction theory approach was summarized by H. Gross [5.5]. The diffraction pattern was described using plane wave illumination. Since the optics that we are using is MO illumination optics, it is necessary to verify the different line width diffraction pattern and report about its influence. MO exposure optics uses different elements to get a uniform illumination. The

coherence management is also different in MO exposure optics as comparing to the normal (plane wave or parallel) illumination. A difference between the diffraction patterns of parallel illumination and MO illumination is represented below.

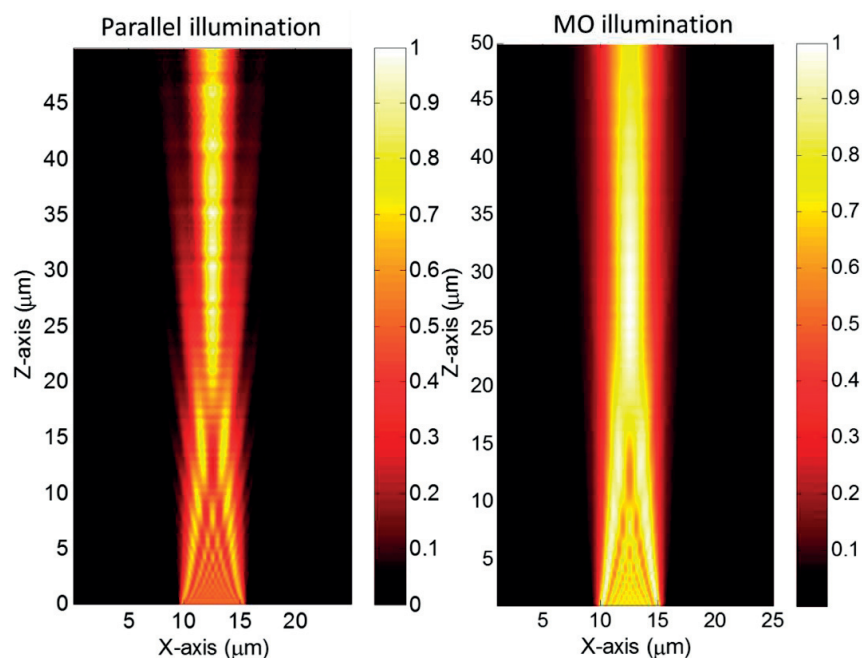


Figure 5. 1: Simulation result of light evolution (x - z) from a $6\ \mu\text{m}$ line width structure until $50\ \mu\text{m}$ proximity gap using parallel illumination and MO exposure optics.

The simulated light evolution from $6\ \mu\text{m}$ line width structure is shown above in Fig. 5.1 with two different illumination techniques. One is the normal parallel illumination and other is the MO exposure optics. As one can notice, MO exposure provides uniform and limited diffraction imaging compared to the normal illumination. MO exposure optics is used with HRA illumination filter plate which provides an angle of 3° during propagation. The diffraction features (interferences) and scattering is also less pronounced with MO exposure optics. In what comes next, our main focus is on the diffraction pattern from different line widths with MO illumination optics to study the feature size and proximity gap restrictions of proximity printing.

5.2 Measurements and recordings

Simulations are done with MO illumination with $405\ \text{nm}$ as wavelength using Layout LAB. The experimental measurements are carried out using an LED (RSW-P05-400-0) of $405\ \text{nm}$ to simulate the illumination regime of a mask aligner. The beam will pass through a Köhler illumination setup and through a beam splitter afterwards. The beam splitter splits the beam's path to object arm and reference arm. Since we are analyzing the aerial intensity image only, the reference arm is not used for the current measurements. In the object MO illumination optics is placed (Fly eyes, Illumination Filter Plate (IFP), final lens). IFP used for the simulation is HR A

with 3° of diffraction angle. The objective used for the measurement is a high resolution 20X/ NA 0.75 dry objective (NIKON CFI Apochromat VC), corrected for 405 nm.

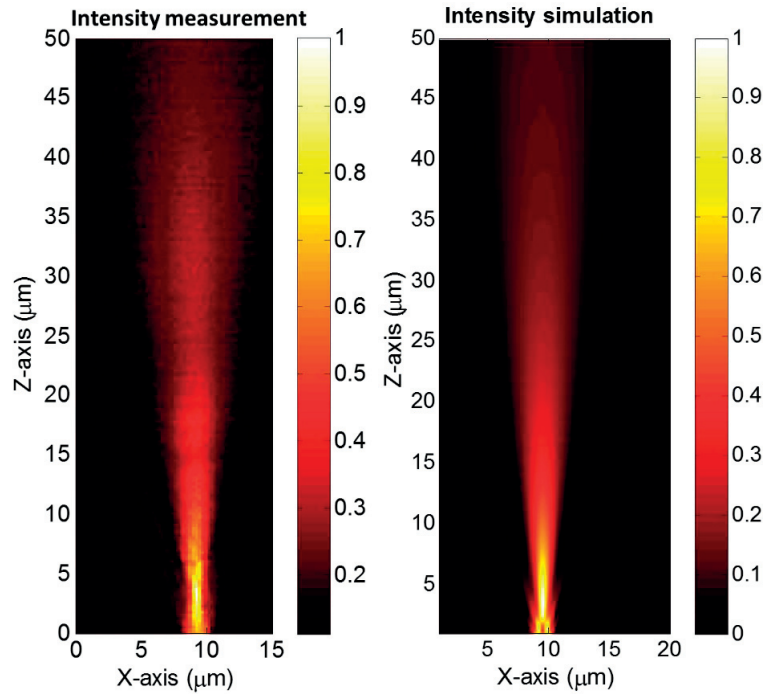


Figure 5. 2: HRIM and simulation result of light evolution (x - z) from a $2 \mu\text{m}$ line width structure until $50 \mu\text{m}$ proximity gap.

The discussion starts with the smallest feature in the evaluation structure, $2 \mu\text{m}$. The light evolution from $2 \mu\text{m}$ line width structure to $50 \mu\text{m}$ proximity gap is theoretically studied and experimentally measured with the help of LAB software and z - axis scanning stage in HRIM respectively in Fig. 5.2. The image clearly shows the intensity drop during the evolution and also the change in the structure definition (width). Understanding of diffraction effects will be easy if the image is studied at different proximity gap.

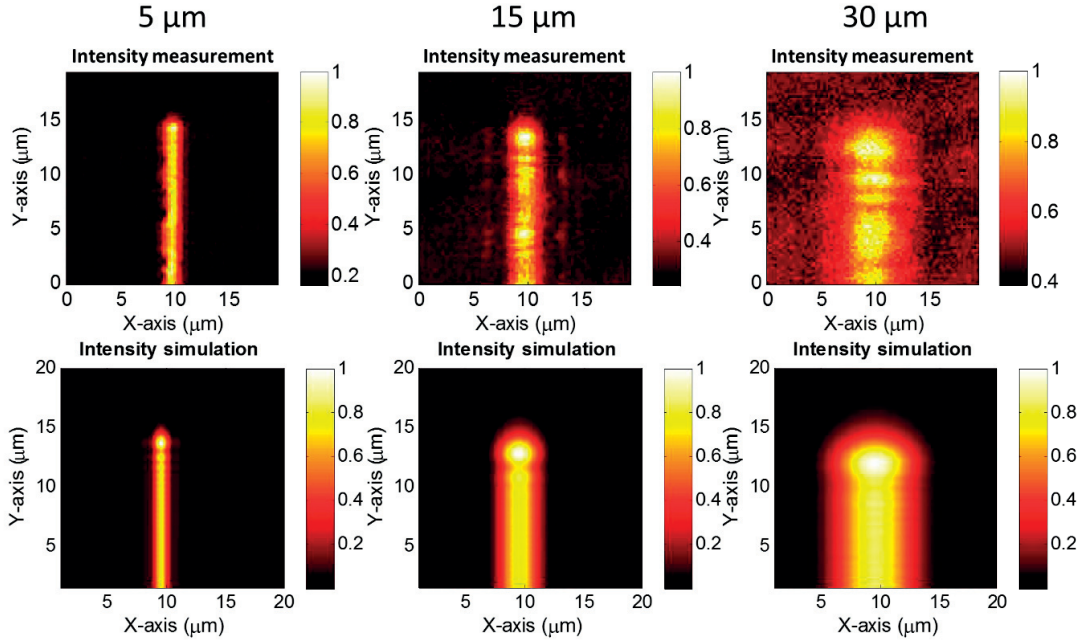


Figure 5. 3: HRIM and simulation intensity images(x - y) at different proximity gaps. Proximity gaps are written on the top of the images.

Figure 5. 3 shows the x - y intensity images of $2\ \mu\text{m}$ line width structure at different proximity gaps. The distance (proximity gap) at which the Fresnel number turns 0.5 ($N_F = 0.5$) is

$$Z = \frac{a^2}{\lambda N_F} = \frac{1}{0.2025} = 4.93\ \mu\text{m} = 5\ \mu\text{m}.$$

The Fresnel number defines the threshold of proximity printing with the parameters like feature shape, size, proximity gap and illumination parameters [5.6]. From Fig. 5.2 it is visible that the structure tries to maintain its properties till $5\ \mu\text{m}$ distance, after that the intensity is scattered out. In almost all cases the proximity printing zone is defined above $N_F > 0.5$. After that, the line width changes with decrease in intensity. The x - y intensity images (Fig. 5.3) show the line width variation and the line width increase with a complete change in original line width. At $5\ \mu\text{m}$ proximity gap, structure shows the desired line width ($2\ \mu\text{m}$). Higher the proximity gap, higher the line width also. At proximity gaps of $15\ \mu\text{m}$ and $30\ \mu\text{m}$, the line width of the structure is higher. Since the intensity values are normalized in the images the exact intensity drop won't be seen. To better see the intensity drop, contrast and line width variation (scattering of light) a line plot is represented below in Fig. 5.4.

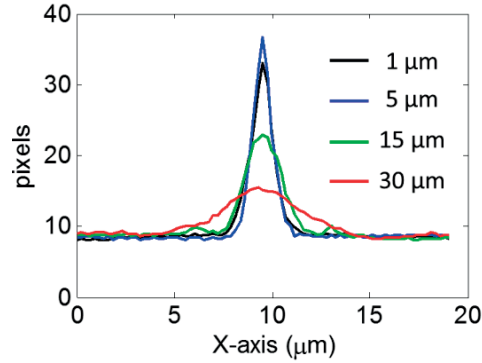


Figure 5. 4: HRIM line plots from(x-y) images of 2 μm line width structure at different proximity gaps.

Figure 5.4 shows the line plots averaged over 30 micrometers. The image clearly represents the structure shape at different proximity gap and also the intensity drop. 1 μm proximity gap is just above the mask level and structure shows its features and the exact line width. When the distance starts getting longer, the structure also modifies its shapes and width. The interesting fact that can be noticed is the rounding of corners at the line ends. Even at 5 μm proximity gap the line ends get rounded and showing high intensity at rounded corners. At 15 μm proximity gap, the intensity is dropped by half and structure width also started increasing. Proximity gap 30 μm is the region where intensity almost dropped to 1/4th of the initial intensity and structure width almost reached up to 10 μm . If we calculate the Fresnel number on those regions, it becomes

$Z = 15 \mu\text{m}$, N_F becomes

$$N_F = \frac{a^2}{\lambda Z} = \frac{1}{6.075} = 0.16$$

$Z = 30 \mu\text{m}$, N_F becomes

$$N_F = \frac{a^2}{\lambda Z} = \frac{1}{12.15} = 0.08$$

The Fresnel number value above show that's $N_F < 0.1$ the structure fidelity is completely lost for independent lines and spaces. The aerial image study explains that printing an independent 2 μm line at large proximity gap (50 μm) is impossible without using resolution enhancement technologies. Printing at lower proximity gap (2 μm – 5 μm) to get good contrast and structure fidelity is also not possible because of the mask and/or wafer damage. To get more information about the independent lines, wider line width features need to be studied.

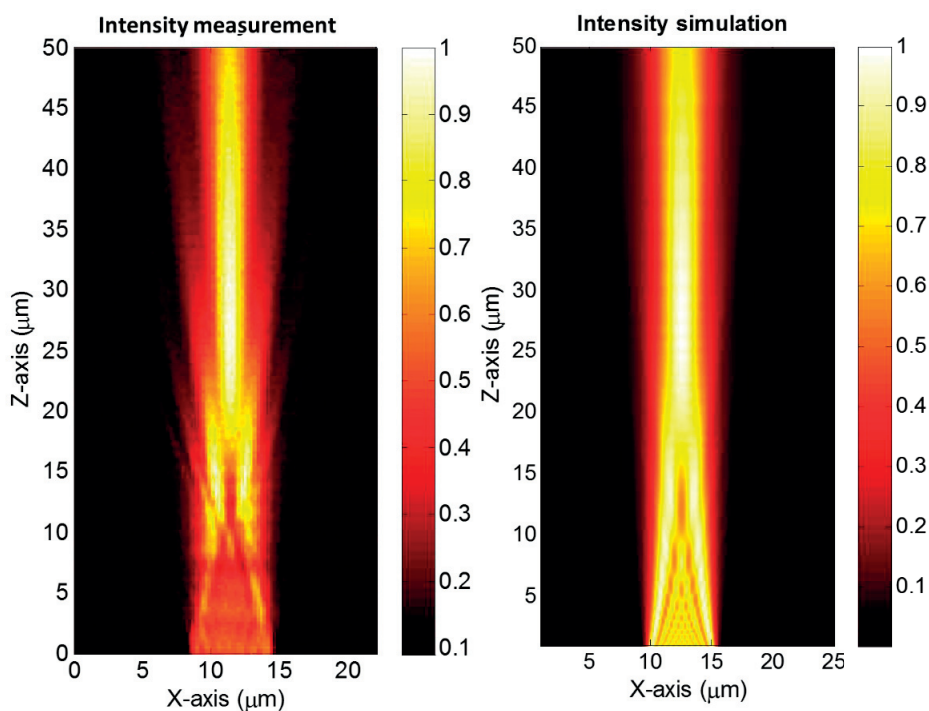


Figure 5. 5: HRIM and simulation result of light evolution (x - z) from a $6 \mu\text{m}$ line width structure until $50 \mu\text{m}$ proximity gap.

Figure 5.5 represents the propagation result of simulation. The diffraction pattern is different at different proximity gaps. The diffraction pattern formations are classified into three main zones. Contact printing region or the small proximity gap region is not considered here. Damaging of mask is having higher chances at contact zone, but printing in the contact region gives higher structure fidelity. The first zone for the study is where the intensity splits in to several units giving intensity hikes at both the edges. The split continues until the whole intensity split into two parts and leaves a dark region between the intensities. The Fresnel number at this region is two ($N_F = 2$). This is the second zone. Final zone is where all the intensity is formed back to the single line propagation. The third zone is usually defined between $0.5 < N_F < 1$ for proximity printing. Printing beyond this region will create drop in the intensity patterns and also the scattering of light. Printing regions vary with each structure definition. Process window optimization is needed to evaluate each line width [5.7]. Process window is considered by several parameters like aerial image intensity, resist parameters, vertical side wall angle etc. The above defined zones are represented with x - y plots in Fig. 5.5 for $6 \mu\text{m}$ line width structure.

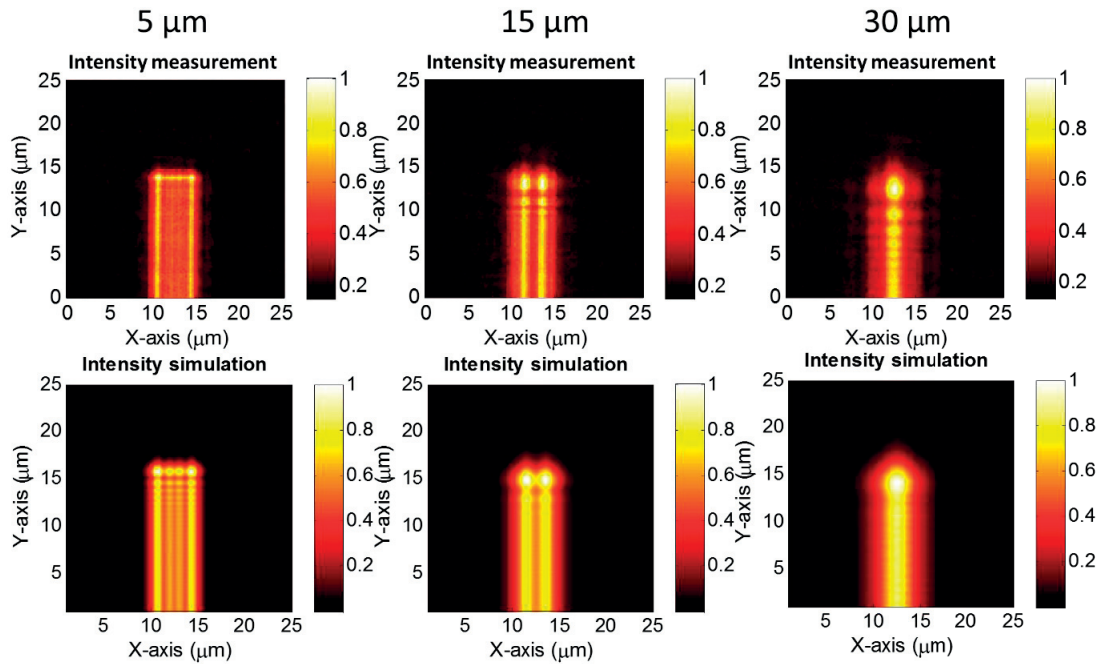


Figure 5. 6: HRIM and simulation intensity images(x - y) at different proximity gaps for $6 \mu\text{m}$ line. Proximity gaps are written on the top of the images.

The aerial image at different proximity gaps explain the same results that have been discussed in the propagation analysis. At $5 \mu\text{m}$ proximity gap, it is observed that the aerial image looks like the desired pattern with an intensity hike on the edges and several intensity drop regions in between. During the propagation further away, the intensity splits into two parts giving a double lobe structure. This is the second characteristic of lines at the regions near to Fresnel number two. The printing of lines at these regions give a double lobe structure. Proximity gaps large than this always shows the third characteristic nature of line called corner rounding. To know more about this, intensity line plots are plotted at different proximity gaps and represented in Fig. 5.7.

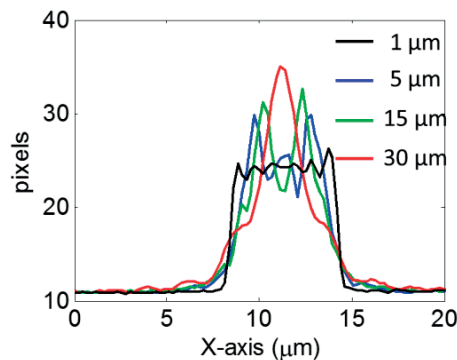


Figure 5. 7: HRIM line plots from(x - y) images of $6 \mu\text{m}$ line width structure at different proximity gaps.

In the intensity line plots, black line shows the structure just above the mask plane (contact region). Structure shape is similar to the desired linewidth pattern. Blue line started representing the first zone where the intensity hike at edges is visible. This hike usually starts above the contact printing region. The intensity hike continues until the intensity fully splits in to two parts. This is what we call the second zone, where the double lobe formation happens. The side walls are also not steep in this region. The final zone where the intensity forms back in to a single line (Gaussian profile like) with high intensity distribution and is represented with red line in Fig.5.7. The corner rounding is prominent in this zone. The regions are mentioned with its Fresnel number on Table 1.

Line width, $w = 6 \mu\text{m}$, Therefore, $a = (w/2) = 3 \mu\text{m}$; $\lambda = 405 \text{ nm}$ ($0.405 \mu\text{m}$)

Zone	Characteristics	Distance, z	Fresnel number N_F
1	Intensity hike in edges	$2 \mu\text{m} - 10 \mu\text{m}$	$10 - 2.2$
2	Double lobes	$11 \mu\text{m} - 15 \mu\text{m}$	$2.0 - 1.5$
3	Corner rounding	$15 \mu\text{m} -$	< 1

Table 5. 1: Fresnel number for $6 \mu\text{m}$ structure

This evaluation chart helps to define the proximity gap where they can print the structures with its different characteristics. To study whether these characteristics of lines are followed by all line widths, some more lines of larger width need to be evaluated.

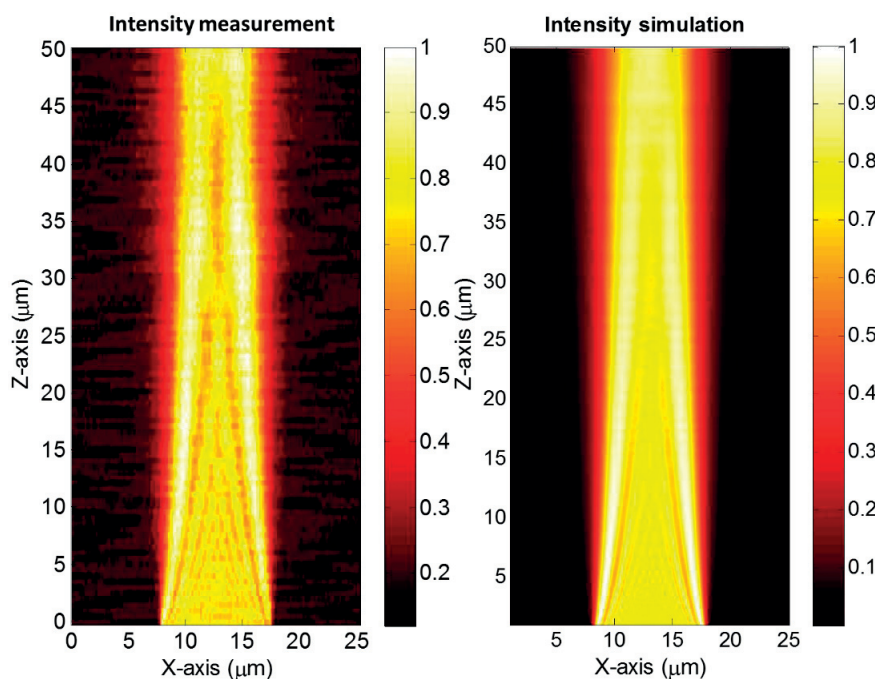


Figure 5. 8: HRIM and simulation result of light evolution (x - z) from a $10 \mu\text{m}$ line width structure until $50 \mu\text{m}$ proximity gap.

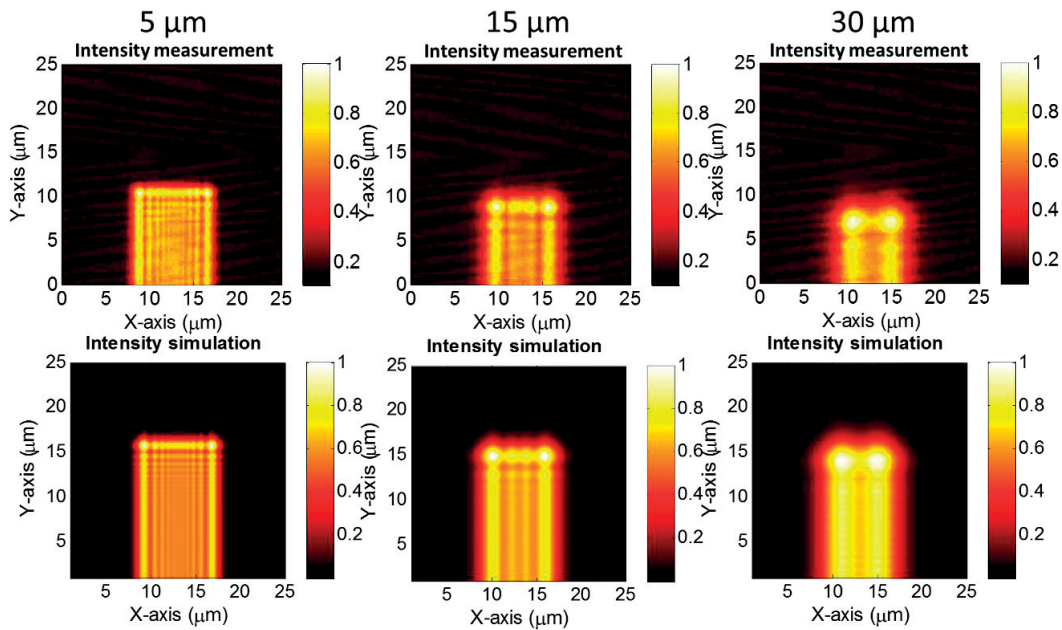


Figure 5. 9: HRIM and simulation intensity images(x - y) at different proximity gaps for $10\ \mu\text{m}$ line. Proximity gaps are written on the top of the images.

For a propagation of $50\ \mu\text{m}$ proximity gap, $10\ \mu\text{m}$ line can also be classified with three zones. First zone ($5\ \mu\text{m}$) usually falls on the region of lower proximity gap which shows intensity hike on the edges. Normally proximity printing prefers $30\ \mu\text{m}$ as a standard gap to print structures because of technical issues. But for this case, at $30\ \mu\text{m}$ gap the line shows the double lobes structure since the Fresnel number 2 falls at that position. Final zone or the Fraunhofer regime starts at a proximity gap of $61\ \mu\text{m}$. The detailed analysis is explained with line plots (Fig. 5.10).

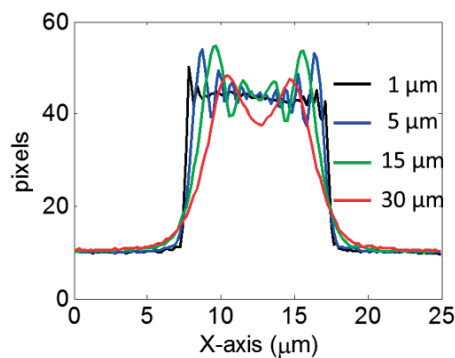


Figure 5. 10: HRIM line plots from(x - y) images of $10\ \mu\text{m}$ line width structure at different proximity gaps.

The line plot gives the above discussed information in a clear form. In contact region, around $1\ \mu\text{m}$ proximity gap, the structure fidelity will be high. After that the intensity hike at the edges starts to develop which is represented with a blue line and green line on the figure. The

intensity split in to two parts is happening around 30 μm proximity gap. Table. 5.2 below explains the variation of structure with proximity gap and Fresnel number.

Line width, $w = 10$ Therefore, $a = (w/2) = 5$; $\lambda = 405 \text{ nm}$ ($0.405 \mu\text{m}$)

Zone	Characteristics	Distance, z	Fresnel number N_F
1	Intensity hike in edges	6 μm – 28 μm	10 – 2.2
2	Double lobes	30 μm – 44 μm	2.1 – 1.5
3	Corner rounding	61 μm –	<1

Table 5. 2: Fresnel number for 10 μm structure.

As the line width of the structure increases, the characteristic zones of the line decreases in the normal printing gap (30 μm). It is well known that the diffraction effects of higher line width structure for shorter proximity gap will be less prominent.

5.3 Results and findings

From the above calculations and figures it is clear that there are mainly three characteristic gestures that a line can make during the propagation with MO exposure optics in dark field mask. All line width form different patterns at line ends and also changes the line width. Line ends can modify to: edge rounding with projection in corners, double lobes formation and corner rounding. These features happen at different proximity gap and also depends on the line width of the structure.

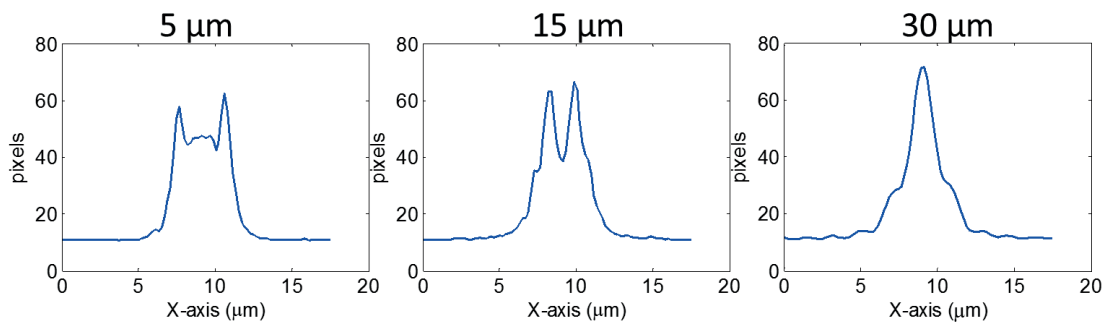


Figure 5. 11: Intensity line images of characteristic features observed for a line (6 μm) at different proximity gaps.

Main parameters which define printing are edge slope and the contrast. From the above figure one can notice that, there is high slope and contrast at proximity gap of 5 μm . The slope and contrast started reducing for proximity gap of 15 μm and the 30 μm proximity gap gives small slope and high contrast. The importance of edge slope was already discussed in previous chapter. Lines can be printed at different proximity gaps but need to compromise on edge slopes and contrast. These natures are depending on the Fresnel number also. One can define the printing

proximity gap by calculating the Fresnel number and the line width behavior at that proximity gap.

Conclusion

The study of lines and its characteristics changes during the propagation of light is very important for printing industry. Solutions for the problem can only be figured when the nature is studied. Here, a thorough study on lines and its natures have been discussed. Proximity printing industry prints the structures in the range of micrometers. So the structures sizes of 2 μm to 10 μm with a proximity gap of 50 μm printing range is discussed above. Fresnel number relation with line width printing is also discussed in the chapter. The characteristic changes of the lines that we observed can be classified as three. They are as follows: Intensity hike on the edges, double lobe structure and corner rounding. These characteristics happen one after another for a line. According to the line width of the structure, these characteristics may fall on the printing proximity gap and can be analyzed by calculating Fresnel number.

References

- [5.1] C. J. R. Sheppard and P. Török; "Effects of Fresnel number in focusing and imaging"; *Proc. SPIE International Conference on Optics and Optoelectronics '98* **Vol. 3729**; pp. 458-472(1999).
- [5.2] B. J. Lin; "Optical Methods for fine line lithography"; *Fine Line Lithography edited by Roger Newman, North Holland publishing company*; pp. 107 – 141(1980).
- [5.3] H. J. Yoo; "An analysis of diffraction intensities in the Fresnel region for the x ray lithography process optimization"; *Proc. SPIE Electron-Beam, X-Ray, and Ion-Beam Submicrometer Lithographies for Manufacturing II* **Vol. 1671**; pp. 411-418(1992).
- [5.4] M. Born and E. Wolf; "Principles of Optics"; *Peragmon press*; (1980).
- [5.5] W. Singer, M. Totzeck and H. Gross; "Handbook of Optical Systems"; *WILEY-VGH Verlag GmbH & Co. KGaA, Weinheim*, **Vol. 2**; pp. 58-60(2005).
- [5.6] B. J. Lin; "A new perspective on proximity printing: From ultraviolet to x ray"; *J. Vac. Sci. Technol. B* **Vol.8, No.6**; pp. 1539 – 1546(1990).
- [5.7] R. Voelkel, U. Vogler, A. Bramati, A. Erdmann, N. Ünal, U. Hofmann, M. Hennemeyer, R. Zoberbier, D. Nguyen, J. Brugger; "Lithographic process window optimization for mask aligner proximity lithography"; *Proc. SPIE Optical Microlithography XXVII* **Vol. 9052**; pp. 90520G 1-10(2014).

CHAPTER 6

2D correction structure in amplitude mask – Corner

Study of lines and characteristic natures in the dark field was interesting. The different structural behavior at different proximity gap was a promising study. Now, the question that comes up is how to solve this structural behavior change and get back the desired pattern. The motivation of this chapter is to find an easy solution for solving one of the earlier problem with line printing called corner rounding. The goal is to define a simple and universal rule based optical proximity correction for mask aligners which can be used to print any line width with precision on the same wafer at same proximity gap and in a single exposure. We proceed to a detailed analysis of the results using simulation, optical characterization and printing [6.1].

6.1 Designing of the corner correction structure

Rules defined by rule based optical proximity correction can be implemented easily but it may not work for all the features on the same way. In other words, error factors are high on rule based corrections. The different type of rules and their formations are explained in some patents [6.2, 6.3]. The major portion of the solutions are for solving either line shortening or corner rounding. One of the common method to solve corner rounding is serif method [6.4, 6.5, 6.6]. The methodology and its features are usually defined for projection printing technology compared to proximity printing technology [6.7, 6.8]. Here, the aim is to find a simple and unique rule based correction for corners specifically for mask aligners. It is similar to the pattern based correction methodology [6.9].

The previous chapter discussed about the different line width characteristics at different proximity gaps starting with smallest line width of 2 μm . The propagation measurement has shown the change of structure pattern from the desired pattern and the propagation was with MO exposure optics. MO exposure optics has been included in all the simulation, experimental and printing results. The wavelength regime is 405 nm and LED is used as the source of illumination for HRIM measurements.

The first step is to find out the minimum line width for which a correction can be applied to overcome the corner rounding. Normally, the printing industry chooses a proximity gap of 20 μm and above it (up to 50 μm) to reduce the mask damage. A fixed proximity gap of 30 μm has been chosen for all the printing experiments and simulations. In general, proximity gap plays a

vital role in designing the correction structures for mask aligners. Aerial images of lines with different line widths have simulated at $30\ \mu\text{m}$ proximity gap and shown in Fig. 6.1.

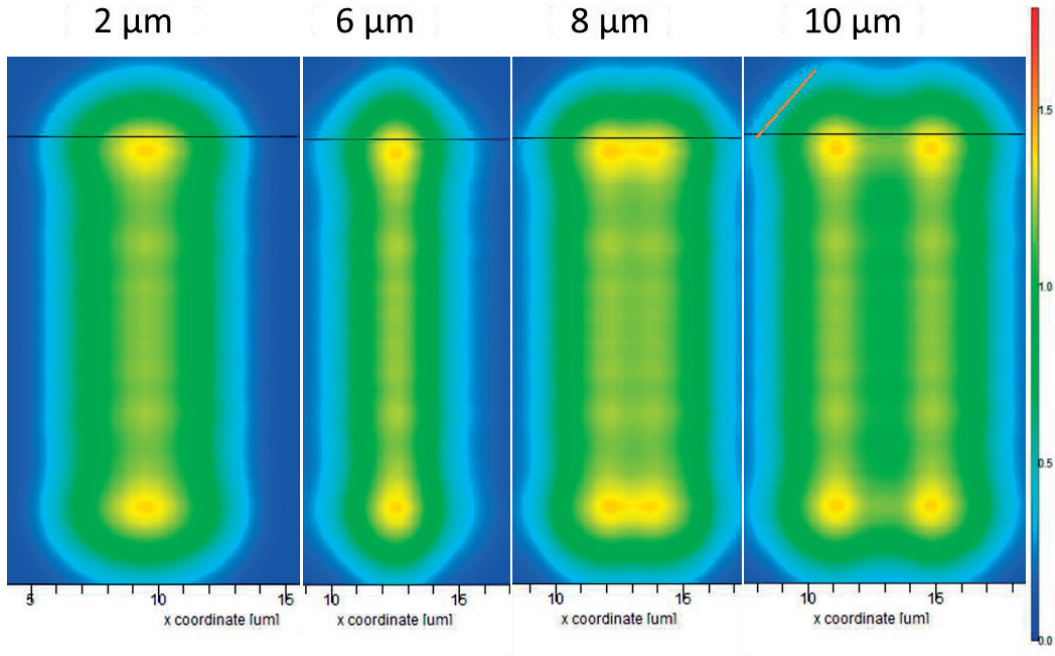


Figure 6. 1: Simulated aerial images of different line widths at $30\ \mu\text{m}$ proximity gap. Blue shows the low intensity regions and red shows the high intensity regions.

In Fig. 6.1 openings are shown, which means that blue is low intensity and red is highest intensity and one can also observe the self-imaging areas. Small structures at $2\ \mu\text{m}$ lead to strong diffraction and the effective line width will be much larger than $2\ \mu\text{m}$ for the desired printing gap. These effects have been described in the previous chapter also. Corners are rounded and cannot be corrected, as the whole aerial image is diffraction limited. At $6\ \mu\text{m}$, the aerial image is comparable with the original structure in width but the line ends are single rounded and there is no flat top end. For $8\ \mu\text{m}$ line width also, the line ends are changing in to a single rounded shape with very small flat top. However, for $10\ \mu\text{m}$ lines the edge or corner rounding happens at $30\ \mu\text{m}$. Both the corners at the line end changes to form round shape (and 45° slope), marked with orange line on the figure. Here, in the images we can see two types rounding at lines ends. One is the line end where both the corners are combined and forms a single rounded shape (eg: $6\ \mu\text{m}$, $8\ \mu\text{m}$). The other one is formed at $10\ \mu\text{m}$ line width, where both the corners on the line end changes its shapes to round, two corner rounding. Having this in mind, one can state that there is a minimum line width for which a correction can be applied to overcome the line end corner rounding. In our case, at $30\ \mu\text{m}$ proximity gap this seems to be a $10\ \mu\text{m}$ line width.

Keeping these factors in mind, the next step is to verify the previous rules and their effects at different proximity gaps. The study starts by comparing the aerial image simulations of

different correction features for a 10 μm line width and 30 μm proximity gap. Results are shown in Fig. 6.2 for different cases: no correction, a conventional serif corrected line end and our result. In serif method, the correction features that are added will hang outside the both ends of the line and it can be a small square, a small rectangle, a small circle, a small triangle or in general more complicated shapes. They are designed by considering the rule that additional feature is $1/4^{\text{th}}$ or less than that of the original line width.

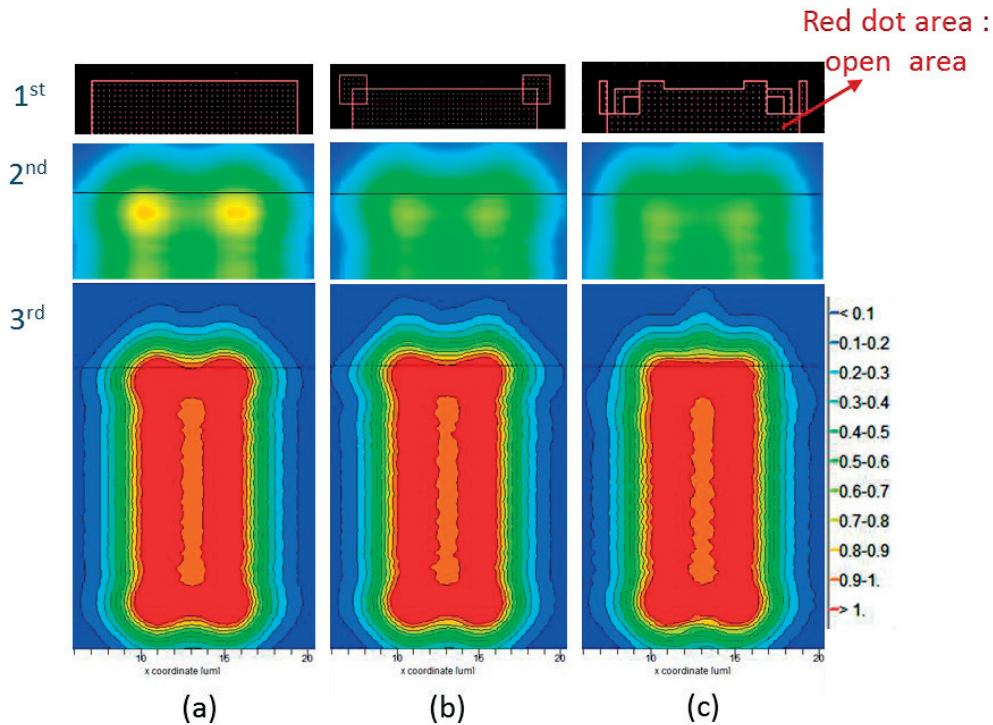


Figure 6. 2:(a) Feature (slit) with no correction, (b) Result obtained with the serif correction methods with conventional feature size and (c) result with the new rule based correction method using sub-resolution features. Here, the images are represented as three sets, first set is the drawing of the pattern, second set is the aerial image and third set is the aerial image in detail with intensity levels.

In Fig. 6.2 images that visualize the different exposure levels are represented by equal intensity lines normalized to one. The edge rounding is appearing in the original mask structure (Fig. 6.2(a)) due to the sharp (or perfect) corner shape. One can modify or reduce the diffraction effects of the sharp corner with sub-resolution features positioned around the edges of the structures. Serif like structures adding openings are shown in Fig. 6.2(b) and more complex structures are given in Fig. 6.2(c). To design a new rule based correction method we first consider the effects of the well-known method used for corner rounding: the serif method. In this method, the addition of corner projection improves the corner rounding. The first look of the aerial image (2nd set) shows the improvements of corners, (the blue and green image 6.2(b)) but the detail

analysis with different line plots with different intensity levels does not show any convincing improvements with serif. The results show that working conditions (dose and development) are difficult to define for serif correction due to the shallow contrast of the improved aerial image. The serif method does not work very well at $30\ \mu\text{m}$ proximity gap for mask aligners with MO exposure optics, which is why a new correction has been designed. The approach is based on modifying corner diffraction by adding much smaller shapes. The new correction method is designed by keeping the knowledge of previously set rules and their definitions. The serif technology of adding extra features on the side has also been used. Here, the aim is to correct the 45° slope of two corners at the line ends.

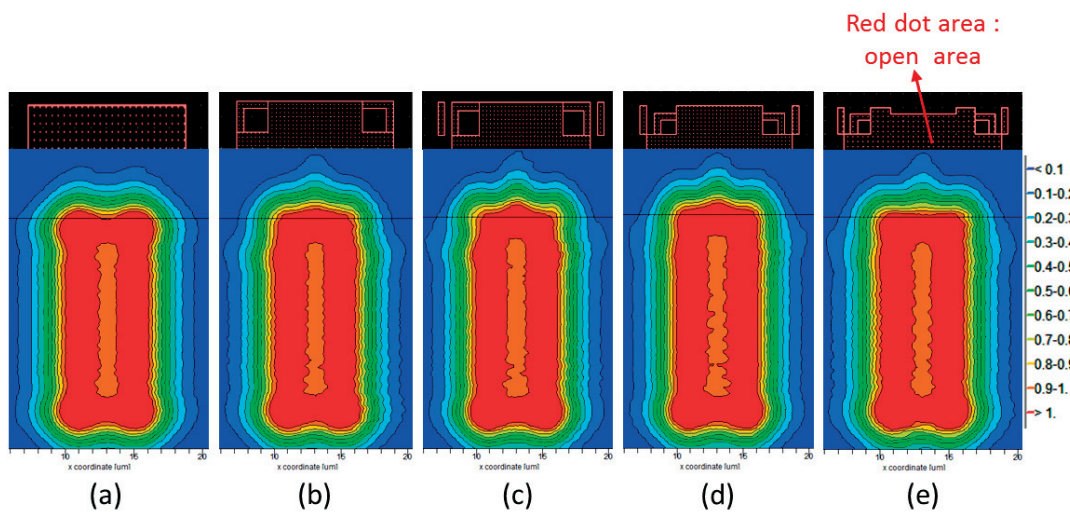


Figure 6. 3: Simulation aerial images of different correction structures at $30\ \mu\text{m}$ proximity gap. The fine black line is printed to guide the eye.

The main motto is that the feature being added should be in the size of sub microns, only then the superposition of the main structure and correction structure creates the effects, which tend to form the desired pattern. In Fig. 6. 3(b), the corners of the structure are carved in to L – shapes to increase the concentration of light. Adding extra lines to the feature increases the slope and steepness of the edge, which is an already well known in chapter 4 (correction technique for edges). This has been shown in Fig. 6.3(c). To reduce the light intensity at the top, some parts of the top is carved inside. This makes the corner and top layer more flat. Figure 6.3(d) and 6.3(e) defines these flat tops by cut off regions in the rectangle and the middle valleys. The target is to preserve the desired shape by preventing the dispersion of light. The optimal values for the widths of correction features are found after several numbers of rigorous simulations and analysis. Each feature size and position in the structure is changed separately and a best fit is searched. The best fit (figure or merit) is considered as the highest steepness of intensity change at a certain position in space or the smallest radius of curvature. At a time, only one feature size

is changed and the value for the best result is kept. In the next iteration the next feature is modified. The change can be either in feature width, length or it can be the distance between the features. After the optimization of all structures a second iteration of the procedure is done for selected structures to verify the quality of the result. An example is shown in Fig. 6.4.

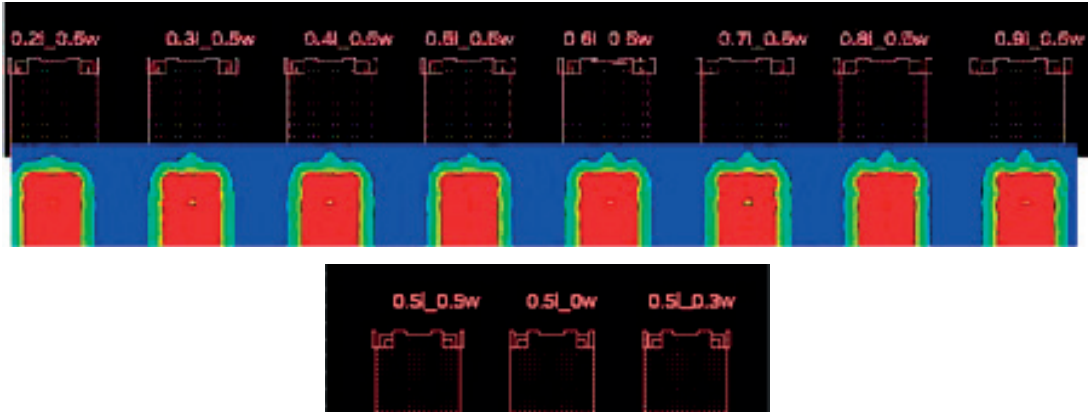


Figure 6. 4: Parameter variation in the OPC structure.

As we could see in Fig. 6.4, small feature helps to increase the resolution and gives the best optimized results. But considering the fact of Mask Rule Constraints (MRC), the dimensions below 500nm are not possible to write on the mask because of the pitch restriction and considerably increasing fabrication costs. Additionally, mask writing errors might be higher if the features sizes are small. Figure 6.5 shows the new rule based design for corner correction for mask aligners.

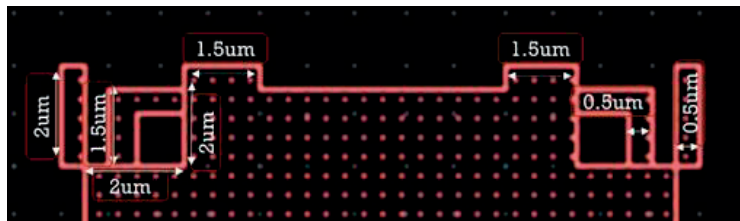


Figure 6. 5: The designed rule based structure for corners.

6.2 Characterization of the corner correction structure

The simulation and measurement starts with a structure of 10 μm and continue the characterization to printing of the structure on wafer also. The wafer used is a polished silicon wafer with 750 nm AZ1518 resist coated on it. Several wafers have been used with different exposure doses and exposure times to find out the exact parameters. The exposure parameters are varied from 37.5 mJ/cm^2 (1.5 sec) to 75 mJ/cm^2 (3.0 sec). The wafer was developed for 60 s in AZ 351B developer diluted at a rate of 1:6 with water. The clearing dose of the current wafer

setting was 37.5 mJ/cm^2 . The aerial images of simulation and measurements, and printing results for $10 \text{ }\mu\text{m}$ line width structure are represented in Fig. 6.6.

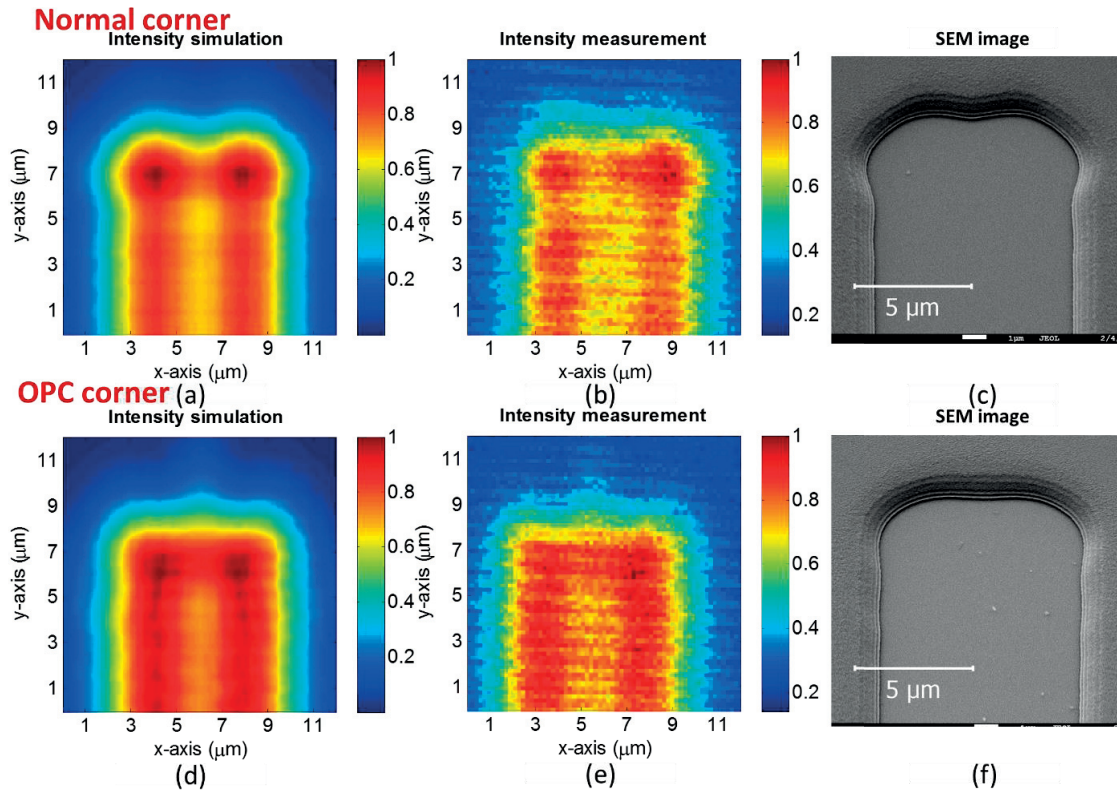


Figure 6. 6: The simulation, experimental intensity and SEM images on wafer of $10 \text{ }\mu\text{m}$ line width: normal (a, b, c) and corrected structure (d, e, f).

Figure 6.6(a) and 6.6(d) are the simulation results of the $10 \text{ }\mu\text{m}$ line width normal structure and optical proximity corrected structure, respectively, at $30 \text{ }\mu\text{m}$ proximity gap. Figure 6.6(b) and 6.6(e) are the experimental intensity image results from HRIM of the structure at $30 \text{ }\mu\text{m}$ proximity gap. The results show quite good similarity between simulation and experimental results. The SEM images (Fig 6.6(c) and 6.6(f)) of printing results on the wafer of a normal structure and OPC structure show the improvements on corners due to the high resolution features. The corner rounding at the line ends has been reduced considerably with the new corrected structure. The different intensity levels in simulation and experimental images can be interpreted in the form of exposure dose. From the images, it is clear that the color code with yellow (0.6) gives sharper corners and the lower intensity regions (0.2 - 0.4) changes the shape at the center by creating peaks and valleys on the structure. From the results in Fig 6.6, it is observed that the high intensity region (Fig 6.6 (d) region between 0.8- 1.0 intensity) is showing a change in the line width compared to the desired line width. It is therefore interesting to analyze such effects more and to study where exactly the intensity regions are falling for the different

printing doses. Figure 6.7 shows SEM images of the printing results for different exposure doses and its comparison with different intensity levels of the simulation.

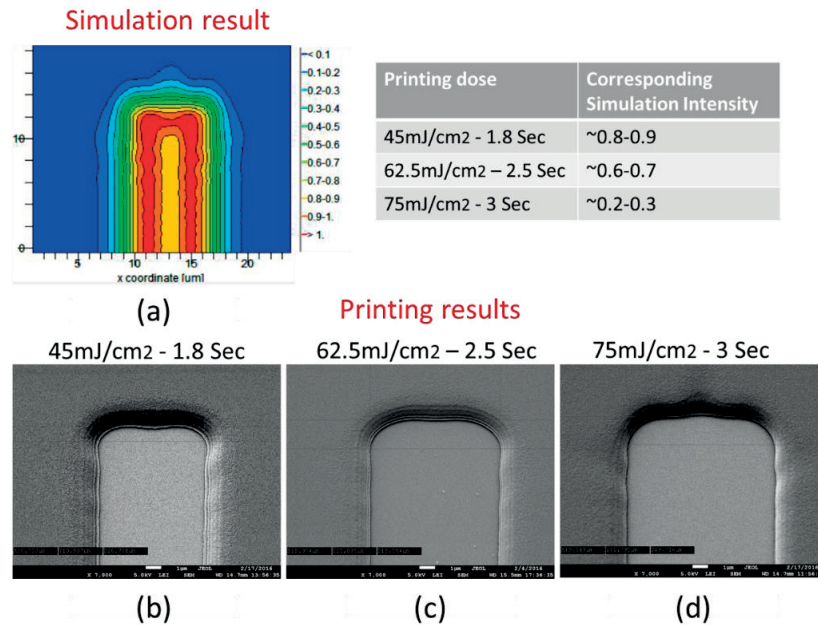


Figure 6. 7: SEM images of the 10 μm line width correction structure at different printing doses.

The dose at which all resist is removed from the wafer after uniform (no structure) exposure is named clearing dose. It depends on several factors like resist material, resist treatment (baking), resist thickness and development condition (developer concentration and time). In the current scenario (silicon wafer with 750 nm AZ1518 resist coated on), the clearing dose is 37.5 mJ/cm² (1.5 Sec). Often, the working point for the dose is set to two times the clearing dose. The simulation result of the corrected structure for 10 μm line width with its normalized intensity levels from 0.1 – 1.0 is represented too (Fig.6.7 (a)). The normalized intensity value 1 in the intensity scale corresponds to a clearing dose value of 37.5 mJ/cm² and the intensity 0.1 in the intensity scale corresponds to values more than two times the clearing dose (near to 80 mJ/cm²). The rest of the scale is a linear change of the intensity and each intensity level corresponds to an exposure dose. The SEM images of the printed structure on wafer are also shown in the figure for different exposure dose values (Fig. 6.7(b), 6.7(c) and 6.7(d)). With simulation intensity results and printed dose results, a comparison table has been prepared to define a process window for the structures. From the table it is inferred that, for the current structure, it is better to use a dose between 2.2 sec - 55 mJ/cm² (1.5 times the clearing dose) to 2.6 sec - 65 mJ/cm² (1.8 times the clearing dose). The clearing dose and just above clearing dose makes ear shapes at both end of the corners and also line width variation will turn up at these doses. Higher dose levels change the feature pattern by other characteristics variations, as one can notice in the small bumps that are present in the middle of the structure with a dose of 75 mJ/cm².

6.3 Results and findings of the corner correction structure

The findings with the above characterization can be defined with the help of process window. One important factor, which decides the process window, is the line width variation with exposure dose. The line width reduction will be different at different exposure doses.

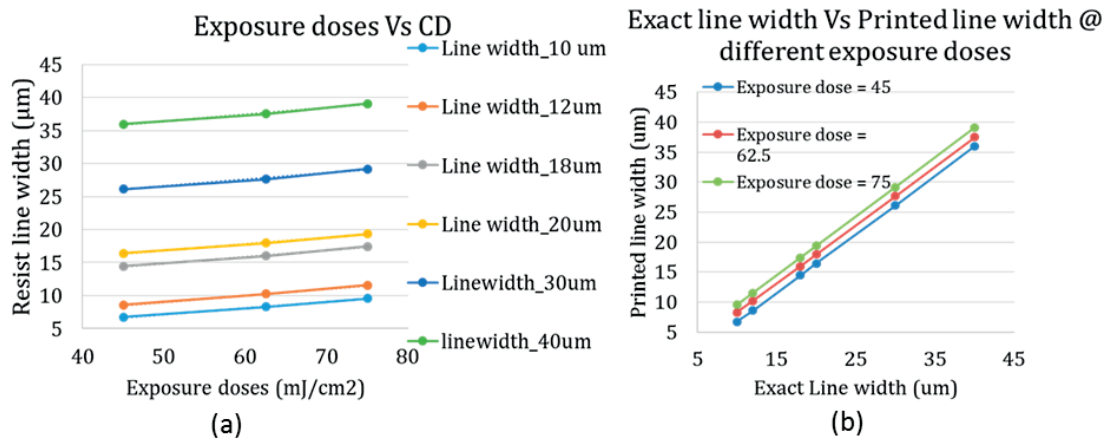


Figure 6.8: Line width variation at different exposure doses.

Figure 6.8(a) shows the line width variation with doses (Bossung plot) and Fig 6.8(b) shows the printed line width versus exposure doses. From Fig 6.8(a), lower dose of 1.8 sec - 45 mJ/cm² creates the reduction of the line width around 4 µm. The dose at 3 sec - 75 mJ/cm² (two times the clearing dose) gives almost the desired line width of 10 µm. The region which gives sharper corner reduces the line width between 1.5 µm to 0.5 µm. The process window can be defined at this point where the exposure dose is between 55 mJ/cm² (2.2 sec) and 65 mJ/cm² (2.6 sec). For Bossung plot, a linear regression was fit to each of the resist line width vs. exposure dose curves and the slopes were extracted. All the slopes are positive and the slope values are between 0.092 and 0.104.

In order to describe the corner rounding, we use the radius of curvature as another characterization parameter. The inner radius of curvature at the corners is used to point out the improvement provided by the new rule. Figure 6.9 shows an example of a radius of curvature definition for exposure of 2.2 sec and for a line width of 10 µm. All the defined curvatures are tabulated with the help of a circular fitting algorithm in Matlab. Circular fitting has been done by finding the position where curving of the line starts and making a 90° fitting with the line to get the radius of the circle.

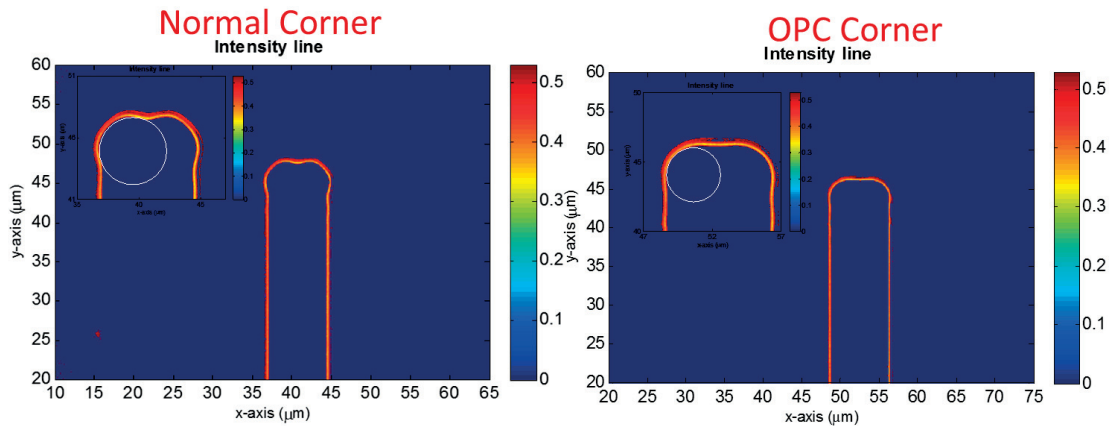


Figure 6.9: Inner radius of curvature definition for $10\ \mu\text{m}$ line width structure.

It is noticed that, for a normal corner the radius of curvature value is $2.72\ \mu\text{m}$ and for OPC corner the value is $1.95\ \mu\text{m}$. The corner with no correction (normal corner) is having higher radius of curvature compared to the proximity corrected design. The normal structure forms a dumbbell shape at both ends of the line at $30\ \mu\text{m}$ proximity gap. These dumbbell formations are reduced with the new correction method and it leads also to a reduced radius of curvature. The radius of the curvature can be reduced further using smaller feature sizes in the correction structure. In current optimized structure we have used a minimum feature size of $500\ \text{nm}$. But $200\ \text{nm}$ feature will give better resolution enhancement, but because of MRC, we are not using that. The minimum radius of curvature that one can obtain with respect to the above optimized structure is $1.3\ \mu\text{m}$. To illustrate this better, simulated values of the structure and inner curvature are plotted in Fig. 6.10.

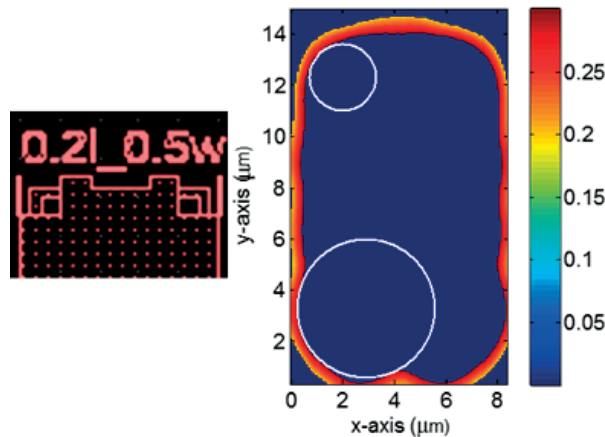


Figure 6.10: Minimum inner radius of curvature of optimized structure having $10\ \mu\text{m}$ line width.

Minimum radius of curvature value has been calculated with the simulated aerial images using Matlab algorithm which is mentioned above. A normal corner radius of curvature has also been included in the image at the bottom. One can notice the radius of curvature difference for a

normal corner and an OPC corner at a single sight. As explained earlier, high resolution correction features can be used for any line width structures in their Fresnel regime.

In order to verify that the new OPC correction rule can be applied to any larger line width, we show result of 40 μm line width.

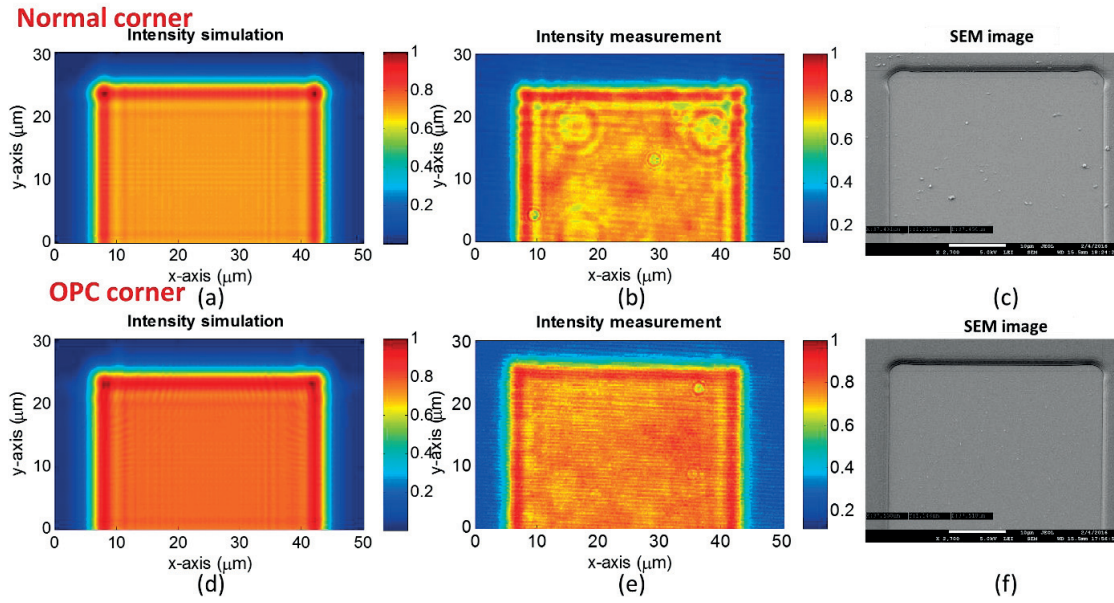


Figure 6. 11: The simulation, experimental intensity and SEM images of 40 μm line width: normal (a, b, c) and corrected structure (d, e, f).

The designed correction structure improves the corner and can be used for printing any line width on the same wafer at single proximity gap and with a single exposure dose. The radius of curvature improvement for different line widths and at different exposure doses has been tabulated in Table 6.1 for further reference.

Line width Vs inner radius of curvature

Line width (μm)	Expo 2.6sec normal (μm)	Expo 2.6sec OPC (μm)	Expo 2.2 sec normal (μm)	Expo 2.2sec OPC (μm)
10	2.85	1.85	2.725	1.75
20	2.85	1.95	2.75	1.85
40	2.95	1.9	2.75	1.8

Table 6. 1: The radius of curvature of different line width structures at different exposure times.

The radius of curvature varies only slightly for different exposure doses. The reduction of radius of curvature of the corner is more than 30%. The inner radius of curvature decreased to 2/3rd. The results with the line width change at exposure doses and the radius of curvature can now be used to define the operation point of the rule based corner correction design. With the above results, the optimal operation point is found as 1.5 times of the clearing dose (exposure

time of 2.2 sec, exposure dose: 55 mJ/ cm² in current scenario) since that gives better improvement values as compared to others.

Conclusion

A simple rule based correction method for corner solutions is defined to use in mask aligners based on free space propagation. A complete analysis cycle including designing, measurement, characterization and printing has been done to define the best process window. The universal correction structure can be applied to different line width and it is optimized for a printing gap of mask aligners set to 30 μm. The main advantage of the new correction structure is that different sizes of structures can be corrected and printed at same exposure condition (dose, distance and development) with high precisions at a single process step. The new OPC structure will be able solve the corner rounding problems in the industry up to certain level. The analysis so defined is purely based on the intensity evolution of light from structures and aerial image studies. The missing part is the phase evolution characterization and the following chapter will discuss the phase propagation.

References

- [6.1] K. Puthankovilakam, T. Scharf, H. P. Herzig, U. Vogler and R. Voelkel; “Unified rule based correction for corners in proximity lithography mask using high resolution features”; *IEEE microelectronic engineering*, **Vol. 172**; pp. 35-44(2017).
- [6.2] K. Yamamoto, S. Miyama, K. Koyama and S. Inoue; “Optical proximity correction method”; *US patent No. US005879844A*; (1999).
- [6.3] C.-J. Hsieh, J.-R. Hwang and J.-T. Huang; “Correcting the polygon feature pattern with an optical proximity correction method”; *US patent No. US006767679B2*; (2004).
- [6.4] N. Lu; “Serif mask design for correcting severe corner rounding and line end shortening in lithography”; *US patent No. US006127071A*; (2000).
- [6.5] O. Bula, D. Cole, E. Conrad, and N. Lu; “Serif mask design methodology based on enhancing high spatial frequency contribution for improved printability”; *US patent No. US 6,214,494 B1*; (2001).
- [6.6] K. E. Wampler and T. L. Laidig; “Method for generating proximity correction features for a lithographic mask pattern”; *US patent No. US005663893A*; (1997).
- [6.7] B.J. Lin; “A comparison of projection and proximity printings —from UV to x-ray”; *IEEE Microelectronic Eng.* **Vol. 11, No.1**; pp. 137-145(1990).
- [6.8] W. Henke, R. Schwalm, M. Weiss, and J. Pelka; “Diffraction effects in submicron

contact or proximity printing”; *IEEE Microelectron Eng.* **Vol. 10, No. 2**; pp. 73–89(1990).

- [6.9] D. M. Newmark, S. Vaidya, J. Segen, and A. R. Neureuther, “Large-area optical proximity correction using pattern-based corrections”; *14th Annual BACUS Symposium on Photomask Technology and Management*; pp. 374–386 (1994).

CHAPTER 7

Phase analysis of amplitude mask structures

- 1D and 2D

Until now, the chapters discussed aerial image study or intensity distribution of light. But there is no concrete study about the phase propagation from mask features and its developments on the mask. Here, the main aim is to observe both phase and intensity propagation from amplitude mask features. Structures used for the study are simple edges and corners in 1D and 2D respectively. The focus of the study is to understand the phase originating from sub resolution features or optical proximity correction structures and their effect on main structure parameters.

7.1 Importance of phase in light propagation

Phase plays a vital role in light propagation. Phase measurements are equally important as the intensity measurements. The imaging and visualization of optical phase and its modulations is always a challenge in optical industry. Interferometric technique is one of the best method to extract the phase information [7.1]. Sample arm (object arm) and reference arm will interfere and outputs can be recorded. Phase contrast imaging is one of the prominent techniques in microscopy to analyze the specimen. In lithography, phase transformations can be applied in beam shaping [7.2].

It is noticed that shaping of beam is the most important factor in proximity printing. The beam needs to be modified in way that the desired structure can be printed on the wafer. Intensity variation is the best way to modify the shape of the beam. The phase of the wave is having an enormous effect on intensity variation. To study and verify this factor, phase evolution from 1D correction structure is studied in more detail below.

7.2 Phase evolution from edge structure (1D)

Edge slope and steepness have been studied in the earlier chapter with simple edge and OPC edges. Slope of the edge is improved by adding sub resolution lines near to the edges (one-line and two-line edge correction structure). Here, the analysis is to study the phase propagation from the corrected edge defined for 30 μm proximity gap. The sample analyzed here is the edge with two line corrections. Simulations are carried out by CST Studio Suite FDTD simulation

because of the phase analysis [7.3]. Experimental results are done with HRIM with TOPTICA laser (405) nm. The reference arm having a mirror and mounted on piezo actuator allows the phase shifting for the phase measurement.



Figure 7. 1: 1D OPC structure for phase analysis

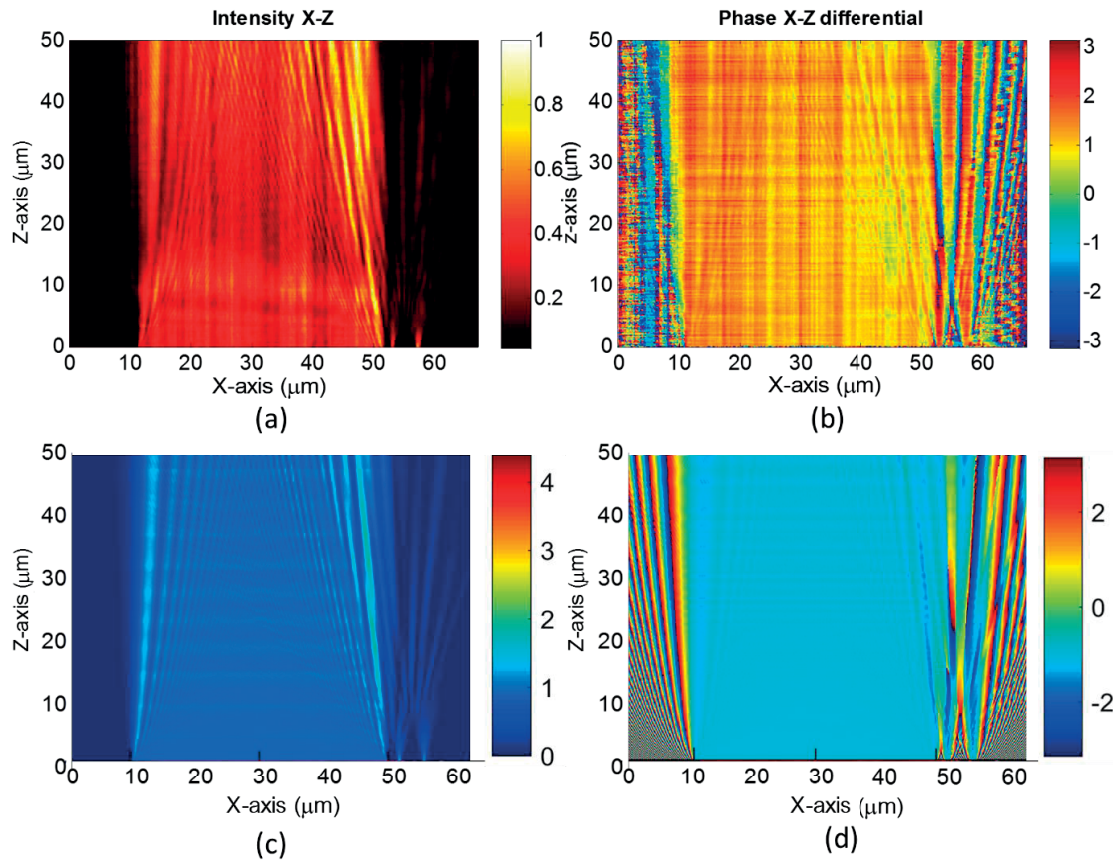


Figure 7. 2: Intensity and phase behind an OPC structure similar to that one given in Fig.7. 1. (a) and (b) HRIM measurement intensity and phase. (c) and (d) are FDTD simulation results.

The measurement technique used to calculate phase is the differential phase [7.4]. When a wave is propagated through a sample region, it gets perturbed. The waves outside the sample region won't be perturbed and it will continue to propagate as normal plane wave. The normal wave propagation is the reference zone and the phase in that region is considered as a constant phase. The difference between reference zone phase (constant phase) and the perturbed wave phase is called as differential phase. This is represented in Fig. 7.2(b) and (d). Both the simulation and measurement results behave in the same pattern. One can notice that, adding small features near to the edge has shown change in the phase distribution. A closer look at the figure shows that, the phase on the left side of the figure (no correction feature) is having a continuous phase and on

the right side (with correction feature), the phase varies. The intensity is also behaving in the same way. The side with the correction feature got higher intensity values as compared to the other side with no correction feature, after 10 μm propagation distance. The interesting region here is the 30 μm proximity gap zone since the correction structure was defined for 30 μm gap. A strong fluctuation of phase is visible around this region. The phase has almost changed from 0 to π . It shows that the phase variation from the samples is having a greater effect on intensity fluctuation. This understanding helps us to think about creation of phase singularities.

Phase singularities are zero intensity regions. If the phase difference between two neighboring points in the space is close to π , then the intensity distribution between these points will be near to zero. This is named as phase singularity or optical vortex [7.5]. Micro and nano structures that can create phase singularities were theoretically and experimentally studied some years ago [7.6, 7.7]. Creation of optical vortex with different phase level mask was introduced by M. D. Levenson in 2002 to create 80 nm contact nodes in lithography [7.8]. The vortex was composed of four regions with phase of 0° , 90° , 180° and 270° to print sub resolution structures. Meeting point of all four phases creates a phase singularity and the end result was vertical steep walls [7.9]. As we know, the Phase Shifting Masks (PSM) are costly for defining four phase shifts. The question here is whether the creation of vortex is possible in amplitude mask by designing the OPC features wisely. If the technique is successful, then it will be more economic when compared to the PSM technique. To understand the phase propagation from amplitude features, 2D correction features designed for a corner correction in amplitude mask is studied below. Results of 2D correction feature is partially published in SPIE proceedings [7.10].

7.3 Phase evolution from corner structure (2D)

The goal here is to study the light evolution from OPC structures defined for corner correction at 30 μm proximity gap. The aim is to study the interplay between phase and intensity. Whether phase singularity creation can define the structure or not is also studied.

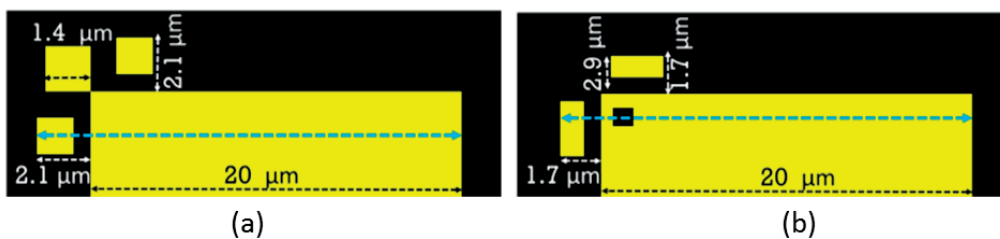


Figure 7.3: 2D OPC structure for phase analysis.

The correction features in Fig.7.3 consist of squares and rectangles that are less than 2 μm in size. The structure on the Fig.7.3 (a) consist of 3 squares near to the corner to increase the resolution and the other one (Fig.7.3 (b)) consist of rectangles and one negative square inside the open area

near to the corner. The small amplitude features creating sharp phase changes is not yet discussed in many literatures and here the study is to get a full potential about such an approach.

The blue dashed line in Fig. 7.3 represents the x-z plane for propagation analysis (line cut for propagation) and the dashed line crosses on the correction structures. The phase and intensity propagation analysis has been done for a proximity gap of $40\ \mu\text{m}$.

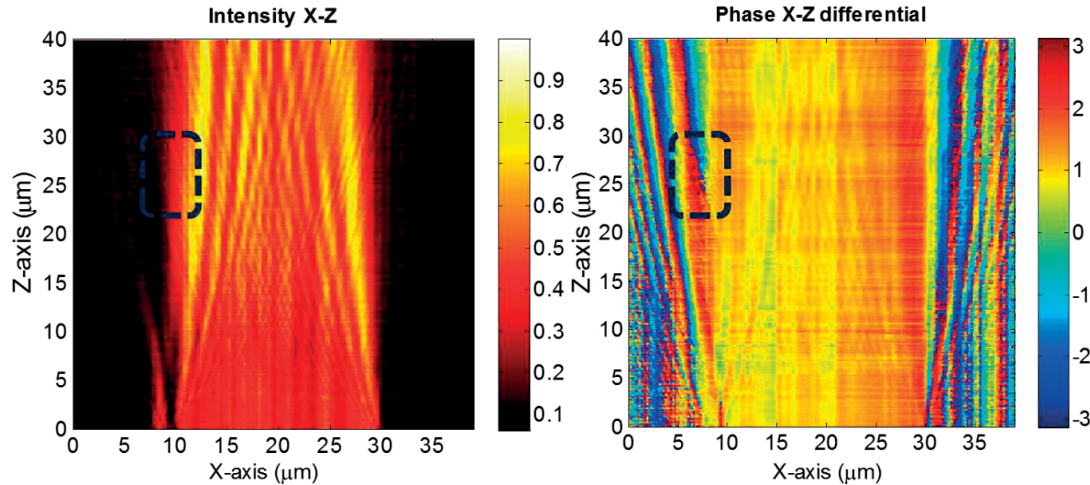


Figure 7. 4: Intensity and phase behind an OPC structure similar to that one given in Fig.7. 3(a).

The phase image clearly shows the propagation difference when compared to a corner without any correction (right side of phase image) and corrected corner (left side of the phase image). As described earlier, the correction structure was designed for printing at $30\ \mu\text{m}$ proximity gap. After $25\ \mu\text{m}$ of propagation, there is an abrupt change in the phase visualized by blue dashed line rectangle. One difficulty to interpret phase images is that many features are usually found in the zones where there is no light. For normal corners, the high intensity zones and contrast variations are coming at $x = 30\ \mu\text{m}$ but the phase stays almost constant during the propagation. This is different for the corrected structure where the phase change ($x = 10\ \mu\text{m}$) is close to intensity edge and seems to be created at this position. The small squares as correction structures shapes the phase to get higher contrast and sharper corner. The problem is of course more complicated because of its three dimensional nature. Therefore, to understand more about the shaping, closer look at the x-y planes of different proximity gap settings is needed. Fig. 7.5 gives an idea about the intensity and phase images at different proximity gaps.

Figure 7.5(a) shows the intensity and phase image just above the plane, in the so called contact region. In the contact region, the diffraction effects are not prominent. The intensity shows the same features as the mask pattern and the phase is constant for all openings (blue and dark red). As discussed above, the phase change happens approximately after $25\ \mu\text{m}$. In order to gather more details, the intensity and phase x-y images at $20\ \mu\text{m}$ and $30\ \mu\text{m}$ are plotted for the comparison.

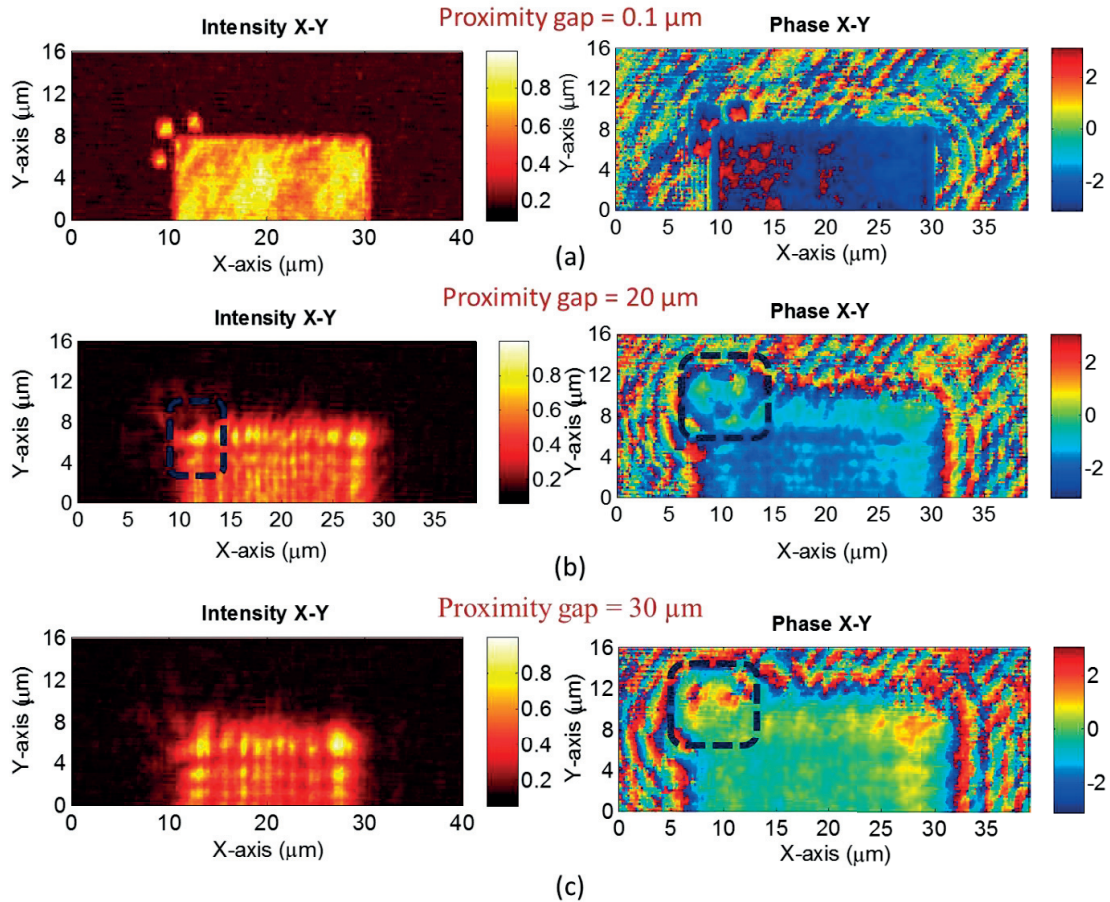


Figure 7. 5: The measured intensity and phase image of the corner structure at different proximity gaps between the mask and observation plane. (a) Image at 0.1 μm proximity gap, (b) image at 20 μm proximity gap and (c) image at 30 μm proximity gap.

Figure 5 (b) is the intensity and phase image at 20 μm proximity gap. A closer look at the intensity images of Fig.5 (b) and 5(c) (dashed line rectangle), reveals that the corners with correction structures are becoming sharper without much spreading due to a hotspot creation. The contrast of the structure with correction features is much better at 30 μm proximity gap. In the intensity image of the corner without correction, the diffraction from the corner is the dominant mechanism that changes the intensity field. The phase images of Fig. 5(b) and Fig. 5(c) show the phase changes that are involved to modify the light pattern. The blue dashed squares in the phase images represent the phase formation. At 20 μm proximity gap, phase changes due to corner correction is not sharp. The color code in the phase images represent the phase changes that is happening in the corners. At 30 μm , the correction structure makes a sharp phase change of π (green- 0 to red-3) around the high intensity spot considered as the corners tip. The phase changes help to shape the light to make sharp corners by surrounding it with abrupt phase changes. To understand more about such phenomenon, one more corner correction structure and

its intensity and phase evolution will be analyzed. This time an inversed amplitude element is also involved as a correction feature. The corner having two rectangles near the corner and having a negative square is represented in Fig.7.3 (b) and, the evolution measurement along the blue line, intensity and phase evolution is plotted in Fig.7.6.

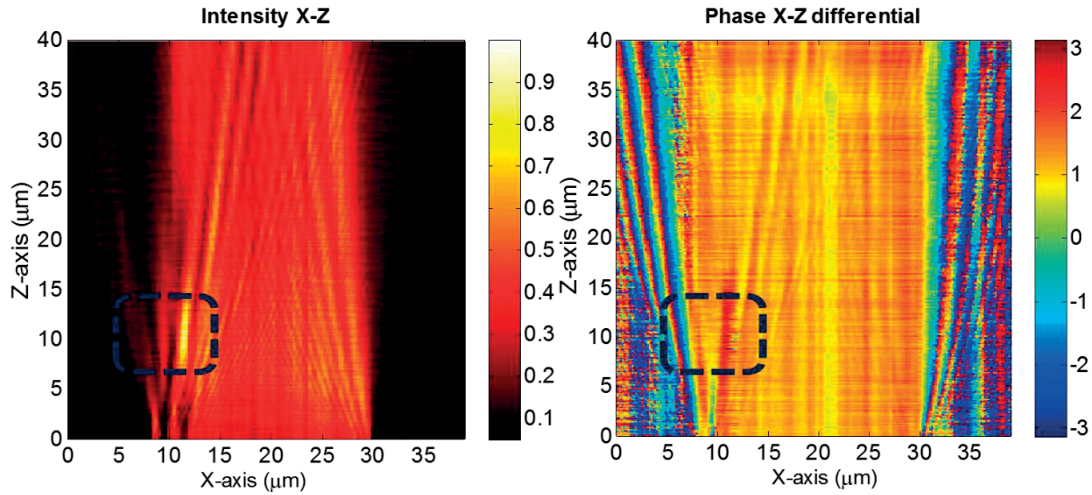


Figure 7. 6: Intensity and phase behind an OPC structure similar to that one given in Fig.7. 3(b).

In Fig.7.6, from the inverted square region a phase fluctuation and an intensity hot spot are visible around 10 μm distance behind the mask (represented by blue dashed rectangles on the images). At 10 μm , the obstacle (negative square) creates the concentrating point with sharp intensity. What we also see is that nothing particular happens anymore after this for the propagation, neither in amplitude nor in phase. Figure 7.7 gives the corresponding x-y plane images at proximity gaps just above the mask plane and proximity gaps of 10 μm and 30 μm . At mask plane, the intensity image shows the correction structures of two rectangles and the small negative square. The phase image in the mask plane clearly shows the uniform phase in the open regions of the mask and undefined values shown as color speckles of the opaque zones. The obstacle seems to have an initial phase shift, the value is close to π phase difference (light blue represents 0 for negative square and dark blue represents the $-\pi$ for open areas from the color codes of phase image). The intensity images at proximity gaps of 10 μm and 30 μm show how diffraction from small features changes the pattern configuration. High contrast and bright spot (blue dashed line square) created at the corners of 10 μm proximity gap have higher probability to build the desired pattern than at higher gaps. The phase image at 10 μm is modulated by the bright spot and sharp phase change of π occurs (the red bright spot inside the blue dashed line square). The consequence of such a focusing regime is a higher sensitivity to proximity gap distances compared to the situation with positive correction structures only (compare to Fig. 7.4). At 30 μm proximity gap, there is not much change of phase compared to the intensity changes. This correction structure may work better at lower proximity gaps than at a higher gap.

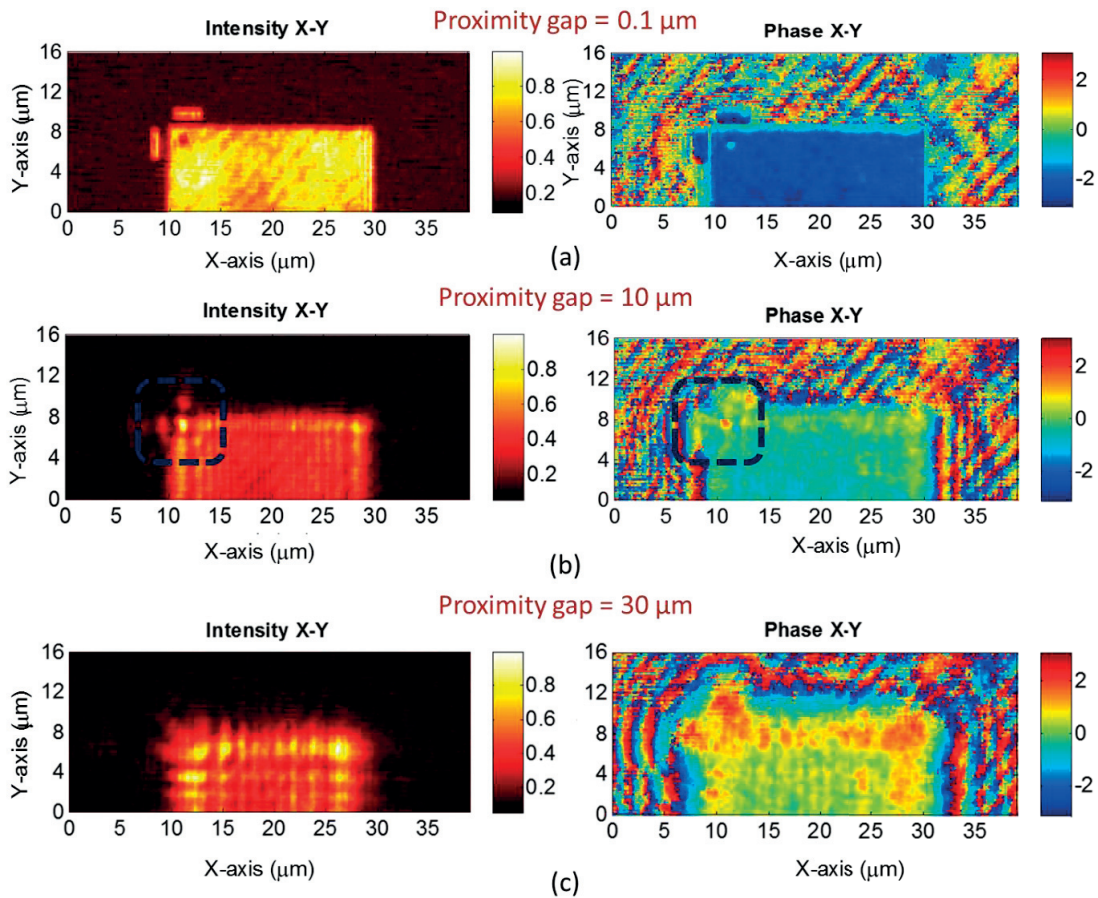


Figure 7.7: The measured intensity and phase image of the corner structure at different proximity gaps between the mask and observation plane. (a) Image at $0.1 \mu\text{m}$ proximity gap, (b) image at $20 \mu\text{m}$ proximity gap and (c) image at $30 \mu\text{m}$ proximity gap.

This is the first set of measurement that analyses how submicron optical proximity correction structures play their role in the propagation of phase and shaping the light to desired pattern. The above images and results show that steep phase variations can be induced with amplitude structures at a large distance behind the mask. It seems that more OPC elements are needed to find a reliable design scheme with sufficient parameters to move the phase singularities to the desired position.

Conclusion

The importance of aerial images or the intensity distributions for getting the desired pattern at printing level has been known to the lithography industry for some time. The coherence management with microlenses, Illumination Filter Plates (IFP) also play a major role in aerial image formations. However, the significant role played by phase for shaping the light to get the

desired pattern for amplitude structures was not recognized. The above studies reveal the phase distributions and phase evolution of different optical proximity corrected structures at different proximity gaps. A first situation is with 1D correction structure for edges where the phase made a sudden phase shift to get the desired pattern. This result paved the idea of creation of phase singularities by OPC features. A Second case was discussed with 2D correction features – OPC correction features for corner at 30 μm proximity gap - and explains where the phase evolution limits the spreading of light. Third situation is explained with negative square and it shows that, focusing of light can be achieved by small obstacle. Phase analysis reveals that more studies are needed to define exact OPC feature for the creation of phase singularities. But this phase definition will help the printing industry to reach higher resolution limits.

References

- [7.1] J. Glückstad and D. Palima; “Generalized Phase Contrast”; *Springer, Netherlands*; pp. 1-5(2009).
- [7.2] R. Barer; “Some Applications of Phase-contrast Microscopy”; *Journal of Cell Science* **Vol. 88, No. 4**; pp. 491-499(1947).
- [7.3] Computer Simulation Technology (CST); “STUDI SUITE – Microwave studio” 3D electromagnetic simulation software.
<https://www.cst.com/>
- [7.4] M.-S. Kim, T. Scharf, C. Etrich, C. Rockstuhl, and H. P. Herzig; “Longitudinal-differential interferometry: direct imaging of axial superluminal phase propagation”; *OPTICS LETTERS* **Vol. 37, No. 3**; pp. 305-307(2012).
- [7.5] H. Aagedal, M. Schmid, T. Beth, S. Teiwes and F. Wyrowski; “Theory of speckles in diffractive optics and its application to beam shaping”; *Journal of Modern Optics* **Vol. 43, No. 7**; pp. 1409-1421(1996).
- [7.6] C. Rockstuhl, M. Salt and H. P. Herzig; “Theoretical and experimental investigation of phase singularities generated by optical micro- and nano-structures”; *Journal of Optics A: Pure and Applied Optics* **Vol. 6**; pp. S271- S276 (2004).
- [7.7] G. Gbur and T. D. Visse; “Phase singularities and coherence vortices in linear optical systems”; *Optics Communications* **Vol. 259**; pp. 428–435(2006).
- [7.8] M. D. Levenson, G. Dai and T. Ebiharac; “The Vortex Mask: Making 80nm contacts with a twist!”; *Proc. SPIE 22nd Annual BACUS Symposium on Photomask Technology* **Vol. 4889**; pp. 1293-1303(2002).

- [7.9] M. D. Levenson, T. Ebiharab, Y. Morikawac and N. Hayashic; “Vortex Via Validation”; *Proc. SPIE 23rd Annual BACUS Symposium on Photomask Technology* **Vol. 5256**; pp. 93-102(2003).
- [7.10] K. Puthankovilakam, T. Scharf, H. P. Herzig, U. Vogler, A. Bramati and R. Voelkel; “Phase analysis of amplitude binary mask structures”; *Proc. SPIE Optical Microlithography XXIX* **Vol. 9780**; pp. 97800V 1-7(2016).

CHAPTER 8

Phase and intensity analysis of phase mask structure

Phase shifting mask (PSM) technology is one of the most prominent resolution enhancement technology in the field of lithography. The previous chapter gives a hint about the propagation in amplitude mask, but the question still exists about the phase and intensity propagation in phase masks. This chapter characterizes a phase shifting mask structure which is designed for corner corrections. The Intensity and phase propagation analysis and also the importance of Lohmann images will be discussed. Of particular interest are tolerance against proximity gap variation and the theoretical explanation of the resolution in printed structures. The chapter is based on the results published in Journal of Micro/Nano Lithography, MEMS, and MOEMS [8.1].

8.1 Phase mask and structure definition

The success of phase mask technology is in the creation of high contrast difference by proper structuring of the mask levels [8.2]. The test structure is a group of corners or elbow structures from a phase shifting mask [8.3]. Tina Weichelt (Friedrich-Schiller-Universität Jena) has developed the mask. The structure and details of the selected structure are described in Fig. 8.1.

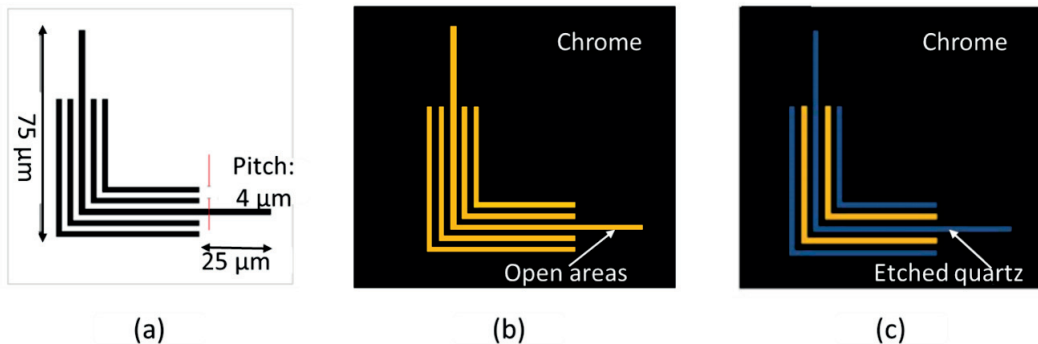


Figure 8. 1: Structure considered for our experiments, (a) is the geometry of the structure, (b) amplitude structure [yellow lines are the open areas] and (c) shows the structure with phase shifts [yellow lines are the open areas and violet areas are the etched quartz] of π or half wavelength.

The structure has a pitch of 4 μm and field size of 75 μm*75 μm. The substrate material is fused silica (quartz) and the structure is etched in such a way to get a phase shift of π or half

wavelength for the design wavelength, which was 365 nm. The smallest feature size is a 2 μm line and the objective is to print the structure at a distance of 30 μm .

A stabilized monomode laser with coherence control from TOPTICA (TopMode CHARM) having a wavelength of 405 nm and 50 mW power is used to achieve a fully coherent illumination regime. For the current measurements, we are using a high resolution 20X/ NA 0.75 dry objective (NIKON CFI Apochromat VC) corrected for 405 nm with the corresponding tube lens. The reference arm has a mirror and is mounted on piezo actuator to allow the phase shifting and a proper reconstruction of the measured phase. Differential phase is used to visualize the phase field [8.4].

8.2 Measurements and recordings from structures

First step is to visualize and observe the intensity and phase behavior of amplitude mask and phase mask structures respectively. The study is just above the mask plane and results are represented in Fig. 8.2.

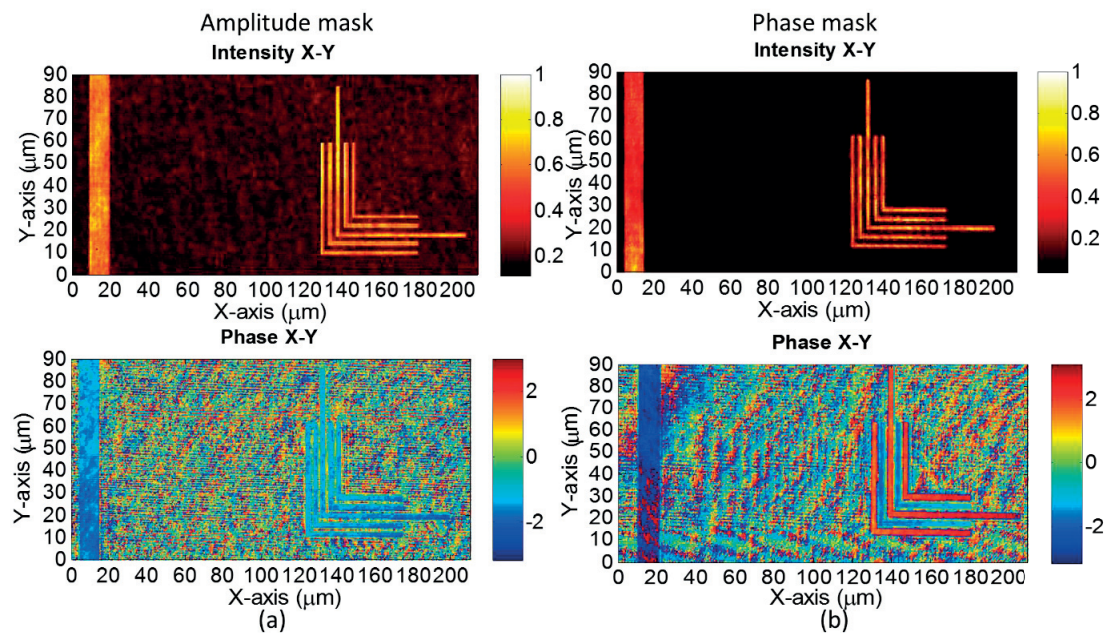


Figure 8. 2: The measured intensity and phase image at 0.1 μm proximity gap between the mask and observation plane. (a) Amplitude mask and (b) Phase shift mask. The intensities are normalized from 0 to 1, and phase values are from $-\pi$ (-3.14) radian to π (3.14) radian.

The intensity images of both amplitude structure and phase structure in Fig. 8.2(a) and Fig. 8.2(b) clearly shows the structure definition and its features. As reference zones, we are using the wide open areas in the field of view which are far away from the measurement area to ensure that the reference line does not influence the measurement. In Fig. 8. 2(a), the phase image shows constant phase at openings indicated by uniform color. In zones without intensity beside the high

intensity zones, the phase could not be evaluated which causes an undefined phase pattern. In Fig. 8. 2(b) within the opening of the mask, one can clearly see the phase difference ($4/5\pi$) between the open chromium and etched quartz in the corner structures with the color code: one part is red and the other part is blue respectively. The blue color refers to a certain phase level that is the same as the non-etched openings of the functional structure. Images in the above figures clearly show the phase measurements and differences between a normal amplitude structure and phase structure.

8.2.1 Propagation Measurement: x-z

The main focus in the experiment is the propagation measurement from a phase mask (propagation axis is z). The measurement evaluation will be easy if the simulation results are available. The first step for that is to create the structure and verify the simulation results. The selected two structures, one amplitude and the other with phase structure are plotted with same parameter conditions including reference line. The line cut region of mask structure will look like the structures in Fig. 8.3. This makes the simulation easy and one-dimensional. The wavelength used for the simulation is 405 nm. A perfectly collimated (parallel) illumination is chosen in order to make sure that simulation and measurement conditions are as close as possible.

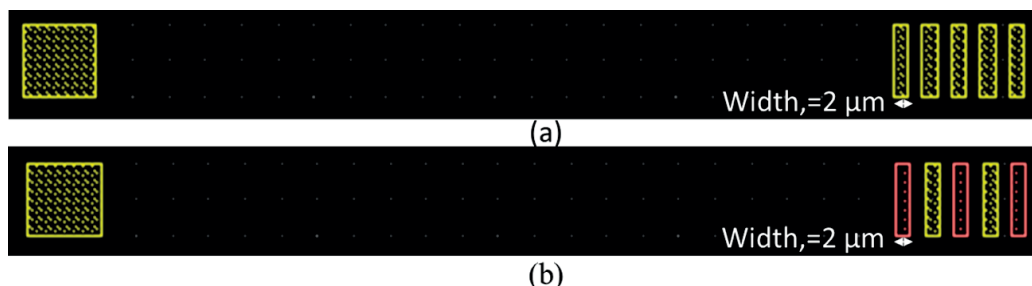


Figure 8. 3: The simulation structure. (a) Amplitude structure with 2 μm openings and 4 μm period (b) represents the PSM Structure of 2 μm openings and 8 μm period with phase changes similar to the measurement structure.

Figure 8.3 shows the structures used for simulation in one-dimension (line profile shape). The amplitude structure (Fig. 8.3(a)) is of lines with a width of 2 μm and a pitch of 4 μm. The phase structure (Fig.8.3 (b)) has phase difference between consecutive openings of half a design wavelength (π). The opening at the left is used as a reference. The width of the phase structure feature is 2 μm and the period is 8 μm because the phase structure alternates which leads to a doubling. To retrieve propagation data in z direction, line cuts of the desired areas are used (white dashed line on the intensity images of Fig. 8.2(a) and Fig. 8.2(b)).

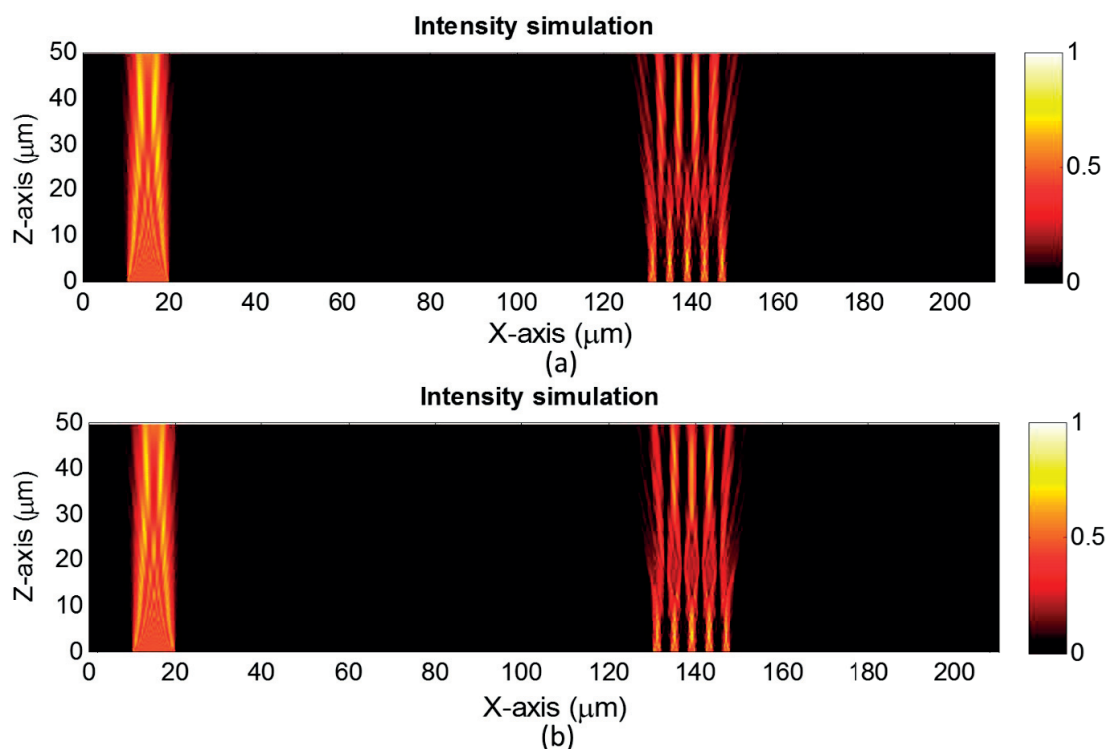


Figure 8. 4: The simulated light field propagation through (a) Amplitude structure and (b) PSM structure for a proximity gap of 50 μm . Intensities are normalized to the maximum intensity.

Figure 8.4 reveals that the diffraction of light leads to varying intensity profiles at different proximity gap as expected. One can observe that, regions of highly confined light fields and diffraction effects are different for a normal amplitude mask and the phase mask. The diffraction effects depend on Talbot length also. For lithographic printing, several parameters are important: the contrast of the structure, the definition of the structure and its position. To get the complete picture, the mask structure is analyzed with HRIM propagation measurement. Figure 8.5 describes the evolution of light through the measured region of the structure at a position indicated by the white line in Fig. 8.2(a). The aerial images are recorded at different distances between mask and wafer with increasing distance of z from the mask.

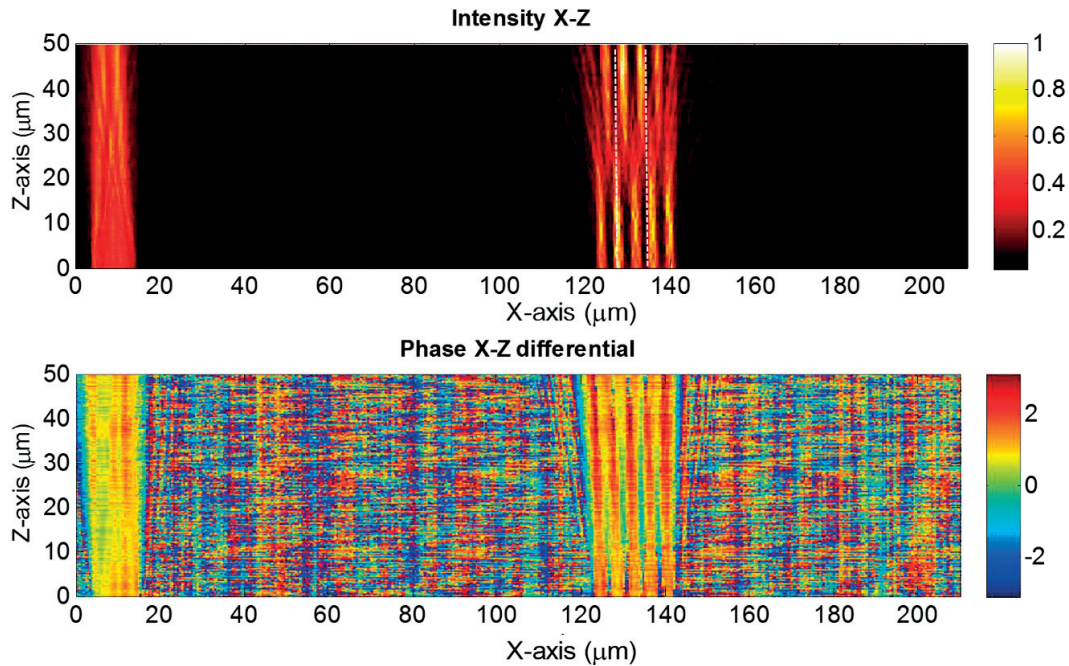


Figure 8. 5: The measured intensity and phase image of the light evolution for a proximity gap of $50\ \mu\text{m}$ in amplitude structure.

In the above figure, it is observed that particular light bundles are visible in the intensity images that have a well-defined phase value. At zones with low intensity, for instance between $30\ \mu\text{m}$ and $110\ \mu\text{m}$ lateral positions (x-axis), the phase cannot be evaluated. Different interesting regions for printing can be defined and verified by the intensity measurement for different zones of proximity gap. The regions till $20\ \mu\text{m}$ of the proximity gap, all the lines are visible and good for the printing. However, just after that one can see the diffraction effects are prominent and lines are not any more differentiable. The regions just above diffraction regions, the contrast is coming back for the lines. One counts only four intensity highs and sees a change of position shift. To guide the eye, white dashed lines are added in the intensity image of Fig. 8.5. Simulations of the amplitude structure in Fig. 8.4 (a) also verify this change in features and positions. The position shift is explained by the Talbot effect and further explanation is in the discussion section below. To avoid the lateral shift and to print the correct structure on the exact positions of the mask, phase shifting mask can be used. Figure 8.6 shows the propagation of light through the phase shifting mask structure through the white dashed line region defined in Fig.8.2 (b).

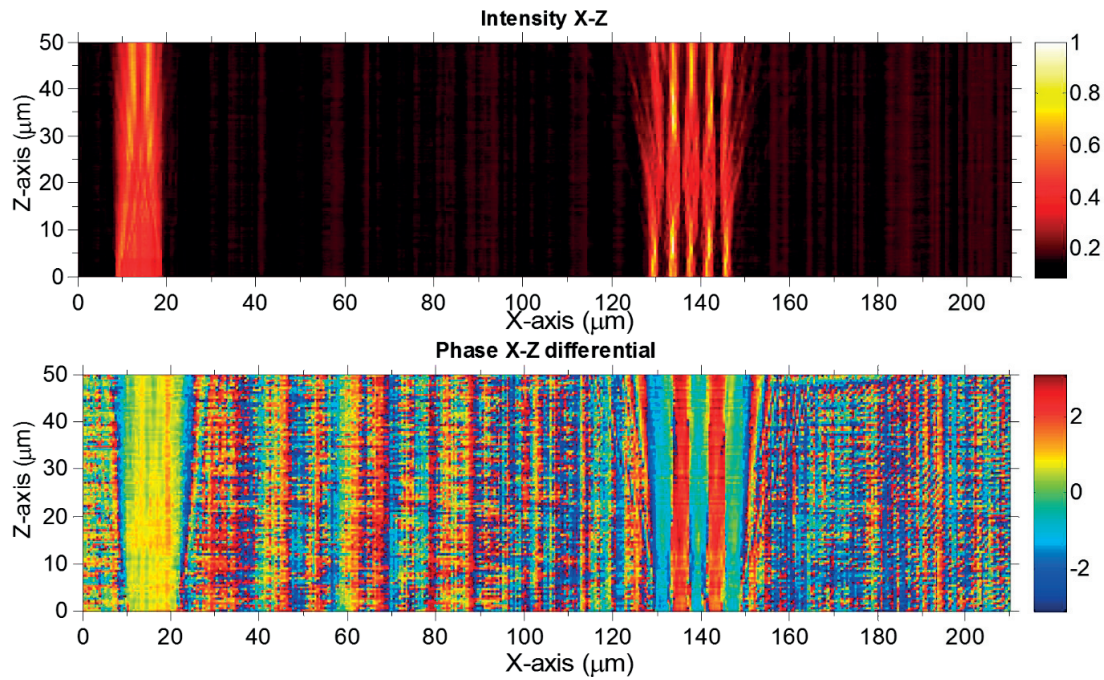


Figure 8. 6: The measured intensity and phase image of the light evolution for a proximity gap of $50\ \mu\text{m}$ in a phase structure.

In intensity image (Fig. 8.6), the high contrast region after the diffraction effect appears at the same position and has the same high intensity distribution exactly at the opening. Phase image clearly shows the phase difference between open chromium and etched quartz during the propagation of light and how it carries the information all along the propagation distance. To discuss the particularities of propagation, a closer look at the propagation measurement of intensity is needed. There are three zones which are distinguished along the propagation direction (z -axis). The first zone is just above the mask or the so-called contact region and extends from mask level to approximately $10\ \mu\text{m}$ proximity gap. Here the structures have high contrast and all openings lead to intensity peaks. Printing in this region gives good results, but a small proximity gap carries the risk of touching the masks and damaging it - a known problem for contact printing. A second zone defined between $10\ \mu\text{m}$ and $32\ \mu\text{m}$, where one can clearly observe the washing out of the well-defined intensity profile by diffraction effects. The contrast and shape of the structures are almost lost in this region and printing would lead to unsatisfactory results. The third zone extends just after this diffraction zone and ranges from $32\ \mu\text{m}$ to $50\ \mu\text{m}$. In this zone, at some regions, the profile regains its properties but usually with less contrast. Especially the high intensity lobes at the outer area are altered. To understand better what causes such behavior, all the three regions are evaluated more carefully with x - y plane intensity and phase images.

8.2.2 Image plots: x-y

To make a better judgment on resolution and process window, image plots and line plots are studied in detail at different proximity gaps. Figure 8.7 represents the intensity and phase images of the x-y plane at 5 μm proximity gap and also the line intensity plots which have been averaged over several lines along the y-axis (35 μm to 55 μm) to increase the quality of the plot.

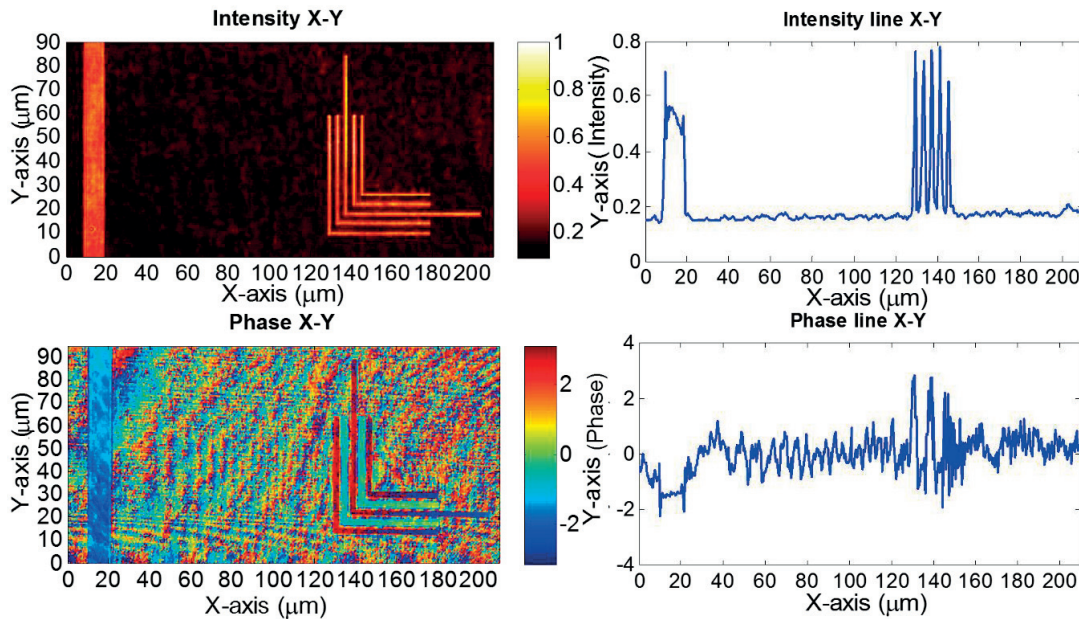


Figure 8. 7: The measured intensity, phase and line image of the phase shifting mask structure at 5 μm proximity gap.

The intensity image at 5 μm proximity gap represents an ideal situation and shows all desired features of the structure, the five intensity maxima with good contrast. The phase image represents a phase shift of π or half wavelength between the etched quartz and open chromium at the designed position. The peaks in the line plots of Fig. 8.7 show very good agreement with the set phase shift of π within the precision of this measurement. The second zone of interest is between 10 μm and 32 μm , where diffraction plays a major role. This zone is the typical working distance where standard mask aligners would deliver sufficient precision for positioning of the mask and wafer. Therefore, it is very interesting for technical applications. Figure 8.8 represents the second zone line image at 22 μm proximity gap. From the intensity x-y image, it is clearly observed that the intensity image does not show the designed features anymore.

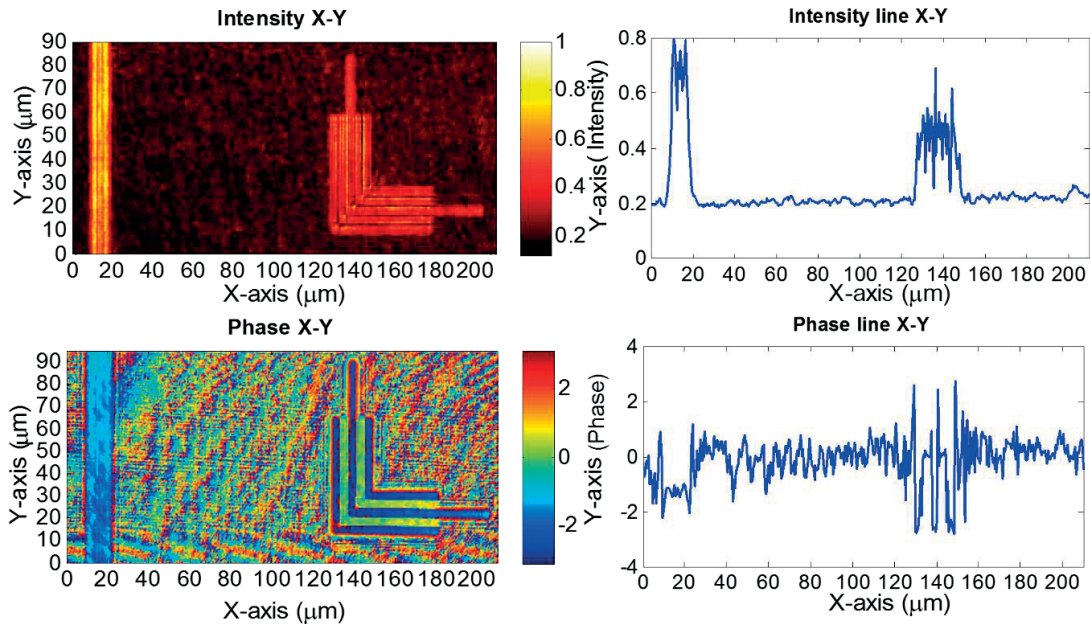


Figure 8. 8: The measured intensity, phase and line image of the phase shifting mask structure at $22\ \mu\text{m}$ proximity gap.

From Fig. 8.8, the specific intensity profile of five peaks is lost as well as the good contrast. The low intensity regions between the multiple structures that are important for printing are washed out. Contrary to the intensity images, the phase images are still showing pronounced phase separation between zones. At some positions, zero intensity is found which is visible when comparing the intensities and phases in Fig. 8.8. Main observation here is that, intensity zero regions are becoming very fine features and cannot be used for proper structure definition in printing. Because printing is based on intensity profiles, the region between 10 and $32\ \mu\text{m}$ should be avoided for the geometry considered here (feature size and period). The reason for this will be clear by considering the Talbot effect, which is discussed later. It shall be noted that the creation of phase singularities with phase masks still keeps the information on the structure. Information with its zero intensities are at right position, but the contrast and intensity profiles cannot be used for printing anymore.

Surprisingly the situation changes when light propagates further. The measurement in the third zone is of interest. The evaluation is at a larger distance behind the mask from $40\ \mu\text{m}$ to $50\ \mu\text{m}$. The result of the measurement is shown in Fig. 8.9. Intensity profile shows very good similarity with the desired one (compared to Fig. 8.2(b)). The contrast is high and the intensity is low at the low light zones. To see the effect of the alternating phase mask on a series of lines compared to a single structure, one can just examine the structure definition of a single line at the end of the corner structures in Fig. 8.9.

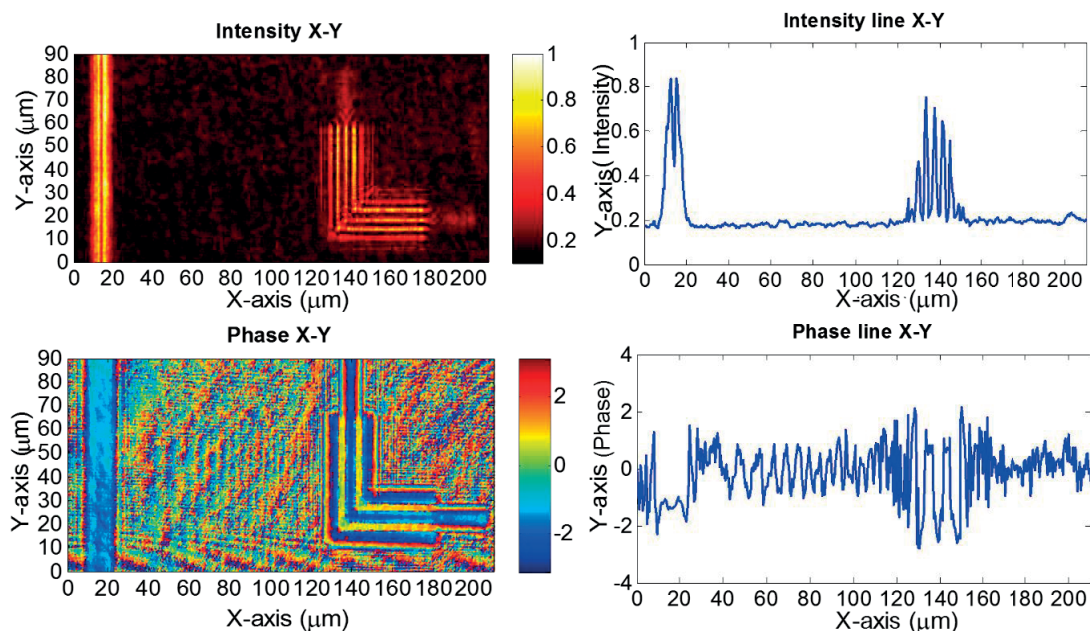


Figure 8. 9: The measured intensity, phase and line image of the phase shifting mask structure at 40 μm proximity gap.

At 40 μm proximity gap, the single line loses its definition completely while the multiple corner structures can still be successfully printed and appear in good contrast. The x-y intensity images show that the structure re-establishes the profile again, but lacks some of the original properties. The only difference is that the outward intensity peaks will have less intensity compared to the inner ones. This might lead to different line width of outer and inner structures, but can be partially corrected using a particular dose setting or process window when printing.

8.3 Results and discussion

The experiments show propagation effects of light through an amplitude and a phase shifting mask with repetitive features. Although the structure we selected has only very few repetitions, interpretation can be made by assuming a periodic structure. When light falls on periodic structures such as gratings, Talbot images appear behind the structure. Talbot effect is also valid for small grating periods [8.5]. The Talbot effect leads to varying light distribution and phase anomalies behind the grating [8.6].

This concept can be applied here also. The wavelength used for the measurement is 405 nm. For the amplitude only mask structure with a period of $d = 4 \mu\text{m}$, one finds a Talbot distance $Z_T = (2d^2 / \lambda) = 79.01 \mu\text{m}$ and half Talbot distance will be around 40 μm . It is known that at half Talbot distances, self-imaging occurs. These images are phase-shifted by half a period, which means that the image position will be laterally shifting by half the width of the grating period.

This corresponds to simulation and experimental findings of the high contrast region at 40 μm distance behind the amplitude mask illustrated in Fig. 8.4 (a) and Fig. 8.5.

For a phase shifting mask with base period $d = 8 \mu\text{m}$ (the combination of amplitude and phase structures, compare with Fig. 8.1) will result in a Talbot distance $Z_T = (2d^2/\lambda) = 316 \mu\text{m}$. This length is much longer than the distance range we are using for printing, which ranges only up to 50 μm usually. In one of the early papers, Lohmann pointed out that phase grating would form amplitude image copies at fractional Talbot distances [8.7, 8.8]. This kind of imaging is only possible for certain phase grating configurations and the image formed is called fractional Talbot image or Fresnel image. The Talbot distance depends not only on the period of the structure but also on the phase step.

In this case, the phase structure on the mask is neither a standard binary phase nor amplitude only grating. It is a complex structure having openings and phase shifts with a phase difference of π . According to Lohmann's interpretation, the new Talbot distance z can be linked to the original Talbot distance (Z_T) and numbers P and Q (where $P < Q$, and are positive integers that depend on the width of the structure w and period d). The fractional Talbot distance z becomes $z = (P/Q) Z_T$.

Self-imaging formed at different distances are explained according to the proper structuring of mask. As discussed by Thomas J. Suleski [8.9], phase structure of π phase difference and a width to period ratio 1:4 will lead to fractional Talbot image length (z) and Talbot length (Z_T) ratio of 1:8. Applying this to the case, the width to period ratio is 1:4 ($2/8$) and the phase difference is π between etched quartz and open chromium. Then, the fractional Talbot image falls at a distance of $z = 1/8^{\text{th}}$ of $Z_T = 316 \mu\text{m} / 8 = 40 \mu\text{m}$ (approx.). This finding corresponds very well to the simulation and experimental findings of the high contrast region at 40 μm distance behind the phase mask in Fig. 8.4(b) and Fig. 8.6. For distances below 40 μm , complex light patterns appear that cannot be optically resolved anymore with our measurement system. In printing, these zones will lead to non-useful operation zones. An additional aspect is the limited number of periods. In such cases, the established pattern is washed out and contrast is reduced which leads to an additional worsening of the pattern definition below the 40 μm distance limit.

The other option to print at this zone is to design an OPC structure. The light evolution from OPC structure designed for printing 30 μm proximity gap is discussed below. The OPC structure is designed using Wave Propagation Method (WPM) and Iterative Fourier Transfer Algorithm (IFTA) [8.3].

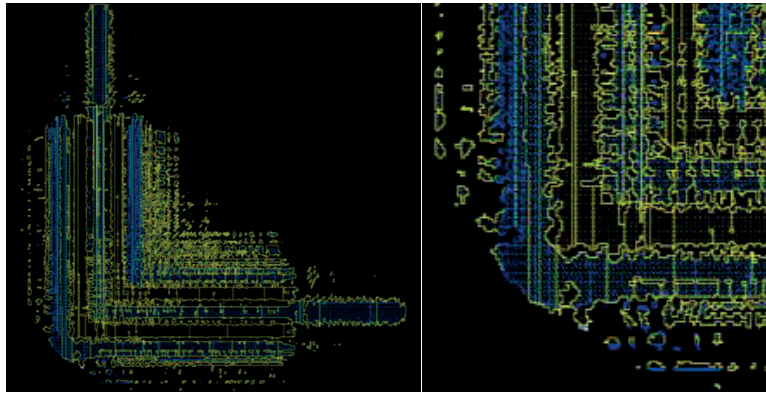


Figure 8.10: OPC structure designed in PSM for printing at $30\ \mu\text{m}$ proximity gap. Left side image is the full image figure and right side image represents the zoom in version of the edge position to see the details.

The OPC structure designed above is a solution to print the defined structure (Fig. 8.1) at $30\ \mu\text{m}$ proximity gap. The amplitude and phase x-y images of the structure are plotted below at different proximity gaps.

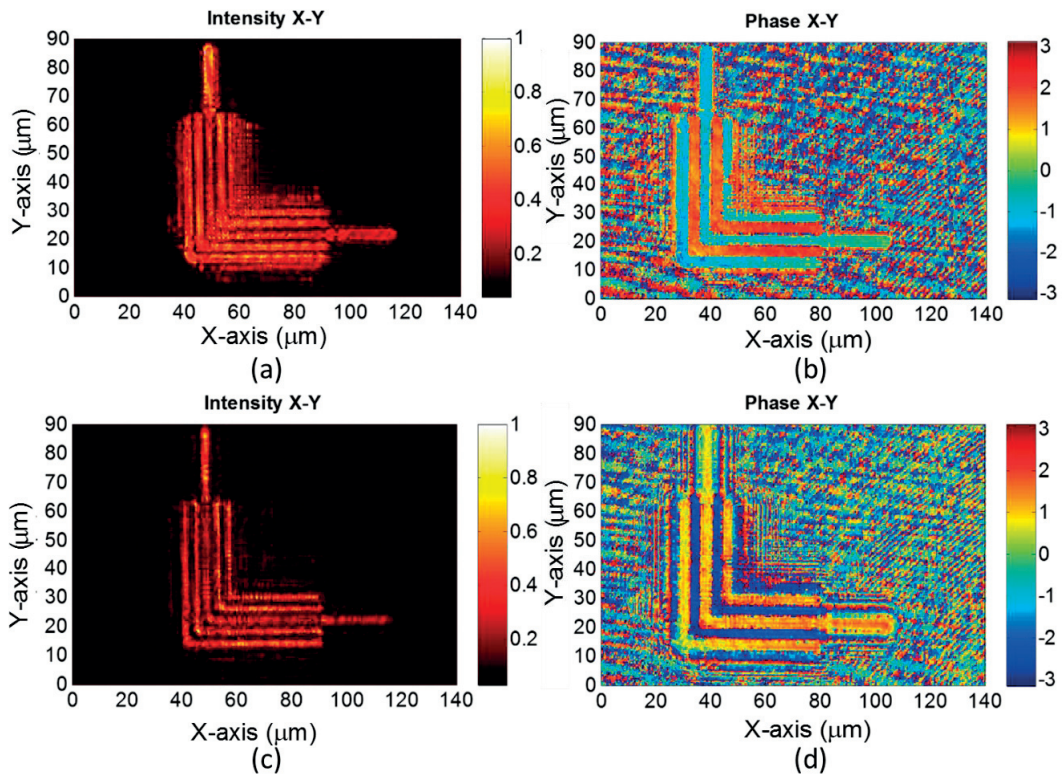


Figure 8.11: The measured intensity and phase images of the OPC phase shifting mask structure at different proximity gaps. (a) and (b) represents the images at $0.1\ \mu\text{m}$ proximity gap. (c) and (d) represents images at $30\ \mu\text{m}$ proximity gap.

The above images expound how the structure pattern is changed by OPC designs. The intensity image at starting point of the light evolution (Fig.8.11(a)) shows all the sub resolution

features in its designed way and the phase image (Fig.8.11(b)) clearly shows the phase difference between different layers and also between the sub resolution features. After 30 μm distance of light propagation, the intensity image reproduced the desired pattern (Fig.8.11(c)). But the phase image (Fig.8.11 (d)) at 30 μm proximity gap does not show any change. This shows that phase variations can propagate larger distance like the creation of phase singularities.

Conclusion

The study presents the phase and intensity profiles behind a phase mask structure in the proximity region up to 50 μm . The results show how the phase encoding preserves the information when correctly applied. The experimental evaluation of the structure at different proximity gaps allows us to understand the different effects. It became clear that the proximity gap for printing a structure can be decided only after studying different parameters and conditions that are triggered by diffraction effects and influenced by the resist properties. The above structure was evaluated at proximity gaps of 5 μm , 22 μm and 40 μm . The above studies changed some ideas that existed till now in printing industry, namely that shorter proximity gaps (but not contact) might give better results. To improve printing on those proximity gaps where diffraction effects are prominent, an OPC structure can be used. An OPC structure designed with PSM is also evaluated. The study shows that the phase shift and singularities will propagate larger distances once it is designed.

References

- [8.1] K. Puthankovilakam, T. Scharf, M.-S. Kim, A. Naqavi and H. P. Herzig, T. Weichelt, U. Zeitner, U. Vogler and R. Voelkel; "Intensity and phase fields behind phase-shifting masks studied with high-resolution interference microscopy"; *Journal of Micro/Nanolithography, MEMS, and MOEMS*; **Vol. 15, No. 2**; pp.021203 1-8(2016).
- [8.2] M.D. Levenson, G. Di, T. Ebihara G. Dai, Y. Morikawa, N. Hayashi and S. M. Tan; "Optical vortex masks for via levels"; *Journal of Micro/Nanolithography, MEMS, and MOEMS*; **Vol. 3, No. 2**; pp.293-304(2004).
- [8.3] T. Weichelt, U. Vogler, L. Stuerzebecher, R. Voelkel and U. D. Zeitner; "Resolution enhancement for advanced mask aligner lithography using phase -shifting photomasks"; *OPTICS EXPRESS* **Vol.22, No.13**; pp. 16310-16321(2014).
- [8.4] M.-S. Kim, T. Scharf, C. Etrich, C. Rockstuhl, and H. P. Herzig; "Longitudinal-differential interferometry: direct imaging of axial superluminal phase propagation"; *OPTICS LETTERS* **Vol. 37, No. 3**; pp. 305-307(2012).

- [8.5] M. V. Berry and S. Klein; "Integer, fractional and fractal Talbot effects"; *Journal of modern optics* **Vol. 43, No. 10**; pp. 2139–2164(1996).
- [8.6] M.-S. Kim, T. Scharf, C. Menzel, C. Rockstuhl and H. P. Herzig; "Phase anomalies in Talbot light carpets of self- images"; *OPTICS EXPRESS* **Vol. 21, No. 1**; pp. 1287-1330(2013).
- [8.7] A. W. Lohmann and J. A. Thomas; "Making an array illuminator based on the Talbot effect"; *APPLIED OPTICS* **Vol.29, No. 29**; pp. 4337-4340(1990).
- [8.8] A. W. Lohmann, J. Schwider, N. Streibl and J. Thomas;" Array illuminator based on phase contrast"; *APPLIED OPTICS* **Vol.27, No. 14**; pp. 2915-2921(1988).
- [8.9] T. J. Suleski; "Generation of Lohmann images from binary-phase Talbot array illuminators"; *APPLIED OPTICS* **Vol. 36, No. 20**; pp. 4686-4691(1997).

CHAPTER 9

Conclusions

The thesis is mainly concentrated on finding the limitation of proximity printing and to increase the resolution of the technology using different techniques. It is for the first time that a complete study including simulation, observation of aerial images and printing for proximity technology has been carried out. The study is intended to highlight the current possibilities and shortcomings of proximity printing over projection printing and to provide resolution enhancement techniques to overcome such. A complete loop of optimization has been performed, starting from simulating the aerial images, to the measurement of intensity plots and finally the printing of structure pattern with mask aligner.

The main novelty that is included in the optimization was that the special illumination technique called MO exposure optics (or MOEO) from Süss MicroOptics that was implemented in both simulation and experimental setup. MO exposure optics gives a uniform and homogeneous illumination regime controlling field uniformity and illumination angle on the mask plane using micro lens arrays, illumination filter plates and Fourier lenses. The simulation tool from GenISys Layout LAB allows to accurately calculate the aerial images and resist profiles. The diffraction pattern was calculated using Rayleigh-Sommerfeld diffraction theory and transfer matrix method which was briefly discussed. The experimental analysis using a measurement setup for different mask structures having MO exposure optics has never been done before. The study was performed with the measurement system called high resolution interference microscopy. It is an instrument working on the principle of Mach-Zehnder interferometer. The instrument consists of mainly two arms: object arm having a sample stage and reference arm consisting of a moving mirror. The instrument efficiently measures the intensity and phase fields that evolve from the mask designs. This helped to accurately define the new aspects of diffraction effects and aerial image intensities at different proximity gap.

The study started with designing corrections for a one dimensional structure. The structure selected was a simple edge. A complete edge study with different correction features at different proximities has never been done before in proximity printing. The study was carried out by defining different parameters at different edge intensity positions which revealed the aspects, such as edge falling position, resist exposure points, for defining edge slope. It also explained the

similarity between simulation and experimental results. The results were subsequently published in SPIE conference proceeding. This gave a good platform to take the research to a higher dimension.

A unified correction structure has been designed for solving the corner rounding problem in proximity printing for a proximity gap 30 μm for all line widths. The complete study from designing the correction structure using simulations, verification by measurement system and printing using mask aligner was carried out using MO exposure optics. The novelty is that the correction structure can be used to print any line width at single proximity gap with single exposure on the same wafer. All the correction structures were usually defined by characterizing intensity or amplitude changes. The aerial image importance is already known but the change in the phase had not really been studied.

It is for the first time, that the phase evolution from different amplitude structures is studied to understand the role played by phase for shaping the light carpet behind microstructures. The study started with 1D correction structure edges. The phase evolution from 1D amplitude structure was never studied before. The phase evolution in the structure made a phase shift at the desired proximity gap which seems to be mediated by phase singularities. Phase singularities or optical vortices have a phase shift of π for neighboring regions and are characterized by zero intensity at the phase jump position. The concept of phase singularity and phase shift gave more insight to study the 2D structures. 2D structures having small amplitude corrections are analyzed with phase evolution. Furthermore, the diffraction effects from different correction features which shape the light were also studied. The phase study shows that more analysis needs to be done for defining the OPC features to get sharp phase shifts and the interpretation will not be easy with amplitude only structures. The phase evolution from amplitude mask structures is a new study and the results were published in SPIE conference proceedings.

Phase and intensity evolution from phase shifting mask were also analyzed. It is a first attempt to study propagations of phase and amplitude of up to 50 μm proximity gap. The study was carried out using a group of corner structures and proved that the ideas like shorter proximity gap gives better results can be misleading. Theoretical concepts like fractional Talbot imaging and Lohmann images are applied to study the effects from phase structures. Optical proximity corrected structures designed in phase shifting mask are also studied and evaluated. The studies showed that phase shifts and phase singularities can propagate longer once the phase shift is designed. The results from phase shifting mask study were published in the journal of Journal of Micro/Nano Lithography MEMS and MEOMS.

A complete propagation study about intensity and phase using different design and verification tools is carried out. The study was performed for different amplitude mask structures and phase mask structures. The intensity evolutionary study helped to define different optical proximity correction structures at different proximity gaps. The study shows that, there exists an open field to continue the research in different micro/nano structures in different masks. Fundamentals principles can also be analyzed with this frame of propagation analysis.

ACKNOWLEDGEMENT

I would like to express my sincere gratitude to all the people for their advice and support in successful completion of my thesis.

Firstly, I would like thank my thesis advisor, Prof. Hans Peter Herzig for giving the opportunity to pursue my dreams in his group. The discussion with him was always interesting and improved my fundamental knowledge in optics. His motivation, patience and enthusiasm for sports helped me to improve my abilities not only in scientific strength but also my personal strength.

I would like to thank my co-thesis director next, Dr. Toralf Scharf. I am really fortunate that I got a chance to work under him. He is the backbone of my thesis. He taught me how to face challenges during the research. He was always helping to make the things perfect, from small alignment problem in optics to writing the thesis in a good form. He was a person easy to communicate not only science but also personal problems. I could not imagine a better advisor than him.

Next, I will express my thanks to Uwe Vogler, Arianna Bramati, Reinhard Voelkel and other members from Süss MicroOptics. They introduced me to lithography field which is the basis of my thesis. I learned all the basics of simulation and proximity printing theory from them.

I express my gratitude to Dr. Myun-Sik Kim, post-doc, who taught me how to handle the instrumental setup which I modified for my thesis. He was a good teacher for me for designing optical setups. I also thank other post-docs, Dr. Gael Osowiecki, Dr. Raphael Barbey and Dr. Nicolas Descharmes for their valuable inputs in my research.

Thanks to Karin Prater for spending four years together in the same office and I had a good time. I would like to thank my former office mate Johana Bernasconi, for helping me with French translations and also my neighbor office mate Richa Dubey to have conversations in 'Hindi'. Besides them, I thank all my colleagues from OPT Lab, Daniel Infante, Gregoire Smolik, Michail Symeonidis, and Babak Vosoughi for all the support and fun times.

I especially thank Brigitte Khan, our secretary, she helped me a lot in setting up my life in Neuchatel. She was very supportive and her advices made my life in Neuchatel easy. I thank Marcel Groccia for providing the electronic facilities and Irene Philipoussis for clean room assistance.

I take this opportunity to thank my former colleagues Sophiane Tournois, Dr. Ali Naqavi, Dr. Sara Santi, Dr. Elsie Barakat, Dr. Qing Tan, Dr. Libo Yu, Dr. Lubos Hvozدارa, Joab di Franscesco, Dr. Armando Cosentino, and Loic Hans, I had a pleasure time working with all of them.

I also take this opportunity to say big thanks to my friends from other labs in Microcity especially GALATEA and AQUA. My final year was amazing and I was able to write my thesis in a relaxed way because of you guys. I really had good fun time during our lunch breaks, coffee breaks and also parties.

Special thanks to my friends in Neuchatel. I thank the family of Von Wyss where I stayed during my first days in Neuchatel. Their warm and loving nature made me love Switzerland and Swiss culture.

May be thanks will be very little for the big group of my Indian friends including Rena. I can't imagine my life in Neuchâtel without them. I enjoyed their company and our Indian parties a lot, especially Arun Bhaiyya, Sheethaldi, Jenni, Keethan, Vineela, Mani, Bhavik, Charmi, Reema and Subha, your homes were second home to me. I never missed India because of you all.

I would express my thanks to my friends in Germany, the Netherlands and Belgium. I have got a chance to see Europe with our trips. Special thanks to my childhood friend Thulsi, she was always an emotional support system for me.

Finally, I acknowledge people who mean a lot to me, my parents (achan and amma), my two caring elder brothers (ettan and aniyettan), sister in laws (edathy and paru) and my loving husband's family (achan (late), amma, oppa and KR ettan, Keshav and Pranav). Their trust and support helped me in achieving my goals. They were my wings to fly. I also thank my cousin, Gautham, whose jokes about my research nature turned in to reality.

I owe a big thanks to one special person, shreeshan, my husband. You were a constant support and encouragement for me during my PhD life. You were always there to correct my stupid mistakes and show me the right path. I am really grateful for having you in my life.

I would like to thank each and every one who came across my life even for a second. The peaks that I have achieved in my life are results of your good wishes and prayers.

List of publications

Journal publications

1. K. Puthankovilakam, T. Scharf, H. P. Herzig, U. Vogler and R. Voelkel; "Unified rule based correction for corners in proximity lithography mask using high resolution features"; *IEEE microelectronic engineering*, **Vol. 172**; pp. 35-44(2017).
2. K. Puthankovilakam, T. Scharf, M.-S. Kim, A. Naqavi, H. P. Herzig, T. Weichelt, U. Zeitner, U. Vogler and R. Voelkel; "Intensity and phase fields behind phase-shifting masks studied with high-resolution interference microscopy"; *Journal of Micro/Nanolithography, MEMS, and MOEMS*; **Vol. 15, No. 2**; pp.021203 1-8(2016).

Conference proceedings

1. K. Puthankovilakam, T. Scharf, H. P. Herzig, U. Vogler, A. Bramati and R. Voelkel; "Phase analysis of amplitude binary mask structures"; *Proc. SPIE Optical Microlithography XXIX* **Vol. 9780**; pp. 97800V 1-7(2016).
2. K. Puthankovilakam, T. Scharf, H. P. Herzig, T. Weichelt, U. Zeitner, U. Vogler and R. Voelkel; "Intensity and phase fields behind Phase Shifting Masks studied with High Resolution Interference Microscopy"; *Proc. SPIE Optical Microlithography XXVIII* **Vol. 9426**; pp. 94260I 1-10(2015).
3. K. Puthankovilakam, T. Scharf, Q. Tan, H. P. Herzig, U. Vogler, A. Bramati and R. Voelkel; "Shaping intensity behind amplitude masks for proximity correction lithography: design, measurement, and realization"; *Proc. SPIE interferometry XVII: Techniques and Analysis* **Vol. 9203**; pp. 92031B 1-8(2014).
4. T. Scharf, K. Puthankovilakam, M.-S. Kim, H. P. Herzig and U. Vogler et al.; "Lightfields behind amplitude masks Creating phase discontinuities"; *15th Workshop on Information Optics (WIO)*; (2016).
5. T. Scharf, M.-S. Kim, K. Puthankovilakam, J. Bernasconi and H.-P. Herzig et al.; "Structured amplitude and phase fields behind microstructures: The quest for high contrast modulation at proximity"; *Proc. SPIE Complex Light and Optical Forces X* **Vol. 9764**; pp. 97640B 1-6(2016).

Presentations and workshops

1. Invited speaker at '*Micro structuring academia*' event organized by **Hilpert electronics**, Baden, Switzerland on 15 Sep 2016.

2. Poster presentation at '*CTI Micro- Nano event*' organized by **Commission for Technology and Innovation CTI**, Basel, Switzerland on 10 July 2016.
3. Oral and poster presentation at '*SPIE Advanced Lithography Conference*' organized by **SPIE**, in San Jose, California, United States, February 2016.
4. Poster presentation at '*Photonics day*' organized at EPFL, Lausanne, November 2015.
5. Poster presentation at '*CTI Micro- Nano event*' organized by **Commission for Technology and Innovation CTI**, Neuchatel, Switzerland on 28 May 2015.
6. Oral presentation at '*SPIE Advanced Lithography Conference*' organized by **SPIE**, in San Jose, California, United States, February 2015.
7. Poster presentation at '*Photonics day*' organized at EPFL, Lausanne, November 2014.
8. Poster presentation at '*SPIE Optics + Photonics Conference*' organized by **SPIE**, in San Diego, California, United States, February 2015
9. Poster presentation at '*Photonics day*' organized at EPFL, Lausanne, November 2013.

List of abbreviations

IC	-	Integrated Circuit
RET	-	Resolution Enhancement Techniques
DOF	-	Depth of Focus
PSM	-	Phase Shifting Mask
OAI	-	Off-Axis illumination
OPE	-	Optical Proximity Effects
OPC	-	Optical Proximity Correction
NA	-	Numerical Aperture
HRIM	-	High Resolution Interference Microscopy
CCD	-	Charge Coupled device
MOEO	-	MO Exposure Optics
IFP	-	Illumination Filter Plate
SMILE	-	SUSS MicroTec Imprint Lithography Equipment
LER	-	Line Edge Roughness
LWR	-	Line Width Roughness
MEEF	-	Mask Error Enhancement Factor
EPE	-	Edge Placement Error
FDTD	-	Finite-difference Time-domain
WPM	-	Wave Propagation Method

Krishnaparvathy Puthankovilakam



EPFL STI IMT OPT,
Optics & Photonics Technology Lab,
Rue de la Maladière 71b
Neuchâtel,
CH 2000, Switzerland
Phone No: +41766235349
Email:krishnaparvathy.puthankovilakam@epfl.ch

➤ RESEARCH INTERESTS

- Optical microsystems and characterization
- Lithography printing, simulation and characterization
- Illumination systems and interferometers
- Experimental data analysis

➤ ACADEMIC QUALIFICATIONS

- Apr2013 – Present **Doctoral student** at Optics and Photonics Technology Lab (OPT), École Polytechnique Fédérale de Lausanne (EPFL), Switzerland.
- July2009 - May2012 **Master of Science and Technology (MSc.Tech)** in Photonics, National Institute of Technology, Calicut, Kerala, India.
- July2006 - May2009 **Bachelor of Science (BSc)** in Physics and Mathematics, Amrita Viswa Vidya Peetham, Kollam, Kerala, India.

➤ WORK EXPERIENCE/INTERNSHIPS

- Apr2013 - Present **PhD student: EPFL, Switzerland**
- Developing a new measurement technique for mask aligners to calculate proximity distance using LED as illumination source.
 - Simulation and characterization of OPC Structures in amplitude mask using High resolution Interference Microscopy (HRIM).
 - Designing new rule based Optical Proximity Correction (OPC) structures for edges, corners and also designing masks for mask aligners (collaboration with Süss MicroOptics).
 - Clean room printing using mask aligners and characterization with SEM.
 - Phase and amplitude analysis of different structures in amplitude and phase shifting mask with HRIM.
 - Studying the theoretical aspects of propagation like Phase singularities, Lohmann Images for designing new rules.
- Nov2012 –Mar2013 **Project Scientific Officer 'B': Tata Institute of Fundamental**

Research (TIFR), Mumbai, India.

- Research and development of muon detectors for India-based Neutrino Observatory project.
- Analyzing and managing the gas flow to the detectors and modify the gas rates.

Dec 2011 – Apr 2012

Master project Student: Tata Institute of Fundamental Research (TIFR), Mumbai, India.

- Simulation and experiments for a prototype laser Interferometer Detector for Gravitational waves – Department of High Energy Physics, under the guidance of Dr. C. S Unnikrishnan.

May 2011 - Jul 2011

Summer Intern: Tata Institute of Fundamental Research (TIFR), Mumbai, India.

- The study and Characterization 2M * 2M Resistive Plate chamber (RPC) under the guidance Dr. Prof. Naba Kumar Mondal and Dr. B. Satyanarayana.
- One of the fully funded scholarship from Indian Academy Of Sciences-India.

May 2010 - Jul 2010

Summer Intern: CERN, Geneva, Switzerland.

- The study and efficiency calculation of Gas Electron Multiplier (GEM) detectors – particle experiments in RD-51 lab, under the guidance of Dr. Archana Sharma.
- One of the few students selected from India with a fully funded scholarship (Central government of India).

➤ JOURNAL PUBLICATIONS

J. mee Vol. 172, 2017

K. Puthankovilakam, et al., *Unified rule based correction for corners in proximity lithography mask using high resolution features.*
[doi:10.1016/j.mee.2017.03.001](https://doi.org/10.1016/j.mee.2017.03.001).

JM³ vol. 15, 2016

K. Puthankovilakam, et al., *Intensity and phase fields behind phase-shifting masks studied with high-resolution interference microscopy.*
[doi:10.1117/1.JMM.15.2.021203](https://doi.org/10.1117/1.JMM.15.2.021203).

➤ CONFERENCE PROCEEDINGS

SPIE Adv. Litho16

K. Puthankovilakam, et al., *Phase analysis of amplitude binary mask structures.* [doi:10.1117/12.2219062](https://doi.org/10.1117/12.2219062).

SPIE Adv. Litho15

K. Puthankovilakam, et al., *Intensity and phase fields behind phase-shifting masks studied with high-resolution interference microscopy.*
[doi:10.1117/12.2085804](https://doi.org/10.1117/12.2085804).

SPIE Opt. Photo14

K. Puthankovilakam, et al., *Shaping intensity behind amplitude masks for proximity correction lithography: Design, measurement and realization.*
[doi:10.1117/12.2060954](https://doi.org/10.1117/12.2060954).

SPIE Phot. West17

Toralf Scharf, et al., *Light fields behind microstructures: study of the Babinet-principle in the Fresnel regime.*

[doi:10.1117/12.2251379](https://doi.org/10.1117/12.2251379).

SPIE Phot. West16

Toralf Scharf, et al., *Structured amplitude and phase fields behind microstructures: The quest for high contrast modulation at proximity.*

[doi :10.1117/12.2214341](https://doi.org/10.1117/12.2214341).

➤ TECHNICAL SKILLS

Matlab, GenISys Layout LAB, Layout editor, Basic CST microwave studio FDTD simulation, Basic Labview and Muon detectors.

➤ LANGUAGES

English	:	Fluent
Malayalam	:	Mother tongue
Hindi	:	Fluent
French	:	Basic

➤ REFERENCES

- I. **Prof. Hans Peter Herzig**, EPFL STI IMT OPT, MC A3 302 (Microcity), Rue de la Maladière 71b, Neuchâtel, CH 2000.
Email - hanspeter.herzig@epfl.ch
- II. **Dr. Toralf Scharf**, EPFL STI IMT OPT, EPFL STI IMT NAM, ELG 241 (Bâtiment ELG), Station 11, Lausanne, CH-1015.
Email - toralf.scharf@epfl.ch
- III. **Dr. Raghu Chathanathi**, Associate Professor, Department of Physics, National Institute of Technology Calicut (NITC), Calicut, Kerala, India.
Email - raghuc@nitc.ac.in

